1995

X-Ray Absorption and Electron Paramagnetic Resonance Studies of Azotobacter Vinelandii Nitrogenase.

Roland Carroll Tittsworth
Louisiana State University and Agricultural & Mechanical College

INFORMATION TO USERS

This manuscript has been reproduced from the microfilm master. UMI films the text directly from the original or copy submitted. Thus, some thesis and dissertation copies are in typewriter face, while others may be from any type of computer printer.

The quality of this reproduction is dependent upon the quality of the copy submitted. Broken or indistinct print, colored or poor quality illustrations and photographs, print bleedthrough, substandard margins, and improper alignment can adversely affect reproduction.

In the unlikely event that the author did not send UMI a complete manuscript and there are missing pages, these will be noted. Also, if unauthorized copyright material had to be removed, a note will indicate the deletion.

Oversize materials (e.g., maps, drawings, charts) are reproduced by sectioning the original, beginning at the upper left-hand corner and continuing from left to right in equal sections with small overlaps. Each original is also photographed in one exposure and is included in reduced form at the back of the book.

Photographs included in the original manuscript have been reproduced xerographically in this copy. Higher quality 6" x 9" black and white photographic prints are available for any photographs or illustrations appearing in this copy for an additional charge. Contact UMI directly to order.

UMI

A Bell & Howell Information Company
300 North Zeeb Road Ann Arbor, MI 48106-1346 USA
313/761-4700 800/521-0600

X-RAY ABSORPTION AND ELECTRON PARAMAGNETIC RESONANCE STUDIES OF *Azotobacter vinelandii* NITROGENASE

A Dissertation

Submitted to the Graduate Faculty of the
Louisiana State University and
Agricultural and Mechanical College
in partial fulfillment of the
requirements for the degree of
Doctor of Philosophy

in

The Department of Chemistry

by
Roland Carroll Tittsworth
B.A., University of Maryland Baltimore County, 1989
August 1995

Acknowledgements

I would like to thank Louisiana State University for providing me with the opportunity to pursue this research. It has been a great privilege.

Also, thanks to the entire faculty and staff of the LSU Chemistry Department for their support and guidance.

I would like to acknowledge the LSU Alumni Association, the LSU Chemistry Department, and Dr. Brian J. Hales for financial support. I would especially like to thank the Chemistry Department for allowing me to teach the General Chemistry and Physical Chemistry Laboratory courses, an experience I found extremely rewarding.

Special thanks to Professor Stephen P. Cramer and his research group at the University of California Davis for their contribution to the EXAFS studies presented here. I learned a great deal from Professor Cramer, Dr. Jie Chen, Dr. Simon George, and Jason Christiansen. Especially Christiansen, since you haven't lived until you've heard him expound at length on the inadequacies of all people, places, and things south of the Mason-Dixon Line at 4 A.M on Beamline X-19A. Of course, that sort of deluded prattle is to be expected from someone whose football team is called the AGGIES. I'd particularly like to thank him for the informative but somewhat ethanolic tour of various Long Island wineries when the monochromator on Beamline X-19A broke.

Thanks to members of the Hales research group, past and present; Dr. Virginia Moore, Dr. Melinda Oliver, Carol Blanchard, Linda Cameron, Laura Efferson, and Renee Johnson, for helpful scientific discussions

I'd especially like to thank my research advisor Dr. Brian J. Hales for his guidance, inspiration, and support. His scientific knowledge and creative skills and his ability to apply them rationally and productively to interesting problems are impressive, to say the least. I consider myself extremely fortunate to have him as a research advisor.

In closing, I'd like to dedicate the work in this dissertation to my maternal grandmother, Mrs. Carrie M. Mellor, whose love, guidance, and support have been immeasurable.

Table of Contents

Abstract

Fe K-edge Extended X-ray Absorption Fine Structure (EXAFS) spectroscopy was used to investigate the metal-cluster structure of both the Mo-containing (Av1) and V-containing (Av1') nitrogenase component 1 proteins of *Azotobacter vinelandii* in their as-isolated and thionine-oxidized states. Using the EXAFS data, plausible distance assignments were made for the cofactor clusters. It was shown that small but consistent distance changes occur in both Av1 and Av1' upon thionine oxidation. Furthermore, the EXAFS of Av1' is very similar to that of Av1, supporting the proposal that the two proteins have homologous metal cluster structures.

Fe K-edge and Mo K-edge EXAFS were used to examine various spectroscopically definable redox states of Av1. It was found that the average metal-metal distances contracted somewhat upon reduction. Also, a split-shell EXAFS analysis was conducted in an attempt to resolve P-cluster and M-center Fe-Fe interactions.

Electron Paramagnetic Resonance (EPR) studies of thionine-titrated Av1 were conducted which verified the existence of S = 1/2 and proposed S = 5/2 EPR signals assigned to the singly-oxidized P-cluster, or P^+. A probabilistic theoretical model was proposed to explain P-cluster oxidation behavior in the P $\rightarrow$ P^{2+} range.

Oxidative titrations were performed on enzymatically reduced Av1' and monitored by EPR spectroscopy. The oxidation behavior of Av1' is similar, but

not identical to that of Av1, in that it follows a consecutive rather than a random model for the $P^{+} \rightarrow P^{2+}$ oxidation. Also, a recently characterized Av1' variant called $Av1'_{A}$ exhibited unique behavior during oxidative titrations. We believe we observe EPR spectral evidence of a redox-gated electron transfer between the P-cluster and the M-center.

Chapter 1 Introduction

1.1 Nitrogen Fixation

Nitrogenase catalyzes the bioreduction of dinitrogen to ammonia, and is the basis for the biological nitrogen cycle. The importance of the nitrogen cycle cannot be overstated, since higher species are unable to reduce nitrogen to ammonia, and depend on single-celled nitrogen fixing organisms to supply it. Nitrogenase is found in bacterial root nodule symbionts of leguminous plants, some phytoplankton, and certain bacteria. The work presented here was done with nitrogenase isolated from the free-living soil bacterium *Azotobacter vinelandii*.

1.2 History

The symbiotic relationship between leguminous plants and nitrogen fixing root nodule bacteria was reported in 1884.[1] The bacterium responsible was successfully cultured in 1888, although the isolated organism was unable to fix nitrogen, apparently because of high oxygen partial pressure in the cultures.[2] Modern quantitative studies of nitrogen fixing bacteria date to 1951, when it was shown that cultures of the free-living soil bacterium *Clostridium pasteurianum* which were supplied with $^{15}N_2$ produced abundant isotopically enriched $^{15}NH_3$.[3]

In-vitro nitrogen fixation was first achieved in 1960 with cell-free extracts of *Clostridium pasteurianum* which were maintained under anaerobic conditions.[4] By 1965, Mortenson[5] and coworkers had shown that the nitrogenase enzyme consists of two different separable metalloproteins called component 1 and component 2. Component 1, also called the MoFe protein, since it contains Mo

and Fe, has a molecular weight of 220,000 to 240,000, depending on the species of origin, and has been shown to be the site of substrate reduction. Component 2, called the Fe protein (it was shown to contain Fe) has an approximate molecular weight of 60,000, depending on the species. Its catalytic function is to supply electrons to component 1.

Commonly accepted nomenclature for nitrogenase includes component 1 and component 2, the MoFe and Fe proteins, and abbreviations using the initials of the parent organism in genus species form. Thus the component 1 protein of *Azotobacter vinelandii* is called Av1, and the component 2 protein is called Av2.

The nitrogen reduction process requires component 1, component 2, MgATP, and a source of electrons.[6-8] In vivo, the source of electrons is thought to be another metalloprotein such as a ferredoxin, but in vitro $Na_2S_2O_4$ (sodium dithionite, sodium hydrosulfite, or DTN) is usually used as an electron donor. The catalytic process involves the association of reduced component 2 with component 1, and the transfer of an electron to component 1 from component 2. Each association has been shown to result in the transfer of only one electron, and for each one transferred, 2 MgATP are hydrolyzed to MgADP by the component 2 protein.[7,9] Also, for every mole of N_2 reduced, 1 mole of H_2 is produced. So, at optimal electron flux, the equation for nitrogen reduction in vitro is:

$$\mathbf{N_2 + 2H^+ + 16MgATP + 8e^- \rightarrow 2NH_3 + H_2 + 16MgADP + 16P_i}.$$

Nitrogenase also reduces numerous other substrates, including acetylene, azide, methylisocyanide, and cyclopropene.[10-13] In fact, the ability to reduce acetylene to ethylene has been adopted as one standard for reporting nitrogenase specific activity, since ethylene is easily detectable by gas chromatography.

The specific catalytic mechanism of nitrogenase seems to be flux dependent, that is, the allocation of electrons to substrates depends on the component 1 to component 2 ratio.[14] In the presence of N_2 and protons in solution, a high component 1 to component 2 ratio will result in low electron flux, with most or all of the electrons going to reduce protons to hydrogen gas rather than dinitrogen to ammonia. Conversely, a large excess of component 2 will result in high flux, and nitrogen will be reduced to ammonia, but one mole of hydrogen gas is always produced, even at "optimal" electron flux.

Pre-steady state and steady state kinetic studies by Thorneley and Lowe have resulted in a proposed kinetic scheme for nitrogenase.[15-19] A large number of "E_n" states (E_0 to E_7) have been proposed in the scheme, each with its own catalytic competence. Only the states E_3 and above are proposed to be involved in the reduction of dinitrogen, although E_2 is able to reduce protons to H_2. To date, no one has reported conclusive spectral evidence of the E_n states higher than E_1 in the component 1 protein. In the MoFe protein, E_0 is an EPR-active state with S = 3/2, and reduction of the MoFe cluster results in the loss of this signal. A steady state turnover mixture at low electron flux results in attenuation

of the MoFe cofactor signal by 50%, which is generally accepted to occur by the mechanism of the cofactor going to the 1 electron reduced form E_1, and then to the 2 electron reduced form E_2, which evolves H_2 and quickly decays to E_0. Since the E_2 state is so short lived, and decays to E_1 before another Av2 can bind and reduce it to E_3, the steady-state turnover mixture has essentially only E_0 and E_1 present at any given time. Since E_1 is EPR silent, a spectrum of a low flux turnover mix is attenuated to 50% of the spectral amplitude of a resting state Av1 sample.

1.3 The Nitrogenases of *Azotobacter vinelandii*

The most dramatic recent breakthrough in nitrogenase research was the publication of a crystal structure of the component 1 protein of *Azotobacter vinelandii* (Av1).[20-22] Rees and coworkers have published a crystal structure for the entire protein, and have also presented models for the nitrogenase metal clusters at 2.2 Å resolution (Figure 1.1). Av1 is an $\alpha_2\beta_2$ tetramer, with a molecular weight of approximately 220,000. Each of the α subunits contains one Fe_8S_9Mo cluster, or FeMo cofactor. Each cofactor, also called M-center or FeMoco, is ligated through Mo to the imidazole nitrogen of histidine at one end and ligated through Fe to a cysteine residue on the opposite end. The Mo in the "nose" of the cofactor is coordinated octahedrally to 3 S in the cofactor cluster, the histidine imidazole nitrogen, and the carboxyl and hydroxyl functional groups of R-homocitrate. R-homocitrate is necessary for enzymatic activity, and may play a role in proton or electron transfer during the catalytic process, since it "points"

toward the P-clusters, which may have some role in electron transfer from Av2 to the cofactor cluster. The P-clusters are composed of two Fe_4S_4 cubanes which are bridged by 2 cysteine thiols and a disulfide bond. One P-cluster spans each $\alpha\beta$ interface, and is ligated through Fe to cysteine residues in each subunit.

The FeMoco clusters are "buried" within the α subunits, although they are accessible to substrate. The cofactor clusters have been shown to be necessary for catalysis. Cofactorless mutants show no catalytic activity. Cofactor may be extracted from intact nitrogenase and inserted into cofactorless mutants, restoring activity. Extracted cofactor is incapable of nitrogen reduction. There is a proposed binding site for the Av2 protein on component 1. It has been speculated that the P-clusters, which are near this region, accept an electron from Av2, and then somehow transfer it to the cofactor, where substrate reduction occurs. To date, there has been no convincing evidence of P-cluster involvement in catalysis, and the role of these clusters remains mysterious.

Rees and co-workers[23] have also published a crystal structure for Av2. Av2 is a γ_2 dimer, with a Fe_4S_4 cluster bridging the subunits at one end, in a "butterfly" configuration. It has a molecular weight of about 70,000. Two proposed binding sites for MgATP have been identified in the crystallographic analysis. It is generally accepted that the binding and subsequent hydrolysis of ATP causes some conformational change in reduced Av2 which allows the reduced Fe_4S_4 cluster to donate an electron to component 1. In fact, MgATP binding causes a change in the radius of gyration of Av2, as confirmed by small

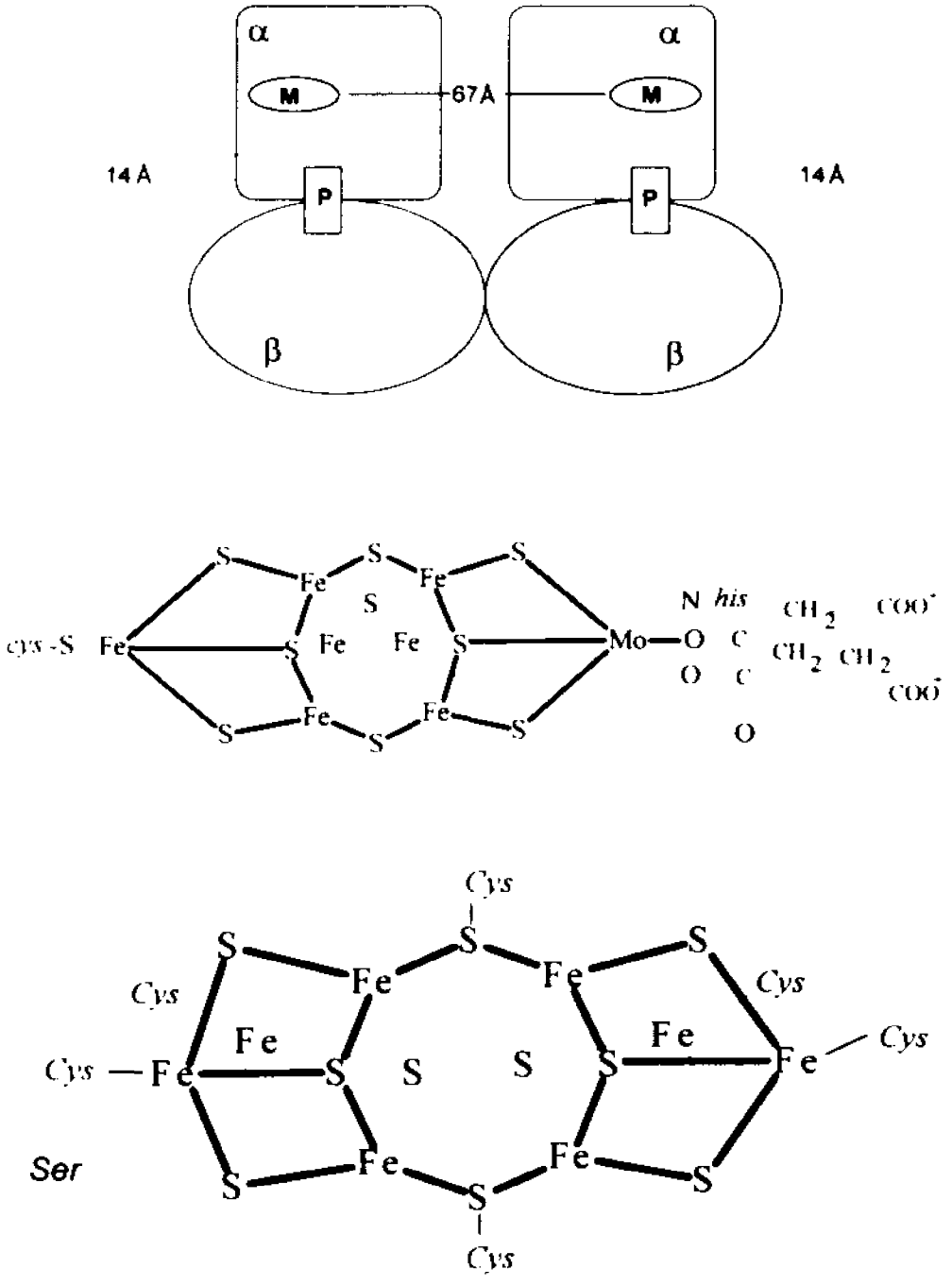

Figure 1.1. Schematic representation of Av1 (top), along with the M-center (middle), and P-cluster (bottom).

angle x-ray scattering experiments.[24] The ATP hydrolysis may supply the energetic "kick" to transfer the electron to component 1. This energy may be spent to change the configuration of residues at the binding sites on both component 1 and component 2 to form a competent electron transfer complex, although this has not been proven.

As-isolated component 1 exhibits an S = 3/2 EPR signal, which arises from the paramagnetic FeMoco cluster.[25] The P-clusters are diamagnetic in as-isolated Av1, but may be oxidized to form paramagnetic species. The existence of EPR observable metal cluster species in Av1 has facilitated investigation of the redox properties of the enzyme. Redox studies of the metal clusters of nitrogenase may be important to the eventual understanding of the nitrogenase catalytic mechanism, since nitrogen reduction is a redox process. Av2 is also EPR active in its as-isolated state, exhibiting a mixed S = 1/2 and S = 3/2 spin state, arising from the Fe_4S_4 cluster.[26]

Azotobacter vinelandii expresses two alternate forms of nitrogenase, one containing V as the cofactor heteroatom instead of Mo, and an Fe-only species. The Fe-only species has not been well characterized, and will not be discussed further. The vanadium containing enzyme, called Av1', was isolated from a mutant strain of *Azotobacter vinelandii*, called LS15, which was developed at LSU in the laboratory of Dr. Brian J. Hales.[27,28] LS15 has been genetically altered so that it may only express the V form of nitrogenase. The V nitrogenase

system also expresses its own component 2 protein, called Av2', which appears to be very similar in structure to the Mo component 2. Av2' is a competent electron donor to Av1, and Av2 also donates electrons to Av1'.

Av1' has not been crystallized, and there is no current structural model available. It does show some striking similarities to Av1, however. It is an $\alpha_2\beta_2$ tetramer, with a molecular weight of approximately 220,000. There are small (molecular weight $\approx$ 15,000) subunits associated with Av1' called δ, but the stoichiometry of this association is not entirely clear. Amino acid sequence homology,[29] metal analysis,[30] and various spectroscopic techniques support the contention that Av1' is very similar in structure to Av1. Recent Mössbauer[31] studies have yielded spectra that are virtually identical to those recorded for Av1. Fe K-edge EXAFS studies of Av1 and Av1' reported in Chapter 3 yield results that are very similar for Av1 and Av1'. Although EXAFS cannot elucidate three dimensional structure, the strikingly similar results for both Av1 and Av1' are probably indicative of significant similarity in the metal clusters of Av1' and Av1.

References

1. Schindler, F. *Jour. Landw.* **1885,** *33*, 324-336.

2. Beyernick, M. W. *Bot. Ztg.* **1888**, *46*, 725-735.

3. Zelitch, I.; Rosenblum, E. D.; Burris, R. H.; Wilson, P. W. *J. Biol. Chem.* **1951**, *191*, 295-298.

4. Carnahan, J. E.; Mortenson, L. E.; Mower, H. F.; Castle, J. E. *Biochim. Biophys. Acta* **1960**, *38*, 188-189.

5. Mortenson, L. E. In *Non-heme Iron Proteins: Role in Energy Conversion*; San Pietro, A. Ed.; Antioch Press: Yellow Springs, Ohio, 1965; 243-259.

6. McNary, J. E.; Burris, R. H. *J. Bacteriol.* **1962**, *84*, 598-599.

7. Winter, H. C.; Burris, R. H. *J. Biol. Chem.* **1968**, *243*, 940-944.

8. Bulen, W. A.; Burns, R. C.; LeCompte, J. R. *Proc. Natl. Acad. Sci.*, U. S. A. **1965** *53*, 532-539.

9. Bui, P. T.; Mortenson, L. E. *Proc. Natl. Acad. Sci.*, U. S. A. **1968**, *61*, 1021-1027.

10. Dilworth, M. J. *Biochim. Biophys. Acta* **1966**, *127*, 285-294.

11. Schollhorn, R.; Burris, R. H. *Fed. Proc.* **1966**, *25*, 710.

12. Hardy, R. W. F.; Burns, R. C.; Parshall, G. W. *Advan. Chem. Ser.* **1971**, *100*, 219-247.

13. McKenna, C. E.; Huang, C. W. *Nature* **1979**, *280*, 609-611.

14. Hageman, R. V.; Burris, R. H. *Biochim. Biophys. Acta* **1980**, *591*, 63- 75.

15. Lowe, D. J.; Thorneley, R. N. F. *Biochem. J.* **1984**, *224*, 877-886.

16. Lowe, D. J ; Thorneley, R. N. F. *Biochem. J.* **1984**, *224*, 903-914.

17. Thorneley, R. N. F.; Lowe, D. J. *Biochem. J.* **1983**, *215*, 393-403.

18. Thorneley, R. N. F.; Lowe, D. J. In *Metal Ions in Biology Vol. 7, Chap. 5*, T. Spiro, Ed.; Wiley: New York, 1984.

19. Lowe, D. J.; Thorneley, R. N. F. *Biochem. J.* **1984**, *224*, 887-894.

20. Kim, J.; Rees, D. C. *Science* **1992**, *257*, 1677-1682.

21. Chan, M. K.; Kim, J.; Rees, D. C. *Science* **1993**, *260*, 792-794.

22. Kim, J.; Rees, D. C. *Nature* **1992**, *360*, 553-560.

23. Georgiadis, M. M.; Komiya, H.; Chakrabarti, P.; Woo, D.; Kornuc, J. J.; Rees, D. C. *Science* **1992**, *257*, 1653-1659.

24. Hodgson, K. O.; Chen, L.; Gavini, N.; Tsuruta, H.; Eliezer, D.; Burgess, B. K.; Doniach, S. *J. Biol. Chem.* **1994**, *269*, 3290-3294.

25. Münck, E.; Rhodes, H.; Orme-Johnson, W. H.; Davis, L. C.; Brill, W. J.; Shah, V. K. *Biochim. Biophys. Acta.* **1975,** *400*, 32-53.

26. Lindahl, P. A.; Day, E. P.; Kent, T. A.; Orme-Johnson, W. H.; Münck, E. *J. Biol. Chem.* **1985**, *260*, 11160-11173.

27. Hales, B. J.; Case, E. E.; Morningstar, J. E.; Dzeda, M. F.; Mauterer, L. A. *Biochemistry* **1986,** *25*, 7251-7255.

28. Hales, B. J.; Langosch, D. J ; Case, E. E. *J. Biol. Chem.* **1986**, *26*, 15301-15306.

29. Bishop, P. E.; Joerger, R. D.; Loveless, T. M.; Pau, R. N.; Michenall, L. A.; Simon, B. H. *J. Bacteriol.* **1990**, *172*, 3400-3408.

30. Eady, R. R.; Robson, R. L.; Richarson, T. H.; Miller, R. W.; Hawkins, M. *Biochem. J.* **1987**, *244*, 963-971.

31. Ravi, N.; Moore, V.; Lloyd, S.; Hales, B. J.; Huynh, B. H. *J. Biol. Chem.* **1994**, *269*, 20920-20924.

Chapter 2 Materials and Methods

2.1 Anaerobic Techniques

Azotobacter vinelandii grows aerobically, and fixes nitrogen under atmospheric conditions, but the purified nitrogenase proteins cannot withstand exposure to oxygen, which results in irreversible oxidative deactivation of the metal clusters. This complication necessitates that nitrogenase be extracted and isolated under anaerobic conditions, and that all experiments be conducted anaerobically.

Nitrogenase proteins were extracted and isolated under strict anaerobic conditions and solutions of purified proteins were stored frozen in liquid nitrogen. When needed for experiments, protein solutions were thawed in a Vacumn Atmospheres glove box with an Ar atmosphere. Oxygen concentration was maintained at less than 1.5 ppm in the glove box by continuous circulation of the box atmoshpere over an oxygen scavenging catalyst bed. Nitrogenase solutions handled outside of the glove box were contained in Ar filled serum vials with gas-tight rubber septa. Tranfers of solutions and gases were effected with gas-tight syringes. All experimental vessels were made anaerobic by repeated cycles of evacuation and filling with Ar on a Schlenk apparatus.

All buffer solutions used in purification or experimentation were deaerated using a Schlenk apparatus. Airtight buffer reservoirs were evacuated to remove air in the headspace and in solution, and then ultra high purity Ar (at $\approx$1.1 atmosphere) was introduced into the headspace through the Schlenk manifold.

Evacuation was then repeated, after which Ar was again introduced into the buffer reservoir. This cycle was repeated at least three times, assuring good deaeration. In most cases, after deaeration was complete, the buffer solutions were made reducing by addition of anaerobic sodium hydrosulfite solution (commonly called sodium dithionite or DTN) to a final concentration of 2 mM. Buffer reducing capability was checked with methyl viologen indicator, which changes from colorless to deep purple upon reduction. Redox studies of the metal clusters of nitrogenase which required that no reductant be present in the buffer solutions were done using buffers that were extensively deaerated on the Schlenk apparatus. The anaerobic condition of these buffers was checked by taking the buffer resevoir into a Vacumn Atmospheres glove box with an Ar atmosphere, opening the resevoir, and stirring the buffer solution while rnonitoring the O_2 detector. $[O_2] < 1.5$ ppm was always maintained.

2.2 Protein Purification

The Mo and V containing nitrogenase of *Azotobacter vinelandii* were extracted and isolated from the appropriate strains using a variation of previously published methods.[1] The bacterial cells were disrupted by osmotic shock. Typically, 300 g of frozen cell paste was taken into the glove box (6 x 50 g aliquots in 250 ml centrifuge bottles) and allowed to thaw. The cells were then suspended in anaerobic 0.025 M Tris-HCl buffer pH 7.4 with 2 mM DTN and 4 M glycerol. The suspensions were allowed to stand for 30 minutes, and the centrifuge bottles were sealed and removed from the glove box. The

suspensions were centrifuged at 10,000 rpm for 20 minutes, and then returned to the glove box. The clear supernatant was decanted, and each cell pellet was rapidly suspended in anaerobic 0.025 M Tris-HCl buffer pH 7.4 with 2 mM DTN and about 6 mg/L deoxyribonuclease, ribonuclease, and lysozyme. The centrifuge bottles were again sealed, removed from the glove box, and centrifuged at 13,000 rpm and 4° C for 1 hr. After centrifugation, the bottles were returned to the glove box, and the dark greenish-black supernatant (lysate) was decanted and pooled. The pooled decantate was then concentrated to a volume of approximately 200 ml with a Minitan membrane concentrator. The crude lysate was assayed for nitrogenase activity using the acetylene reduction assay (see below). In the purification of Mo-nitrogenase, the lysate was usually heat treated to remove non heat-stable contaminants by heating the lysate to 60° C for 5 minutes in a water bath, with subsequent centrifugation to remove heat denatured contaminants. Heat treatment was not done during V-nitrogenase purification, since we have observed that it results in little improvement of nitrogenase activity.

Further isolation and purification of nitrogenase was done by liquid chromatography, starting with ion-exchange chromatography followed by gel-filtration. Concentrated lysate was loaded anaerobically onto a 300 ml DEAE cellulose anion-exchange resin which had been equilibrated with 0.025 M Tris HCl pH 7.4 with 0.08 M NaCl and 2 mM DTN. The column was then rinsed with 0.1 M NaCl buffer until the eluate ran clear. A 1500 ml 0.1-0.5 M linear NaCl

gradient (in above buffer) was then run while collecting fractions in Ar filled serum vials capped with rubber septa. The collected fractions were assayed for component 1 and component 2 activity, and appropriate fractions were pooled and concentrated, using an Amicon membrane concentrator. In the case of the Mo-nitrogenase, ion exchange chromatography was usually successful in resolving the component 1 and 2 proteins, but there was often extensive overlap of the component 1 and 2 peaks in V-nitrogenase.

Gel-filtration on 300 ml Sephacryl S-300 columns was usually the final purification step for both the Mo and the V nitrogenase. 5-7 mL of 50-70 mg/ml (350 mg of protein) protein solution was loaded on the column, and eluted with 0.025 Tris-HCl (pH 7.4) with 0.3 M NaCl and 2 mM DTN. Fractions were collected in Ar filled serum vials capped with rubber septa, and assayed for nitrogenase activity. Appropriate fractions of isolated component 1 and 2 nitrogenase were pooled and concentrated. Protein purity was monitored during the purification process by SDS-PAGE (sodium dodecyl sulfate-polyacrylamide gel electrophoresis).

2.3 Acetylene Assay

Nitrogenase has the capability to reduce substrates other than nitrogen. It readily reduces C_2H_2 to C_2H_4, both of which are easily detected by gas chromatography. The acetylene reduction assay has become a widely accepted measure of nitrogenase activity, and specific activities are often reported in the literature in nmols C_2H_2 reduced min^{-1} mg^{-1} of protein. Neither of the component

proteins exhibits enzymatic activity by itself, so it is necessary to combine them in activity assays.

The acetylene reduction assay mixture consists of 2.5 mM ATP, 30 mM phosphocreatine, 0.125 mg/ml creatine phosphokinase, 20 mM DTN, and 5 mM $MgCl_2 \cdot 6H_2O$ in 38 mM TES-KOH (pH 7.4). The DTN is present as an electron source, and the phosphocreatine and creatine phosphokinase are present for the regeneration of ATP from ADP, so a continous reaction can occur. One ml of this solution was transferred to a 13.5 ml serum vial for each assay. The vial was deaerated on the Schlenk apparatus and injected with an atmosphere of 10% C_2H_2 in Ar. The nitrogenase component proteins were added, and the reaction mixture was incubated in a shaker bath at 30° C.

A Varian 3700 gas chromatograph was used to detect ethylene production. A 0.1 ml sample of the headspace gas was removed from the assay vial with a gas-tight syringe and injected onto a Porapak column. Ethylene was detected with a Flame Ionization Detector (FID), with acetylene serving as an internal standard. The detector was output to a strip chart recorder.

2.4 Protein Concentration

Protein concentration was determined by the biuret method, using a standard curve prepared with BSA (bovine serum albumin). One ml of biuret reagent was added to a 200 µl aliquot of protein solution in an eppendorf tube, and the mixture was allowed to incubate at room temperature for 20 minutes. A

Cary 219 spectrophotometer was used to measure the absorbance of the solutions at 540 nm.

2.5 Extended X-Ray Absorbance Fine Structure Spectroscopy

2.5.1 Introduction

EXAFS (Extended X-ray Absorption Fine Structure) spectroscopy is a powerful technique which is particularly well suited for structural studies of protein-bound metal clusters.[2] EXAFS spectroscopy is ideal for investigations of metalloproteins in solution, since long range repeating order, such as is found in protein crystals, is not necessary. Furthermore, it may be argued that proteins in solution are more likely to be in their "native" configuration than those that are bound in a crystal lattice, since crystal packing may result in structural distortion. Also, EXAFS may be used where crystallization is not possible, which is often the case in ligand-binding and mechanistic studies of metalloproteins. EXAFS spectroscopy yields information about the identity, number, and distance of backscattering atoms in the vicinity of an absorbing atom.[3] It has been shown to yield extremely accurate distance information, especially in the first coordination sphere of backscattering atoms. In most cases, EXAFS is not very useful in the determination of three dimensional structure, which is the domain of x-ray crystallography. EXAFS and crystallography are complementary techniques, since EXAFS can be used to investigate proteins in solution, while crystallographic data can be used to propose three dimensional structural models. Also, EXAFS can often yield information about the distance, identity,

and number of backscattering atoms around a central absorber relatively quickly, while protein crystal structures may take many months to solve.

2.5.2 Basic EXAFS Theory

When an atom absorbs an x-ray photon of the appropriate energy, an electron is ejected from some core energy level of the atom. The x-ray absorbance spectrum shows a sharp rise at this energy. This is commonly called an absorption edge, and the edges are named for the shells of the Bohr atom, with K for n = 1, L for n = 2, M for n = 3, etc. Sometimes, absorption edge features may be interpreted to identify the geometric arrangement of atoms surrounding an absorber, since the edge can show features that are sensitive to electronic structure.[4] Above the edge, in the EXAFS region, x-ray absorption spectra show sinusoidal oscillations if there are neighboring atoms present. This sinusoidal oscillation contains information about the number, type, and distance of the neighboring atoms from the absorber.

The physical phenomenon underlying EXAFS is the interaction of an ejected electron from an absorbing atom with the atoms surrounding the absorber. If one thinks of the ejected electron as an outgoing photoelectron wave and the electronic potentials of the various surrounding atoms as backscattering forces, it is easy to picture the interaction. As the photoelectron energy is scanned by increasing the x-ray energy irradiating the sample, the outgoing wave is backscattered by a neighboring atom. Depending on the frequency, the amplitude of the backscattered wave *at the absorber* will be at its

maximum, minimum, or somewhere in between. This interaction contributes to the transition moment of the absorber, and we observe a damped sinusoidal oscillation in the EXAFS region of the absorption spectrum. The sum of all of the interactions from all of the backscatterers is additive, and comprises the oscillation observed in the EXAFS region of the spectrum. This oscillation may be extracted and analyzed mathematically to tell us the identity, number, and distance of the backscatterers from the absorber.

The damped sine waves contributed by each of the backscatterers are defined by three observable quantities: frequency; amplitude; and phase.[3] The frequency of the wave gives information about the absorber-backscatterer distance, since the modulation of the absorbance in the EXAFS region of the spectrum is dependent on the amplitude of the backscattered wave at the absorber, which changes as the frequency is changed. So, a long absorber-backscatterer distance, which requires many periods of the sine wave to make the round trip from the absorber to the backscatterer and back to the absorber, requires a small change in frequency to go through an entire period of interference at the backscatterer. Since the frequency change is small for this process, the absorbance modulation will occur at a higher frequency compared to the same absorber-backscatterer pair in closer proximity.

The amplitude of the sine wave is determined by the identity and number of backscatterers. Heavier atoms have greater backscattering amplitudes than lighter ones. The amplitude of the resultant wave is additive. For example, 2 S

atoms equidistant from an absorber will each contribute an identical wave to the absorbance spectrum, which will have twice the amplitude of a wave contributed by a single S.

The phase shift is useful in determining the identity of the backscatterer. Different atomic species have different electron densities. The photoelectron wave is phase shifted when it encounters the electorn density of a backscatterer. The size of the phase shift depends on the atom type. It should be noted that the absorber also contributes to the phase shift, since the outgoing wave is phase-shifted as it leaves the absorber and as it returns from the backscatterer.

The EXAFS must be extracted from the absorption spectrum before it can be analyzed. EXAFS is defined as consisting only of the sinusoidal modulation of the x-ray absorption coefficient μ due to absorber-backscatterer interactions. Theoretically, the expression $\chi = \mu - \mu_0 / \mu_0$ defines the normalized EXAFS quantity, where μ_0 is the free-atom absorption coefficient. However, μ_0 is unknown and unmeasurable for any system of interest, so approximate methods must be used to isolate the EXAFS. An alternate form of the above expression, $\chi(k) = \mu - \mu_s / \mu_0$, where the parameter μ_s is defined as the "smooth" part of the absorption coefficient μ, may be used to extract the EXAFS.[5] The quantity k, called the photoelectron wave vector, is defined as $k = [(2m/h^2)(E-E_0)]^{1/2}$, where m is the mass of the electron, h is Planck's constant, E is the spectral energy, and E_0 is the energy origin at wnich $k = 0$ (k is expressed in units of $Å^{-1}$). Generally, the x-ray absorption spectra are background corrected by

extrapolation and subtraction of a function fitted to the pre-edge region of the spectrum. Depending on the concentration of the sample, this may or may not yield a true value for μ, the total absorption coefficient. In very dilute samples the extrapolation is usually only dependable near the absorption edge. However, tabulated values for the energy-dependent change in μ_0 are available, so a single value for μ determined near the absorption edge is all that is necessary for background correction and normalization.[6] The post-edge absorption spectrum is fitted with a cubic spline which approximates μ_s. Subtraction of μ_s from μ and normalization by μ_0 using the Victoreen function yields EXAFS data $\chi(k)$ normalized to a "per absorbing atom" basis.[3] Usually, $\chi(k)$ is multiplied by k^3 so that the small amplitude oscillations far above the absorption edge (farther out in k-space) can be easily visualized during analysis.

The EXAFS is analyzed by curve fitting to some functional form representing $\chi(k)$. The experimental EXAFS may be Fourier transformed from k-space (frequency, $Å^{-1}$) to R-space (distance, Å) as the first step in analysis. The Fourier transforms reveal peaks at various distances R which define the different backscattering "shells", and their approximate distances from the absorber. This information provides a good starting point for the subsequent EXAFS curve fitting analysis. Also, "Fourier filtering" may be used to simplify the EXAFS analysis by isolating different distance shells, thus allowing analysis of short and long distance interactions separately. This is effected by windowing the selected region in the transform with a function that goes smoothly to the baseline. The

windowed portion is then backtransformed, and the resultant EXAFS can be analyzed.

The EXAFS presented here was analyzed by curve-fitting with a non-linear least squares fitting algorithm[7] to the standard curved-wave functional form for single scattering EXAFS:[8]

$$\chi(k) = \sum_i \frac{N_i \gamma_i f_i(k,R_i)}{kR_i^2} e^{-2\sigma_i^2 k^2} \sin[2kR_i + \phi_i(k,R_i)]$$

where the summation is over all backscatterers at a distance R_i, with root-mean square distance deviation σ^2 and coordination number N_i. The functions $f(k,R_i)$ and $\phi(k,R_i)$ represent the distance and energy dependent curved-wave backscattering amplitude and total phase shift, respectively. The amplitude reduction factor γ accounts for inelastic effects and multielectron processes.

2.5.3 Instrumentation

The EXAFS experiments reported here were done at the National Synchrotron Light Source at Brookhaven National Laboratory. Some spectra were also recorded at the Stanford Synchrotron Radiation Laboratory. The high photon flux, plane polarization, and broad spectral range of synchrotron light make it ideal for x-ray experiments on dilute metalloproteins in solution.

Two different detection modes were employed, depending on the sample type. In the EXAFS experiments described here, various synthetic model compounds were used to check fitting procedures and to define the threshold energy shift ΔE_0 for the subsequent protein EXAFS curve fits. The model

compounds were run in transmission mode, using inert-gas ion chambers as detectors. A chamber before the sample monitored beam I_0 and one placed after the sample monitored transmitted beam, I_t. Also, a third chamber was placed behind I_t with a calibration foil (Fe or Mo) over the window, so simultaneous spectral calibrations could be performed.

Since nitrogenase is an extremely large molecule with a relatively small number of absorbers (Fe or Mo) present compared to the substituent residues of the polypeptide, scattering becomes a problem, and transmission detected EXAFS is virtually impossible. All protein spectra were recorded by fluorescence detection of the Fe K_α or Mo K_α fluorescence, respectively. Each element of a Canberra Industries 13-element Ge solid-state diode detector[9] was output to a shaping amplifier, where the sawtooth detector pulse was shaped into a gaussian form proportional to the photon energy striking the detector. The output was windowed with a single channel analyzer on the desired K_α peak. The detector position was adjusted to attain optimal count rates on all elements.

2.6 Electron Paramagnetic Resonance Spectroscopy

2.6.1 Introduction

Electron paramagnetic resonance spectroscopy, or EPR, is a useful spectroscopic technique for probing chemical species that have unpaired electrons.[10] These include free radicals, point defects in crystals, and many transition metal ions. The physical phenomenon underlying EPR is the

Zeeman effect. An electron has intrinsic spin, which can have values of +1/2 and -1/2. In the absence of an externally applied magnetic field, the energies of these two spin states are degenerate. If an external magnetic field is applied, this degeneracy is lifted, and the levels are separated in enegy, as shown in Figure 2.1. The energy separation is a function of the magnetic field

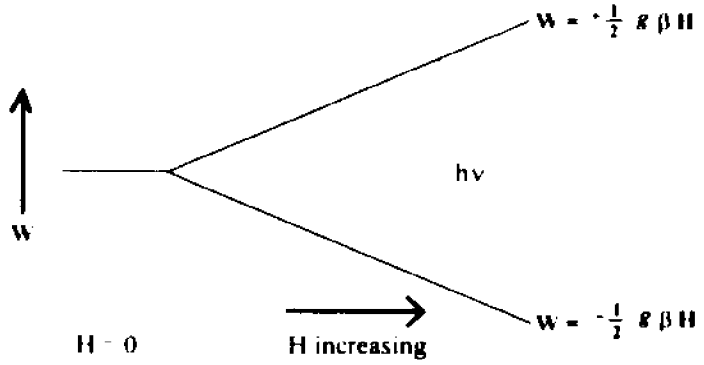

Figure 2.1. Energy splitting of degenerate spin levels by an applied magnetic field.

strength, and increases as the magnetic field is swept to higher values. A transition may be induced between the separated levels by absorption of radiation of the proper energy. This absorption may be detected, and the resulting spectrum analyzed to gain information about the electronic state of the species under investigation.

The EPR transition may be represented quantum mechanically by the spin Hamiltonian operator **H**:

$$\mathbf{H} = g\beta H\mathbf{S}_z$$

where $\mathbf{S}_z$ is the spin operator, H is the magnetic field, β is the Bohr magneton for the electron, and g is a parameter whose value depends on the relative contributions from spin and orbital angular momentum. For the free electron g = 2.0023. Operation on the the spin wave functions by **H** results in two energies for $|+1/2>$ and $|-1/2>$:

$$\mathbf{H}\,|+1/2> = +(g\beta H)1/2$$

and

$$\mathbf{H}\,|-1/2> = -(g\beta H)1/2\ ;$$

and the energy splitting between the two levels is:

$$\Delta W = g\beta H = h\nu\ ;$$

where $h\nu$ is the energy of the microwave quantum for the transition between the two states. Now we can say:

$$g = h\nu/\beta H.$$

The g-factor is the standard parameter for identification of EPR spectral inflections, and can always be calculated with the known frequency of the applied microwave radiation, the magnetic field at which an inflection occurs on the spectrum (since the field is swept, and the irradiation frequency remains constant for a given resonant cavity), and the constant β ($\beta = 9.274 \times 10^{-21}$ erg G^{-1}).

In most cases, the situation is more complex than detailed above, and a more complete Hamiltonian is needed to properly analyze EPR spectra. The system in question may show considerable anisotropy, and have 2 *g*-factors in the axial case ($g_x = g_y$, $g_z \neq g_x, g_y$) or 3 *g*-factors in the rhombic case. ($g_x \neq g_y \neq g_z$), due to different magnetization along the molecular x, y, and z axes. Nuclear hyperfine interaction may occur if a nearby nucleus has a net spin, splitting the EPR spectrum into multiple lines, given by (2nI + 1) where n is the number of identical nuclei, and I is nuclear spin quantum number. In the case of transition metal ions, spin orbit coupling and ligand field effects complicate the picture further. For single ions where symmetry can be determined, the Hamiltonian can often be simplified to achieve an analytical solution.[11] For Fe-S cluster EPR in metalloproteins where symmetry is unknown, numerical diagonalization of the spin Hamiltonian derived energy matrix is the best way to predict spectral features. EPR spectral assignments presented here were calculated with "Rhombo", kindly furnished to us by Professor W. R. Hagen.[12]

The spin Hamiltonian generally used in high-spin biological EPR consists of a crystal field or zero field splitting term and a Zeeman term as follows:

$$H = \mathbf{S} \cdot \mathbf{D}' \cdot \mathbf{S} + \beta \mathbf{B} \cdot \mathbf{g} \cdot \mathbf{S}$$

where;

$$\mathbf{S} \cdot \mathbf{D}' \cdot \mathbf{S} >>> \beta \mathbf{B} \cdot \mathbf{g} \cdot \mathbf{S}$$

in most systems of interest at X-band ($h\nu \approx 0.3$ cm^{-1}) EPR frequencies. The zero field splitting term splits an S = n/2 spin system into (n + 1)/2 Kramer's doublets.

Effectively, this results in an energy separation between the doublets much greater than the microwave quantum, so they behave as independent $|\pm 1/2>$ spin systems.

Effective *g* values are calculated with Rhombo by diagonalizing the energy matrix calculated with the Hamiltonian above rewritten as:

$$H = D[S_z^2 - S(S+1)/3] + E(S_x^2 - S_y^2) + \beta \mathbf{B} \cdot \mathbf{g} \cdot \mathbf{S}$$

where the quantities *D* and *E* are called the axial and rhombic zero-field splitting parameters, respectively. The ratio $|E/D|$ is limited to values between 0 and 1/3. Now, the effective *g*-values can be defined in terms of one parameter, the rhombicity, or $\lambda = |E/D|$. "Rhombograms" (see Chapter 5) depicting predicted *g*-values as a function of λ may be used to visualize predicted *g*-values for a given rhombicity.

2.6.2 Instrumentation

EPR spectrometers consist of three basic components: an electromagnet; a source of radiation to induce spin transitions; and a detection system to monitor the absorbance of the radiation.[13] The sample being investigated is placed in a resonant cavity between the pole faces of the electromagnet, and the magnetic field is swept. Microwave radiation from a klystron is directed down a hollow wave-guide into the resonant cavity, and sets up a standing wave in the cavity. When the splitting induced by the magnetic field matches the energy of the microwave radiation irradiating the sample, detectable absorbance may occur. EPR cavities are designed so that the

magnetic component of the microwave radiation is maximized at the sample location, and the electronic component is minimized, since the transition is a magnetic one. Modern EPR instruments usually employ phase-sensitive detection. The applied magnetic field is modulated by the application of an oscillating magnetic field from Helmholtz coils embedded in the walls of the microwave cavity. The detector only accepts absorbance signals that oscillate near this frequency (commonly 100 kHz), thus improving signal to noise ratio. The amplitude of the modulating field is an important parameter in EPR detection, since if the modulation amplitude is kept small compared to the spectral linewidth, the amplitude of the detected signal will approximate the slope of the absorption curve. If the modulation amplitude is properly adjusted, the resultant spectrum represents the true first derivative of the absorption spectrum. Since the first derivative line shape is what is actually detected, EPR spectra are normally presented in this form.

References

1. Burgess, B. K.; Jacobs, D. B.; Stiefel, E. I. *Biochim. Biophys. Acta.* **1980**, *614*, 196-209.

2. Cramer, S. P. Biochemical Applications of X-ray Absorption Spectroscopy. In *Extended X-ray Absorption Fine Structure*; Konigsberger, D., Prins, R., Eds.; Plenum: New York, 1988: pp 257-320.

3. Scott, R. A. *Meth. Enzymol.* **1985**, *117*, 414-459.

4. *X-Ray Absorption: Principles, Applications, Techniques of EXAFS, SEXAFS, and XANES*; Konigsberger, D., Prins, R., Eds.; Wiley: New York, 1988.

5. Lytle, F. W.; Sayers, D. E.; Stern, E. A. *Phys. Rev. B* **1975**, *11*, 4825.

6. *International Tables for X-Ray Crystallography*. MacGillavry, C. H., Rieck, G. D., Eds.; Kynoch Press: Birmingham; England, 1968.

7 Marquardt, D. W. *J. Soc. Ind. Appl. Math.* **1963**, *11*, 443.

8. McKale, A. G.; Knapp, G. S.; Chan, S. -K. *Phys. Rev. B* **1986**, *33*, 841-846.

9. Cramer, S. P.; Tench, O.; Yocum, M.; George, G. *N. Nucl. Inst. Meth.* **1988**, *A266*, 586-591.

10. *Electron Spin Resonance, Elementary Theory and Practical Applications*. Wertz, John E., Bolton, James R., Chapman and Hall: New York; 1986.

11. *Electron Paramagnetic Resonance of Transition Ions*. Abragam, A., Bleaney, B., Dover: New York; 1986.

12. Hagen, W. R. In *Advances in Inorganic Chemistry: Iron-Sulfur Proteins*. Sykes, A. G., Cammack, R., Eds., Academic Press: New York, 1992; Vol. 38, pp 165-222.

13. *Electron Paramagnetic Resonance, A Comprehensive Treatise on Experimental Techniques*. Poole, Charles P.; Interscience: New York; 1967.

Chapter 3 Fe K-edge EXAFS Studies of the MoFe and VFe Nitrogenase Proteins of *Azotobacter vinelandii*

3.1 Introduction

Crystallographic studies of the nitrogenase component 1 of both *Clostridium pasteurianum*,[1,2] and *Azotobacter vinelandii* [3-5] have been ongoing for a number of years. An x-ray crystal structure for the FeMo-cofactor and the P-cluster of *Azotobacter vinelandii* at 2.2 Å resolution has been published,[4] as well as a crystal structure for the entire Av1 protein.[5] The Fe EXAFS studies reported here were undertaken prior to the publication of the crystal structure of Av1 and were inspired, in part, by x-ray anomalous scattering studies of Cp1 reported by Bolin[1] and coworkers which indicated that Mo was ligated at one end of an apparently symmetrical FeMo cofactor cluster, composed of Fe and S. The P-clusters were shown to be most likely composed of pairs of sulfide/thiolate bridged Fe_4S_4 cubanes. Since the clusters appeared to be at least somewhat symmetrical and Fe is in large abundance in the component 1 nitrogenase protein, Fe K-edge EXAFS on the intact Av1 and Av1' protein seemed feasible, and possibly informative.

The crystal structures of Av1 and Cp1 are still undergoing refinement and revision, and are not yet well enough resolved to give exact interatomic distances. One of the strengths of EXAFS is its ability to give extremely accurate distance information, especially in the first coordination sphere of backscatterers, so information from EXAFS may still be relevant to the further elucidation of the metal cluster structure of Av1. Also, no crystal structure

currently exists for Av1', so EXAFS data is the best source of structural information available for the metal clusters contained in it. Analysis and comparison of Av1' EXAFS with the EXAFS of Av1, for which a cystallographic model has been proposed, follow.

EXAFS of the oxidized component 1 proteins was motivated by the fact that nitrogenase catalysis is a redox process, and it is possible that the metal clusters of nitrogenase undergo redox-induced structural changes. Titration with a small excess of thionine solution oxidizes the M-centers by 1 equivalent and the P-clusters by two equivalents.[6-9] If large structural changes occur as a result of oxidation, they may be detectable by EXAFS.

3.2 Background

Several EXAFS studies of nitrogenase had been done previous to the start of this work. Mo EXAFS studies of the MoFe protein, extracted M-centers (called FeMoco, for FeMo cofactor), and crystals of MoFe protein have yielded average Mo-(O,N), Mo-S, and Mo-Fe distances of approximately 2.1, 2.4, and 2.7 Å, respectively.[10-14] V EXAFS of Av1' has yielded similar results with V-S and V-Fe distances of approximately 2.3 and 2.75 Å, respectively.[15] The only Fe EXAFS of nitrogenase metal clusters previously attempted was of isolated cofactor (extracted M-center) of the Mo and V component 1 proteins, which yielded 2.7 Å Fe-Fe interactions and 3.7 Å Fe-Fe interactions.[16,17]

3.3 Experimental

Nitrogenase proteins were purified by methods discussed in Chapter 2. Typical specific activities were 1800-2000 nmol of C_2H_2 reduced min^{-1} mg^{-1} of Av1 and 230-280 nmol of C_2H_2 reduced min^{-1} mg^{-1} of Av1'. EXAFS samples of the as-isolated component 1 proteins were prepared by concentrating the proteins in 0.025 M Tris-HCl pH 7.4, 0.2 M NaCl, with 2 mM DTN with Minicon membrane concentrators. Thionine oxidized samples were prepared by titrating sodium dithionite-free Av1 with thionine solution in 0.025 M Tris-HCl pH 7.4 with 0.2 M NaCl. The dithionite was removed from the protein solutions by gel-filtration and methyl viologen indicator was used to check for any residual dithionite. Thionine titrated samples were also concentrated with Minicon membrane concentrators. The samples were then made ≈ 40% in glycerol to prevent ice crystal formation. The final sample concentrations ranged from ≈ 130-200 mg/ml, which is ≈ 17-26 mM in Fe and ≈ 1.1-1.7 mM in cofactor (Mo,V). Fe K-edge EXAFS samples were syringe-loaded into 2 cm x 3 mm lucite sample cuvettes with 1 mm path lengths and polypropylene windows, which were machined at LSU. EPR samples were also loaded simultaneously, for verification of oxidation state by EPR spectroscopy. Samples were examined by EPR before and after exposure to the x-ray beam. No apparent spectral changes were evident, and no significant loss of specific activity was found after beam exposure.

Data were collected on unfocused beamline X-19A at the National Synchrotron Light Source, Brookhaven National Laboratory. Slit widths were typically 2 x 20 mm. The beamline was equipped with a Si(111) double crystal monochromator, which was detuned to 50% intensity to reduce the transmission of higher harmonics. Model compounds were run in transmission mode, monitoring incident and transmitted beam intensities with nitrogen filled ion chambers. A third ion chamber was typically employed for spectral calibration, using an Fe reference foil. Spectra were calibrated to the first inflection point in the Fe foil edge jump, at 7111.2 eV. Spectra were recorded at 4-10 K with an Oxford Instruments liquid helium flow cryostat.

Protein spectra were recorded at 4-10 K in fluorescence mode, using a Canberra Industries 13-element Ge solid state diode array detector[18] windowed on the Fe K_{α} signal. Count rates of less than 35 kHz were maintained on each detector, with amplifier shaping time generally set at 0.5 μsec. Spectra were collected in the form F/I_0 vs. eV. Spectral scans spanned from 100 eV to at least 800 eV above the absorption edge. All reported spectra were recorded on at least two separate occasions with different samples, to ensure the reproducibility of spectral features. Before averaging, all spectra were superimposed to be sure that no spectral evolution had occured during data aquisition. Deglitching was done on raw spectral data only, by single point removal. The data presented here represent a total of 50, 40, 38, and 18 scans

of as-isolated Av1, thionine-oxidized Av1, as-isolated Av1', and thionine-oxidized Av1', respectively.

The EXAFS was extracted from the x-ray spectra by standard methods, as discussed in Chapter 2. The photoelectron wave vector $k = [(2m/h^2)(E - E_0)]^{1/2}$ was defined with an initial E_0 of 7130 eV. The spectra were Fourier filtered by Fourier transforming from *k*-space to R-space, and then backtransforming selected regions to *k*-space. The selected regions were then fitted using a Levenberg-Marquardt[19] non-linear least squares curve-fitting algorithm to the curved-wave, single scattering functional form[20] of the EXAFS equation:

$$\chi(k) = \sum_i \frac{N_i \gamma_i f_i(k,R_i)}{kR_i^2} e^{-2\sigma_i^2 k^2} \sin[2kR_i + \phi_i(k,R_i)]$$

where the summation is over all backscatterers at a distance R_i, with root-mean square distance deviation σ^2 and coordination number N_i. The functions $f(k,R_i))$ and $\phi(k,R_i)$ represent the distance and energy dependent curved-wave backscattering amplitude and total phase shift, respectively. The amplitude reduction factor, γ, was held fixed at 0.9 during all fits.

3.4 Results

EXAFS spectroscopy and analysis of a species containing multiple absorbers (30 Fe in Av1) with several possible site symmetries can be a daunting task. Before attempting analysis of the nitrogenase proteins, model compounds were used in an attempt to check the fitting procedures, and to

calibrate ΔE_0 for the different absorber-backscatterer pairs. This is especially important when considering long absorber-backscatterer distances, where the probability of multiple scattering contributions increases dramatically.[21] An $[Fe_6S_6Cl_6]^{3-}$ sulfido-bridged prismane (Figure 3.1) synthesized in the laboratory of Professor Dimitri Coucouvanis was used for this purpose.[22,23]

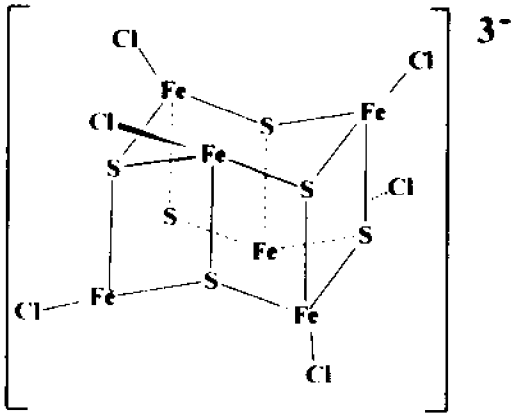

Figure 3.1. The $[Fe_6S_6Cl_6]^{3-}$ prismane model compound.

Since a crystal structure is available for the prismane cluster, the fitting procedure was relatively straightforward. The 1-3 Å and the 3-5 Å region of the EXAFS Fourier transform were backtransformed separately for fitting. The coordination number N_i was held fixed, and the distance R_i, the mean square deviation σ^2, and the threshold energy shift ΔE_0 were used as fitting parameters. All fitting was done within the single-scattering formalism. An EXAFS Fourier transform of the $[Fe_6S_6Cl_6]^{3-}$ prismane is shown in Figure 3.2, and curve-fitting results are presented in Table 3.1, along with results from the nitrogenase fits. Figure 3.2 also shows EXAFS Fourier transforms of Av1 and

Av1' along with the transform of the $[Fe_6S_6Cl_6]^{3-}$ cluster showing similar, but not identical, radial distance distributions.

Interpretation of of the $[Fe_6S_6Cl_6]^{3-}$ EXAFS is straightforward. The large peak at ~ 2.3 Å may be modeled as the sum of the first shell Fe-Cl and Fe-S interactions at 2.22 Å and 2.28 Å, respectively, which are both within 0.01 Å of the cyrstallographically determined value.[22,23] The peak at 2.76 Å can be assigned to a pair of di-μ-sulfido bridged Fe-Fe interactions. A pair of long single sulfur bridged Fe-Fe interactions model the peak at 3.8 Å. A small peak at 4.4 Å and a shoulder at 4.7 Å can be fitted with three cross-cluster Fe-S interactions and a single cross-cluster Fe-Fe interaction, respectively. The assignment of the 4.7 Å Fe-Fe interaction is suspect, since the shoulder is barely detectable. The distances determined by curve-fitting were extremely close to the crystallographic values determined for this compound, with the greatest discrepancies (0.03 Å) appearing in the long-distance (3-5 Å) fits, probably indicating small contributions from multiple scattering for this compound.

Two model compounds with suspected multiple scattering ligands were also analyzed. A phenolate substituted prismane,[22,23] $[Fe_6S_6(OC_6H_4\text{-}p\text{-}Me)_6]^{3-}$, and a formate bridged Fe dimer,[24] $Fe_2(O_2CH)_4(BIPhMe)_2$, both showed significant discrepancies between the crystallographically determined distances

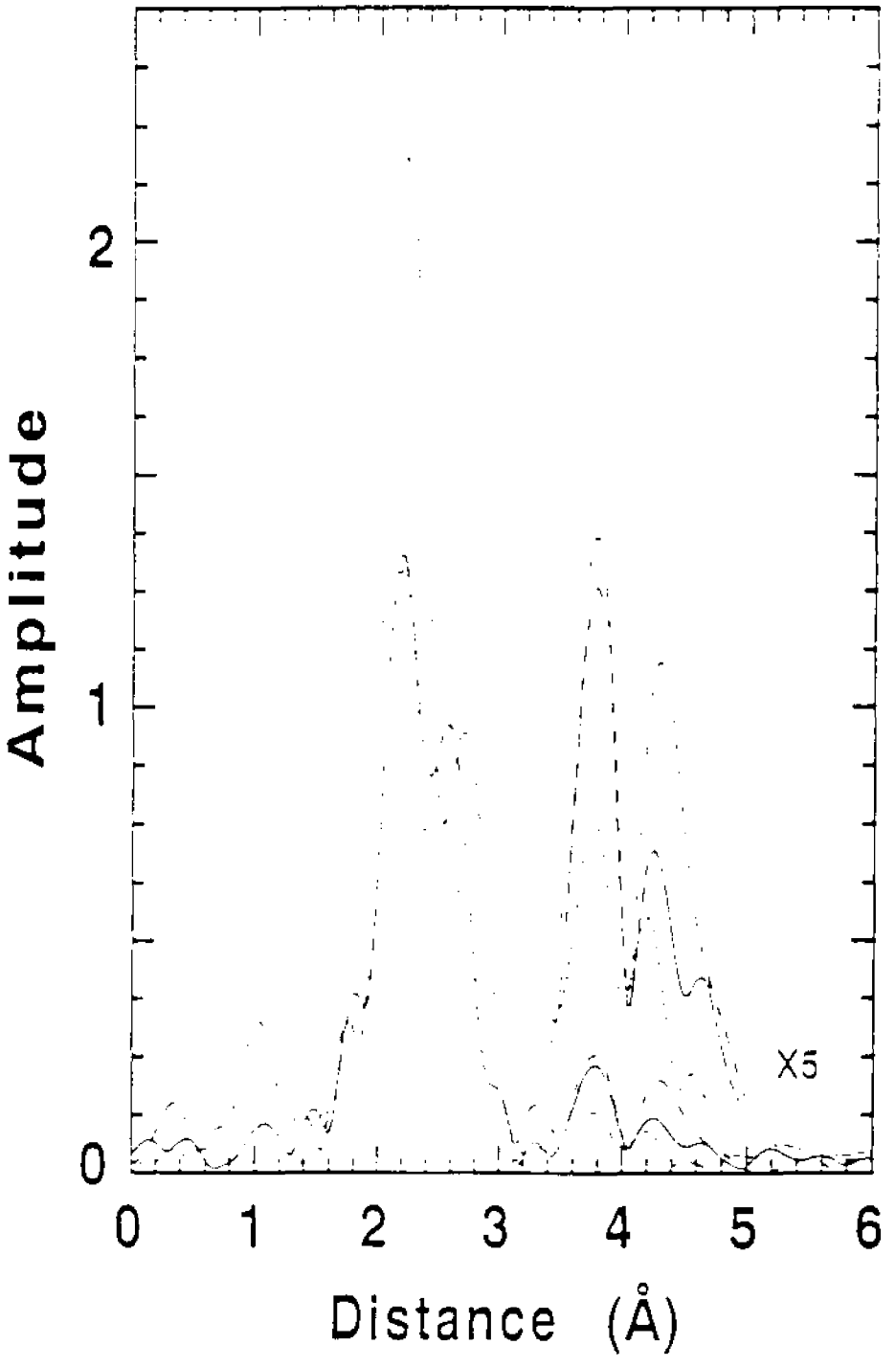

Figure 3.2. Fe EXAFS Fourier transforms of the $[Fe_6S_6Cl_6]^{3-}$ prismane (dashed), as-isolated Av1 (solid), and as-isolated Av1' (short dash)

Table 3.1 EXAFS curve-fitting parameters for the 1-3 Å (top) and 3-5 Å (bottom) regions. [a]Coordination number, held fixed during refinement, unless *, optimized by curve fitting. [b]Interatomic distance. [c]Mean-square deviation of R. ΔE_0 was optimized in prismane fits and held constant for protein fits. [d]Interactions not resolvable.

	Fe-S(Cl) ΔE_0 = -3 eV			Fe-Fe ΔE_0 = -8 eV			Fe-Mo ΔE_0 = -6 eV			Fe-O ΔE_0 = -12 eV		
sample	N[a]	R[b], Å	$10^5\sigma^2$, Å^{2c}	N[a]	R[b], Å	$10^5\sigma^2$, Å^{2c}	N[a]	R[b], Å	$10^5\sigma^2$, Å^{2c}	N[a]	R[b], Å	$10^5\sigma^2$, Å^{2c}
$(Fe_6S_6Cl_6)^{3-}$	4.0	2.277	304	2.0	2.757	355						
As-isolated Av1	3.5	2.317	576	2.0	2.641	535	0.3	2.732	179	5	1.842	7797
Thionine-oxidized Av1	3.5	2.291	513	2.0	2.657	465	0.3	2.696	34	5	1.833	7797
As-isolated Av1'	3.5	2.322	608	2.3	2.674	773				5	1.864	7041
Thionine-oxidized Av1'	3.5	2.289	542	2.3	2.690	688				5	1.869	7041

	Fe-Fe ΔE_0 = -10 eV			Fe-Fe(X) ΔE_0 = -10 eV			Fe-S ΔE_0 = -16eV			Fe-Fe ΔE_0 = -13 eV		
sample	N[a]	R[b], Å	$10^5\sigma^2$, Å^{2c}	N[a]	R[b], Å	$10^5\sigma^2$, Å^{2c}	N[a]	R[b], Å	$10^5\sigma^{2c}$, Å^2	N[a]	R[b], Å	$10^5\sigma^{2c}$, Å^2
$(Fe_6S_6Cl_6)^{3-}$	2.0	3.82	613				3.0	4.41	386	1.0	4.68	487
As-isolated Av1	1.4*	3.78	613	1.6*	4.00	487	2.2*	4.28	386	0.4*	4.68	487
Thionine-oxidized Av1	1.4*	3.74	613	0.7*	3.99	487	*d*			*d*		
As-isolated Av1'	1.0*	3.76	613	0.8*	3.99	487	0.8*	4.30	386	*d*		
Thionine-oxidized Av1'	0.8*	3.76	613	0.5*	4.02	487	0.5*	4.38	386	*d*		

and those determined by EXAFS curve-fitting, especially for the long-distance interactions. The long Fe-Fe interaction at ~ 3.8 Å in the prismane was fitted at 3.90 Å, a 0.06 Å deviation from the 3.836 Å distance from the crystal structure. A long Fe-S interaction modeled by curve fitting at 4.42 Å also deviated from the crystallographic value of 4.455 Å. Presumably, this error arises from interference and/or multiple scattering pathways involving phenolate carbon shells at 3.5 and 4.2 Å. A 0.02 Å error in the short Fe-Fe at ~ 2.8 Å was also observed and is probably due to phenolate carbons at 2.95 Å. The EXAFS analysis of the formate-bridged dimer also shows significant deviation from the crystallographic distances, especially in the 3.574 Å Fe-Fe distance, which was determined by EXAFS fits to be 3.519 Å. Still, even with these discrepancies, the greatest error found between crystallographic and EXAFS distances was ~ 0.06 Å, even where multiple scattering and interference from outer shell light atoms were a factor.

EXAFS of as-isolated Av1 was Fourier filtered and the 1-3 Å and 3-5 Å regions were fitted separately. Figure 3.3 (left, top) shows the raw data and the root mean square deviation (error bars) between 3 EXAFS data sets. The middle panel shows the Fourier filtered EXAFS in the 1-3 Å range, along with the curve fit. The bottom panel show the filtered data and fit for the 3-5 Å region. The long distance interactions (3-5 Å) result in very small peaks, so the root mean square deviations of three data sets were transformed separately and then averaged to assess the noise level, as shown in Figure 3.3 (right, top).

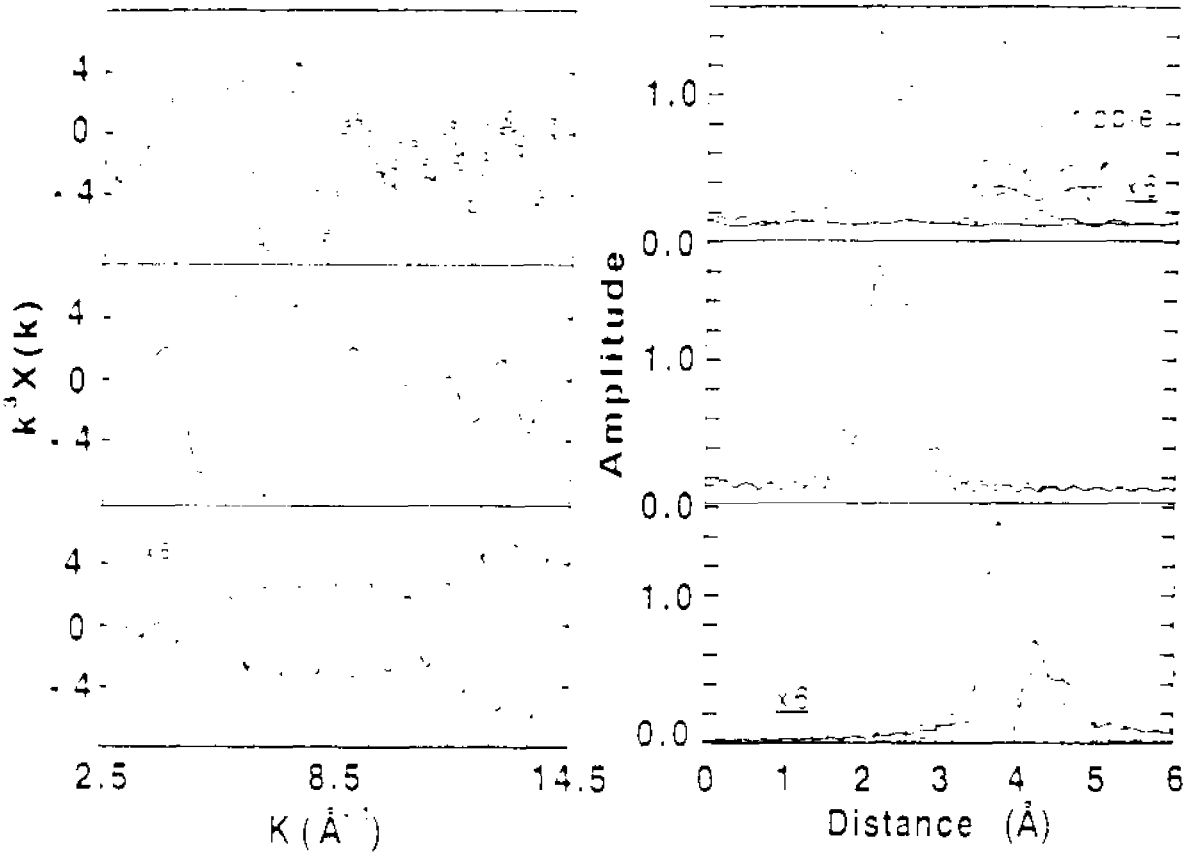

Figure 3.3 Fourier filtering of as-isolated Av1 Fe EXAFS. Left: (top) Raw data and error bars; (middle) filtered data (solid) and fit (dashed) for the 1-3 Å region, (bottom) filtered data (solid) and fit (dashed) for the 3-5 Å region. Right: Fourier transforms of data on left. Data is solid, fits are dashed (top) Fourier transform with noise and truncation ripple, (middle) data and fit for 1-3 Å region, (bottom) data and fit for 3-5 Å region with (long dash) and without (short dash) the 4 Å Fe-X interaction

Also, the Fourier transform truncation ripple level was estimated by Fourier filtering and backtransforming the 1-3 Å region, and then retransforming the data from 0 to 6 Å. It is apparent that the peaks, although small in amplitude, are above the noise and Fourier transform ripple level. Figure 3.3 right middle and bottom show the Fourier transform and fit in the 1-3 Å and 3-5 Å region, respectively. The ΔE_0 parameters used in the protein fits were those determined for the $[Fe_6S_8Cl_6]^{3-}$ prismane at analogous distances.

The Fourier transform of the 1-3 Å region shows two major peaks, which can be modeled with Fe-S and Fe-Fe interactions at 2.32 Å and 2.64 Å, respectively. Using coordination numbers of 3.5 and 2 for these components and optimizing σ^2 results in a reasonable fit (Table 1). Of course, other fits are possible. Locking σ^2 to the value found in the prismane fit results in coordination numbers of 2.3 and 1.9 for the Fe-S and Fe-Fe interactions, respectively, but the resultant fit is not as good. Coordination number (N) and σ^2 are highly correlated parameters and should not, in general, be fitted simultaneously. The necessity to "lock" one of these parameters naturally limits the precision of the EXAFS analysis.[25] "Goodness of fit" in all of these analyses is defined by the magnitude of the fit residual; $R = (\sum_i (\chi'_{exp} - \chi'_{calc})^2 k^6) / N$, where k is the photoelectron wave vector, χ'_{exp} is the observed EXAFS, χ'_{calc} is the calculated EXAFS, and N is the number of data points. The smaller the value for R, the better the fit. Further improvement of the fit is afforded by the inclusion of an Fe-Mo interaction at 2.73 Å, with N = .3. A similar distance

(2.68-2.72 Å) has been reported for fits of Mo EXAFS of Av1 for a Mo-Fe absorber-backscatterer pair.[11,12] Also, Fe EXAFS of the isolated FeMo cofactor has yielded a 2.70 Å distance for an Fe-Mo interaction.[16] Inclusion of an Fe-O interaction at 1.84 Å results in a slightly improved fit. This interaction may be real or a result of systematic errors in the fitting functions.[26] It is possible that some Fe-(O,N) ligands exist in nitrogenase, or some undefined interaction between the metal clusters and H_2O is occuring. The crystal structure depicts a serine in each β subunit that could be ligated to a P-cluster Fe.[3-5] Also, R-homocitrate has been shown to co-extract with the FeMo-cofactor, and it has been modeled in the crystal structure ligated to Mo. One or more of the substituent groups of homocitrate may be in the vicinity of cofactor Fe. In any event, inclusion of this Fe-O interaction gives the best fit to the experimental data, but no meaningful structural interpretation can be drawn from it.

The 3-5 Å region shows a dominant peak at 3.78 Å, which is fit with an Fe-Fe interaction, with N = 1.4. Fits of the long interactions were effected by locking the σ^2 to the values determined for the analogous interactions in the prismane model. Transform features apparent at 4.3 Å and 4.7 Å were tentatively identified as Fe-S and Fe-Fe distances for curve fitting, by examination of the prismane radial distribution. The 4.3 Å feature was assigned to an Fe-S interaction, after eliminating the possibility of other Fe-X interactions, by determining which backscatter-absorber pair resulted in the

smallest difference between the calculated and experimental EXAFS. Similarly, the 4.7 Å distance was assigned to an Fe-Fe interaction.

The backscattering interactions between Fe-Fe (3.8 Å), Fe-S (4.3 Å), and Fe-Fe (4.7 Å) yield a less than perfect fit to the experimental data, as is clearly apparent in Figure 3.3 (right, bottom). However, the fit shows 3 components at radial distances very close to those of the experimental data. Addition of another Fe-Fe interaction at 4.0 Å improves the fit, as does an Fe-S at 3.9 Å. So, the experimental EXAFS may have a contribution from these Fe-Fe and Fe-S interactions or some mix of the two. This is not surprising, since Fe-S distances in the 3.85-3.91 Å range have been reported for cross-cube distances in synthetic Fe-S cubanes[27] and and an average 3.9 Å distance has been observed in a 4Fe-4S protein.[28]

The radial distribution of distances in thionine oxidized Av1 is very similar to that of as-isolated Av1, as shown in Figure 3.4. However, there is a marked variation in the EXAFS Fourier transform amplitudes between the two forms. Curve fitting of the experimental EXAFS data in the 1-3 Å region (Figure 3.5 left, top) yields Fe-S and Fe-Mo distances that have contracted slightly, from 2.32 → 2.29 Å, and 2.73 → 2.70 Å, respectively. The Fe-Fe distance at 2.64 Å expands somewhat, to 2.66 Å. It should be noted that these changes are at or near the generally accepted resolution of EXAFS analysis, which is 0.02 Å for

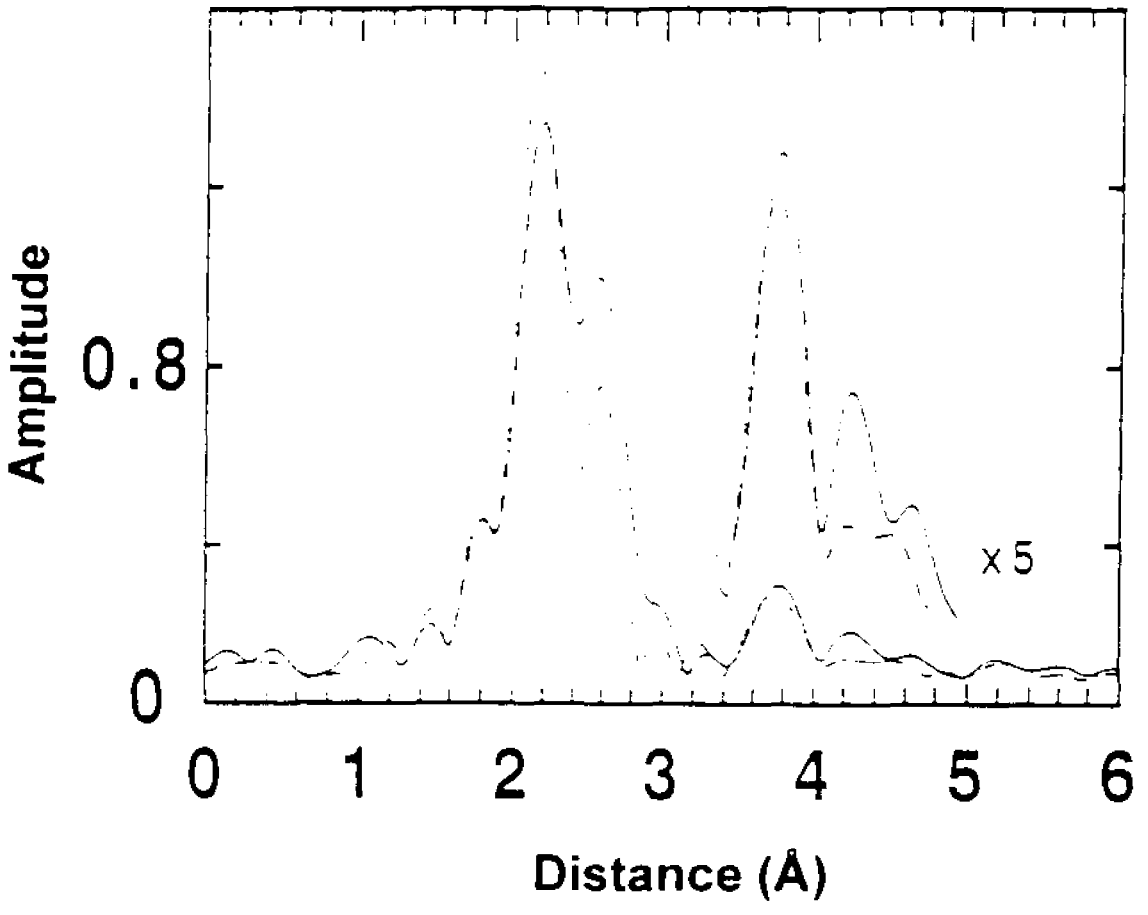

Figure 3.4 Fourier transform of as-isolated vs thionine oxidized Av1 (solid) as-isolated, (dashed) thionine oxidized

well behaved systems. The important result here may well be that the changes in absorber-backscatterer distances are very small upon oxidation, showing no detectable evidence of major metal cluster rearrangement. In an attempt to model the amplitude change in the Fe-S and Fe-Fe peaks, the EXAFS was fit by fixing the coordination numbers to the values for the as-isolated protein, which resulted in σ^2 that were similar for both the as-isolated and the thionine oxidized Av1. If the coordination numbers were allowed to float and the σ^2 was held fixed, the coordination numbers changed from 3.5 → 3.7 and from 2.0 → 1.7 for the Fe-S and Fe-Fe interaction, respectively, as the protein state went from as-isloated → oxidized. These are small changes in coordination number, and are probably not significant. Of all of the EXAFS fitting parameters, coordination number has been shown empirically to be the least dependable, probably due to deficiencies in theoretical backscattering amplitude functions.[20] The changes in the Fourier transform amplitudes are probably due to small changes in interference between overlapping shells upon oxidation.

The 3-5 Å Fourier transform of the thionine oxidized Av1 EXAFS is dominated by a large peak, as can be seen in Figure 3.5 (right, top), which is fit at 3.74 Å. This is a contraction compared to the as-isolated Av1 data which was fit at 3.78 Å. EXAFS distances often become less precise as the fit is extended to outer-shell components due to an increase in possible interference from other components and multiple scattering pathways. These data were

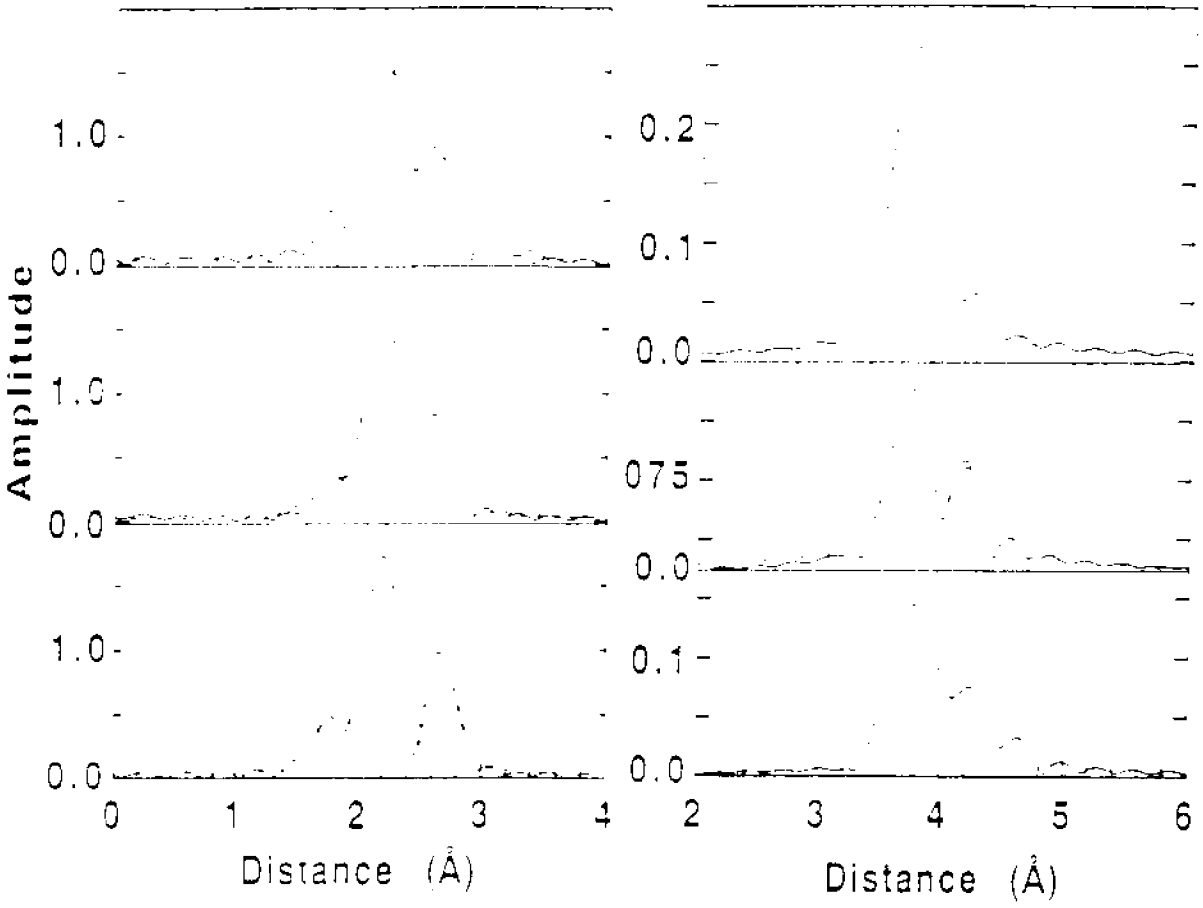

Figure 3.5 Fourier transforms of data (solid) and fits (dashed) for the 1-3 Å region (left) and the 3-5 Å region (right) for (top), thionine oxidized Av1, (middle), as-isolated Av1 (bottom), thionine oxidized Av1

fitted within the single-scattering formalism, so it should be stressed that small changes in long distances cannot be construed as precise. The interactions at 4.3 Å and 4.7 Å are not resolvable in this data, and no fits are reported for them.

Av1' (the V-Fe nitrogenase component 1) exhibits EXAFS that is very similar to that recorded for Av1. The fits for the short Fe-S and the short Fe-Fe are within 0.01 Å and 0.03 Å of the respective distances determined in the Av1 fits (Table 1; Figure 3.5 left, middle). The Fe-Mo distance at 2.7 Å is not needed for the Av1' fit, as expected. The short Fe-Fe interaction is fit at 2.67 Å with a coordination number of 2.3, as opposed to 2.0 for the corresponding 2.64 Å distance in Av1. This is because the expected Fe-V distance at ~2.7 Å cannot truly be resolved, since Fe and V have very similar backscattering phase and amplitude functions, as is the case with elements in close proximity on a row of the Periodic Table. Addition of an Fe-V component at 2.70 Å does result in a slightly improved fit. In any event, the presence of V in Av1' has been demonstrated spectroscopically, and the backscattering contributions from the Fe-V interactions are presumably included in the fits of the Fe-Fe interactions at 2.67 Å. This supposition is strengthened by the observation of slightly longer Fe-Fe fit distances in both as-isolated and oxidized Av1' than in Av1 for the ~2.6-2.7 Å coordination shell. As is the case in Av1, a non-specifically assignable Fe-O interaction also improves the fit.

The 3-5 Å region Fourier transform of the as-isolated Av1' EXAFS (Figure 3.5 right, middle) is dominated by an Fe-Fe interaction at 3.76 Å, similar to the 3.78 Å distance in Av1. There is also an obvious peak at ~ 4.3 Å which was fit to an Fe-S interaction at 4.30 Å. Again, an additional Fe-Fe interaction at 3.99 Å is necessary to achieve a good fit, as was the case in Av1 (above) The signal to noise ratio of the data was not large enough to do reliable fits of the long Fe-Fe shell at ~4.7 Å which was observed in as-isolated Av1.

The long distance fits (3-5 Å) show smaller optimized coordination numbers for Av1' than for Av1 in every shell. This may be due to differing interference effects between the shells, rather than dramatic structural differences between Av1' and Av1. The long distance fits for both Av1 and Av1' were effected by fixing σ^2 and allowing the coordination number to float. Fixing the coordination number and floating σ^2 results in a larger σ^2 for Av1' than for Av1 in each backscattering shell. Examination of the optimized fit values in the 1-3 Å range (Table 1) reveals larger σ^2 for Av1' than for Av1 in the short Fe-S and Fe-Fe shells also. These two shells were fitted by fixing the coordination number and allowing σ^2 to float. The correlation between σ^2 and N makes it impossible to interpret the data more exactly. Also, as was stated above, coordination numbers are the least reliable of the EXAFS fitting parameters and deviations like these in multi-absorber species are not unexpected, especially in the case of long-distance interactions.

Thionine oxidation of Av1' results in EXAFS-determined distance shifts similar to those observed in Av1 (Figure 3.5 bottom, left and right). The average Fe-S distance of 2.32 Å in as-isolated Av1' contracts to 2.29 Å upon oxidation. The short Fe-Fe interaction expands slightly from 2.67 → 2.69 Å with oxidation. The long Fe-Fe interaction remains the same, at 3.76 Å. There is a dramatic change in the long Fe-S interaction at 4.30 Å, which shifts to 4.38 Å in the oxidized data fits, although no corroboration of this interaction is available from the Av1 data (see above). Absorber-backscatterer distances greater than 4 Å in a multicenter cluster may have some contribution from multiple scattering pathways, which can effect both distance and amplitude determinations in the curve-fitting process. Therefore, large distance changes in long range interactions are best interpreted cautiously. It appears, within the limitations of the single-scattering formalism, that the distance does increase to some extent upon oxidation of Av1'.

Again, as is the case in Av1, thionine oxidation results in amplitude changes in the Fourier transform of oxidized Av1' (Figure 3.6). These may be rationalized similarly (see above) as those observed for oxidized Av1. It is very probable that some small structural change is occuring upon oxidation, but the amplitude changes observed are not consistent with any major structural change or significant rearrangement.

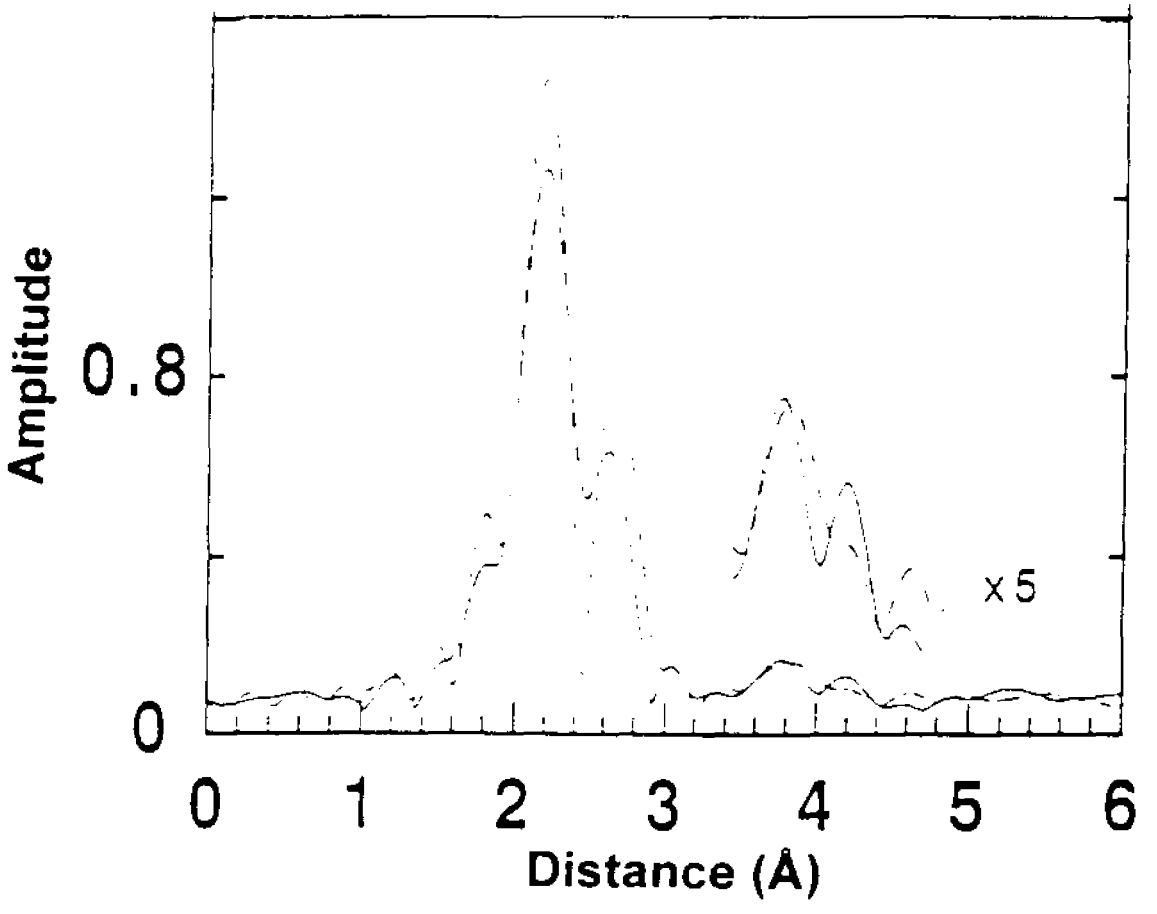

Figure 3.6 Fe EXAFS Fourier transform of as-isolated (solid) vs thionine oxidized (dashed) Av1

3.5 Discussion

The nitrogenase component 1 proteins contain 30 Fe atoms in two different pairs of clusters, the M-centers and the P-clusters. This could mean that there are 15 unique Fe sites, 7 in the M-center and 8 in the P-cluster. Also, the Reese crystallographic model shows that the M-center is only ligated at the ends, through Mo to histidine at one end, and through Fe to cysteine on the other end.[3-5] This loose ligation could result in a fairly flexible cofactor structure and a wide distribution of distances. The P-clusters are ligated through each Fe to a cysteine, but are located in the $\alpha\beta$ subunit interface, where significant structural distortion could occur. However, the EXAFS analysis resulted in generally reasonable coordination numbers and acceptable deviations in average distance determinations. Since EXAFS analysis yields average distances and approximate coordination numbers, it is impossible to make absolute distance assignments within the cofactor cluster or the P-cluster. However, assuming a symmetrical structure (a three fold rotation axis through the Mo and the opposite end Fe) whose major contribution to the EXAFS arises from Fe-Fe, Fe-S and Fe-Mo interactions, plausible cofactor distance assignments can be made, which are shown in Figure 3.7. The bridged double-cubane P-clusters probably contribute mainly short distances to the EXAFS, except for cross-cubane Fe-S interactions at approximately 3.9 Å.

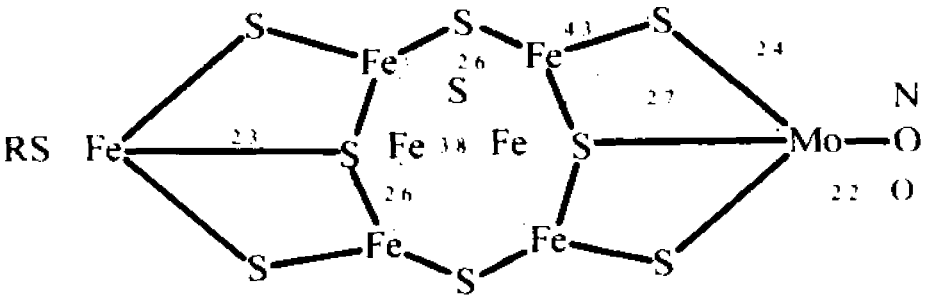

Figure 3.7 Distance assignments in Å for the FeMo cofactor derived from Fe EXAFS. Mo-O and Mo-S distances from other EXAFS studies are included (see text)

The 4.3 Å Fe-S distance has not been observed before in nitrogenase EXAFS. The $[Fe_6S_6Cl_6]^{3-}$ prismane EXAFS analysis includes an Fe-S interaction at 4.41 Å, which is within 0.03 Å of the distance determined by crystallography.[22,23] The fact that the 4.3 Å Fe-S distance is observable by EXAFS in Av1 may be significant. EXAFS is very sensitive to variations in absorber-backscatterer distances. If, in fact, there is large disorder in the cofactor cluster, it is doubtful that such a long cross-cluster interaction would be observable. The observation of this long distance interaction supports the proposal that the cofactor does have significant symmetry.

Oxidation of the metal clusters of Av1 and Av1' resulted in very small distance changes. A slight contraction of the 2.3 Å Fe-S distance was observed for both Av1 and Av1', along with a slight expansion of the 2.7 Å Fe-Fe distance in both proteins. This behavior would argue that no *major* structural rearrangement takes place upon chemical oxidation, since these

short distances actually define the structural core of both metal clusters. The long distance changes observed are also consistent with this proposal, since the greatest change observed was the 4.30 → 4.38 Å Fe-S distance in Av1'.

There is striking similarity between the EXAFS of as-isolated and thionine oxidized Av1 and Av1'. Since there is no crystallographic data available for Av1', the EXAFS results are the most definitive structural data available for it. Although EXAFS cannot determine three-dimensional structure, the similarity of the Av1 and Av1' EXAFS, amino acid sequence homology[29] between Av1 and Av1', recently reported Mössbauer spectroscopy studies,[30] and metal analysis of both proteins certainly make a strong case for very similar metal cluster structure between the two variants.

References

1. Bolin, J. T.; Ronco, A. E.; Mortenson, L. E.; Morgan, T. V.; Williamson, M.; Xuaong, N.-H. In *Nitrogen Fixation: Achievements and Objectives*; Gresshoff, P. M., Roth, L. E., Stacey, G., Newton, W. E., Eds.; Chapman and Hall: New York, 1990; pp 117-124.

2. Kim, J.; Woo, D.; Rees, D. C.; *Biochemistry* **1993**, *32*, 7104-7115.

3. Kim, J.; Ress, D. C. *Science* **1992**, *257*, 1677-1682.

4. Chan, M. K.; Kim, J.; Rees, D. C. *Science* **1993**, *260*, 792-794.

5. Kim, J.; Rees, D. C. *Nature* **1992**, *360*, 553-560.

6. Zimmermann, R.; Münck, E.; Brill, W. J.; Shah, V. K.; Henzl, M. T.; Rawlings, J.; Orme-Johnson, W. H. *Biochim. Biophys. Acta.* **1978**, *536*, 185-207.

7. Hagen, W. R. In *Advances in Inorganic Chemistry: Iron-Sulfur Proteins*; A. G. Sykes and R. Cammack, Ed.; Academic Pres: 1992; Vol. 38; pp 165-222.

8. Surerus, K. K.; Hendrich, M. P.; Christie, P. D.; Rottgardt, D.; Orme-Johnson, W. H.; Münck, E. *J. Am. Chem. Soc.* **1992**, *114*, 8579-8590.

9. Pierik, A., J.; Wassink, H.; Haaker, H.; Hagen, W. R. *Eur. J. Biochem.* **1993**, *212*, 51-61.

10. Cramer, S. P. Biochemical Applications of X-ray Absorption Spectroscopy. In *Extended X-ray Absorption Fine Structure*; D. Konigsberger and R. Prins, Eds.; Plenum: New York, 1988; pp 257-320.

11. Cramer, S. P.; Hodgson, K. O.; Gillum, W. O.; Mortenson, L. E. *J. Am. Chem. Soc.* **1978**, *100*, 3398-3407.

12. Cramer, S. P.; Gillum, W. O.; Hodgson, K. O.; Mortenson, L. E.; Stiefel, E. I.; Chisnell, J. R.; Brill, W. J.; Shah, V. K. *J. Am. Chem. Soc.* **1978**, *100*, 3814.

13. Conradson, S. D.; Burgess, B. K.; Newton, W. E.; Mortenson, L. E.; Hodgson, K. O. *J. Am. Chem. Soc.* **1987**, *109* 7507.

14. Flank, A. M.; Weininger, M.; Mortenson, L. E.; Cramer, S. P. *J. Am. Chem. Soc.* **1986**, *108*, 1049-1055.

15. George, G. N.; Coyle, C. L.; Hales, B. J.; Cramer, S. P. *J Am. Chem. Soc.* **1988**, *110*, 4057-4059.

16. Arber, J. M.; Flood, A. C.; Garner, C. D.; Gormal, C. A.; Hasnain, S. S.; Smith, B. E. *Biochem. J.* **1988**, *252*, 421-425.

17. Harvey, I.; Arber, J. M.; Eady, R. R.; Smith, B. E.; Garner, C. D.; Hasnain, S. S. *Biochem. J.* **1990**, *266*, 929-931.

18. Cramer, S. P.; Tench, O.; Yocum, M.; George, G. *N. Nucl. Inst. Meth.* **1988**, *A266*, 586-591.

19. Marquardt, D. W. *J. Soc. Ind. Appl. Math.* **1963**, *11*, 443.

20. McKale, A. G.; Knapp, G. S.; Chan, S. -K. *Phys. Rev. B* **1986**, *33*, 841-846.

21. *X-Ray Absorption: Principles, Applications, Techniques of EXAFS, SEXAFS, and XANES*; Prins, R.; Konigsberger, D., Eds.; Wiley: New York, 1988.

22. Coucouvanis, D.; Kanatzidis, M. G.; Dunham, W. R.; Hagen, W. R. *J. Am. Chem. Soc.* **1984**, *106*, 7998-7999.

23. Al-Ahmad, S. A.; Salifoglou, A.; Kanatzidis, M. G.; Dunham, W. R.; Coucouvanis, D. *Inorg. Chem.* **1990**, *29*, 927.

24. Tolman, W. B.; Liu, S.; Bentsen, J. G.; Lippard, S. J. *J. Am. Chem. Soc.* **1991**, *113*, 152-164.

25. Cramer, S. P.; Hodgson, K. O.; Stiefel, E. I.; Newton, W. O. *J. Am. Chem. Soc.* **1978**, *100*, 2748-2760.

26. Professor S. P. Cramer, personal communication.

27. Christou, G.; Mascharak, P. K.; Armstrong, W. H.; Papaefthymiou, G. C.; Frankel, R. B.; Holm, R. H. *J. Am. Chem. Soc.* **1982**, *104*, 2820-2831.

28. Adman, E. T.; Sieker, L. C.; Jensen, L. H. *J. Bio. Chem.*, **1973**, *218*, 3987-3996.

29. Bishop, P. E.; Joerger, R. D.; Loveless, T. M.; Pau, R. N.; Michenall, L. A.; Simon, B. H. **1990** *J. Bacteriol. 172*, 3400-3408.

30. Ravi, N.; Moore, V.; Lloyd, S.; Hales, B. J.; & Huynh, B. H. **1994** *J. Biol. Chem. 269*, 20920-20924.

Chapter 4 Fe and Mo EXAFS of *Azotobacter vinelandii* MoFe Protein in Various Oxidation States.

4.1 Introduction

Hopefully, the EXAFS studies discussed in the previous chapter will be of some help in refining the structural model for the metal clusters of nitrogenase. Since EXAFS is well-suited to the determination of short distances and examination of the proposed M-center and P-cluster models reveal many such interactions, the technique may yet yield some interesting and possibly useful information concerning structural changes in the metal cluster(s) induced by different redox states. The analysis presented in the previous chapter revealed small but consistent changes in EXAFS determined distances upon chemical oxidation of the nitrogenase component 1 proteins. What follows is a systematic Fe K-edge and Mo K-edge EXAFS analysis of the MoFe nitogenase (Av1) in four spectroscopically definable redox states.

Mo K-edge and Fe K-edge EXAFS studies of MoFe protein solutions,[1] crystals,[2] and extracted FeMo-cofactor[3] have yielded several interatomic distances and coordination numbers for various absorber-backscatterer pairs. Mo-O(N), Mo-S, Mo-Fe, and Mo-Fe' interactions have been assigned at ~2.1, 2.4, 2.7, and 3.7 Å , respectively. Also, a very long Mo-Fe interaction at ~5.1 Å has been modeled in both solutions and crystals of Av1.[2] Fe EXAFS of intact nitrogenase has yielded average distances for Fe-S, Fe-Fe, and Fe-Mo interactions of ~2.3, 2.6, and 2.7 Å. Fe EXAFS analysis of intact nitrogenase

is complicated by the fact that 30 Fe in 2 types of clusters are present in each molecule, so EXAFS determined distances are averages of P-cluster and M-center interactions. The P-clusters undoubtedly make a significant contribution to the EXAFS in the short distance ranges. Figure 4.1 shows models of the clusters with plausible distance assignments from Mo and Fe EXAFS.

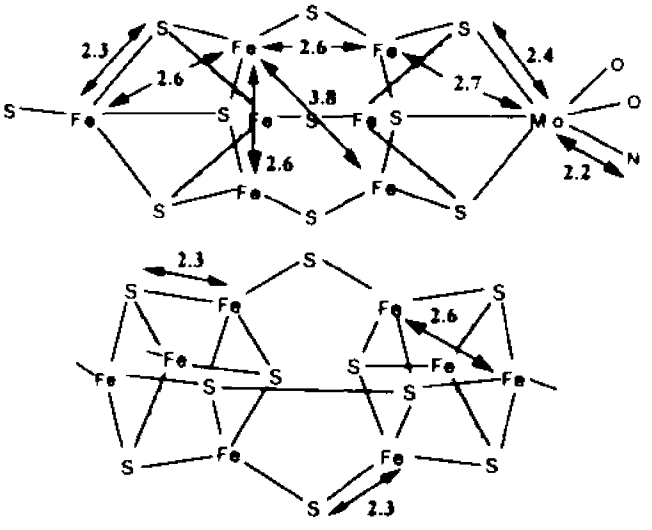

Figure 4.1 Interatomic distances from Mo and Fe EXAFS assigned to the M-center (top), and the P-cluster (bottom).

Now that the crystallographic models are undergoing rapid refinement for the "resting" enzyme, active research can turn toward mechanistic studies from an informed perspective. There has been no EXAFS reported for nitrogenase that has had electrons put into it during catalytic turnover. According to the Thorneley-Lowe[4,5] kinetic scheme, component 1 assumes various E_n states, from E_0 (resting enzyme) to E_7 during dinitrogen reduction. Unfortunately, no one has reported any spectral characterizations of the various

proposed states above E_1. It has been shown that low electron flux steady-state enzymatic turnover of component 1 and component 2 with H^+ as the only substrate present will result in the reduction of the S = 3/2 FeMoco EPR signal by 50%.[4] This has been attributed to the initial reduction of component 1 to E_1 by the transfer of a single electron from component 2. The rate limiting step in the Thorneley-Lowe scheme is the dissociation of component 2 from component 1. The association-dissociation cycle is slow, with a rate of 6.4 s^{-1}. Once component 1 has been reduced by a second electron to E_2, H_2 is evolved rapidly and component 1 relaxes back to E_0. Thus, in a low electron flux steady state turnover mixture E_2 relaxes to E_0 before it can be reduced again to form E_3, so effectively the only states present at any given time are E_0 and E_1. E_1 is EPR silent, so the spectral amplitude is reduced by 50% compared to a control with the same amount of "resting" Av1 present. The electron flux is controlled by limiting the amount of Av2 present in the reaction mixture. Studies of Av1 in reduced states are important, since it has been proposed by Thorneley and Lowe that N_2 does not even bind until the enzyme has reached E_3. Fe and Mo EXAFS analysis of enzymatically reduced, as-isolated, and selectively oxidized Av1 is presented below.

4.2 Experimental

Av1 and Av2 were extracted and purified as detailed in Chapter 2. Specific activities of the purified components ranged from 1800-2000 nmol

C_2H_2 reduced min^{-1} mg $protein^{-1}$ for Av1 and 1400-1600 nmol C_2H_2 reduced min^{-1} mg $protein^{-1}$ for Av2.

To obtain a pure one-electron reduced EXAFS spectrum, we examined a steady state turnover mixture of resting and one-electron reduced MoFe protein from *Azotobacter vinelandii*, in the presence of a small amount of Fe protein. We measured the Fe K-edge EXAFS of these E_0 + E_1 steady state samples and subtracted the 50% E_0 contribution, thus isolating an E_1 spectrum. Specifically, steady state mixtures were prepared by incubating a 5:1 molar ratio of MoFe protein:Fe protein, along with excess sodium dithionite and an ATP regenerating mixture at room temperature in a Vacuum Atmospheres glove box with an argon atmosphere. The O_2 level was held at <1.5 ppm throughout the entire procedure. The regenerating mixture consisted of 0.025 M Tris-HCl pH 7.4, with 10 mM sodium dithionite, 10 mM Mg-ATP, 150 mM creatine phosphate and 0.625 mM creatine phosphokinase. Purified MoFe protein was added to the reaction mixture first, followed by the Fe protein to start the reaction. The reaction was allowed to proceed in the glove box for 8 min., at which time ethylene glycol (as a glassing agent) was added to the reaction mixture, for a final concentration of 40% ethylene glycol, and approximately 20 mg/ml MoFe protein. Samples and simultaneously run controls (without a source of MgATP or the regenerating system) were loaded into lucite EXAFS cuvettes and quartz EPR tubes simultaneously. Samples

were then frozen, typically at 12 minutes from the point of addition of the Fe protein.

The sample condition was verified by EPR spectroscopy. Steady state turnover samples all showed 50% reduction in the amplitude of the S=3/2 FeMo-cofactor signal compared to the control samples in spectra recorded at 3.2 K. EPR spectra were recorded on a computer-interfaced Bruker ER300D spectrometer with ESP 200 data collection software and an Oxford Instruments ESR-900 helium flow cryostat. Temperature was monitored with an FeAu/Chromel thermocouple positioned directly below the sample tube and monitored with an Oxford Instruments ITC-4 temperature controller.

MoFe protein with 2-equivalent oxidized P-clusters was prepared by oxidation with indigodisulfonate (IDS).[6] EPR spectroscopy has shown that the S=3/2 FeMo-cofactor signal remains at full amplitude[7] while integer-spin (S = 3) EPR signals that have been assigned to 2-equivalent oxidized P-clusters appear upon oxidation with excess IDS.[8] P-cluster oxidation with IDS was effected by titrating dithionite-free MoFe protein with anaerobic IDS solution (prepared in 0.025 M Tris-HCl pH 7.4 and 0.2 M NaCl) until the endpoint was reached, indicated by a persistent blue-green color. Sodium dithionite was removed from the MoFe protein prior to IDS titration by gel filtration with Sephadex G-25 (Pharmacia). IDS oxidized samples were concentrated with Minicon membrane concentrators to a final concentration of 90-140 mg/ml. EXAFS cuvettes and quartz EPR tubes were loaded and frozen in liquid

nitrogen simultaneously. All of the above procedures were done in the glove box with the O_2 level held at <1.5 ppm continuously. EPR spectra showed no attenuation of the S = 3/2 FeMo-cofactor signal when compared to untitrated control samples. The S = 3 EPR signal (at g = 11.6 in perpendicular mode) which has been assigned to 2-equivalent oxidized P-clusters was present in the IDS oxidized samples.[9-11] Other EPR signals that are assigned to different P-cluster oxidation states (S = 1/2, 5/2 or 7/2) were not observed.[8,12,13] Thionine oxidations were done as described in Chapter 3.

The samples prepared represent a number of EPR definable redox states of the metal clusters in Av1. As-isolated (P/M), enzymatically reduced (assumed P/M^-), IDS oxidized (P^{2+}/M), and thionine oxidized (P^+/M^{2+}) Av1 were investigated by EXAFS.

The EXAFS spectra were measured in fluorescence mode using a Canberra Instruments 13-element Ge solid-state array detector.[14] During the measurement, the samples were maintained at 8-10 K in an Oxford Instruments CF1208 liquid helium flow cryostat. Amplifier shaping times were set at either 0.5 ms or 1 ms, with total count rates for each channel kept below 35 kHz and 20 kHz respectively. Single channel analyzer windows were set to collect the Fe or Mo K_α signal. The spectra were calibrated by simultaneously collecting transmission spectra of a pure metal foil, setting the first inflection point energy at 7111.2 eV for Fe and 20,000 eV for Mo.

X-ray absorption spectra were recorded on several different beamlines. Steady state turnover Fe EXAFS data were collected on NSLS beamline X-10C running in focused mode with Si(220) and Si(111) monochromator configurations, SSRL beamline 6-2 in focused mode and Si(111) monochromator configuration, and NSLS beamline X-19A in unfocused mode with Si(220) monochromator configuration. IDS oxidized data were collected on NSLS beamline X-19A in unfocused mode with a Si(111) monochromator configuration, NSLS beamline X-10C running in focused mode with a Si(111) monochromator configuration, and SSRL beamline 6-2 in focused mode with a Si(111) monochromator configuration. For beamlines X-19A and 6-2, the second monochromator crystal was detuned to minimize the transmission of harmonics. For beamline X-10C, a mirror feedback system was used for rejection of harmonics [15] Beam spot size was maintained at a maximum of ~2 x 12 mm with focusing optics and/or tantalum slits placed at the beam exit port. The incident beam intensity was monitored with a nitrogen-filled ion chamber. Mo x-ray absorption spectra were recorded at SSRL beamline 7-3, operating in unfocused mode with a Si(220) monochromator, and at NSLS beamline X-19A in unfocused mode with a Si(220) monochromator. For Mo samples, the beam intensity was monitored with argon filled ion chambers and the spot size was maintained by slits placed at the beam exit port.

Reproducibility of the data from all beamlines was checked by overlaying the data sets and comparing the EXAFS over the full range of data. De-

glitching was performed by single-point removal on raw spectral data. The EXAFS oscillations were extracted from the raw data with a cubic spline and normalized with a Victoreen function using routine methods.[16] Values of 7131 eV for Fe and 20020 eV for Mo were used to define the initial magnitude of the photoelectron wave vector $k = [(2m/h^2)(E-E_O)]^{1/2}$. The EXAFS spectra were interpolated onto identical *k*-space grids with $\Delta k = 0.05$ Å^{-1} and then averaged to form a single data set for both the singly reduced mixture ($E_0 + E_1$) and IDS oxidized MoFe protein. The EXAFS spectrum of resting E_0 MoFe protein was also interpolated onto the same k-space grid and subtracted from the $E_0 + E_1$ mixture to yield the EXAFS of the E_1 state.

The EXAFS spectra were Fourier transformed from *k*-space to R-space, and specific regions of the resulting transforms were then Fourier filtered and back-transformed for subsequent curve fitting to the single-scattering, curved-wave functional form of the EXAFS equation[17] using a Levenberg-Marquardt curve fitting algorithm:[18]

$$\chi(k) = \sum_i \frac{N_i \gamma_i f_i(k,R_i)}{kR_i^2} e^{-2\sigma_i^2 k^2} \sin[2kR_i + \phi_i(k,R_i)]$$

where the summation is over all backscatterers at a distance R_i, with root-mean square distance deviation σ^2 and coordination number N_i. The functions $f(k,R_i)$ and $\phi(k,R_i)$ represent the distance and energy dependent curved-wave backscattering amplitude and total phase shift, respectively. The amplitude reduction factor γ was held fixed at 0.9 during all fits.[1]

$(CO)_3MoFe_6S_6Mo(CO)_3$ as discussed in Chapter 3.[1,19] The ΔE_o parameters determined from the model compound fits were held fixed for the protein fits. The protein fits were effected by locking the coordination number (N) to values obtained from the crystallographic models[20-22] while optimizing σ^2 and the radial distance R by curve fitting, using published results as initial values for these parameters.[1,2]

4.3 Results

The Fe EXAFS of IDS-oxidized MoFe protein (P^{2+}/M) is shown in Figure 4.2 along with 4-shell and 5-shell curve fits (see below). For curve fitting analysis, the Fe EXAFS of the IDS oxidized MoFe protein was Fourier transformed (k = 3-14.5 $Å^{-1}$) and then the R-space region from 0-6 Å was back-transformed. Since IDS does not effect the oxidation level of the M-center, a large change in the M-center distances is not expected, so the Fe-Mo distance at 2.71 Å previously determined by Mo K-edge EXAFS of resting enzyme was held fixed for the IDS fit. The best 4 shell single-scattering fit with this constraint (Table 4.1 and Figure 4.2), found average Fe-S and Fe-Fe distances of 2.31 Å and 2.65 Å, as well as a long Fe-Fe component at 3.74 Å.

The fit shown in Figure 4.2 is reasonable but not exact, although EXAFS fits rarely are. Multiple scattering possibilities were examined by Jason

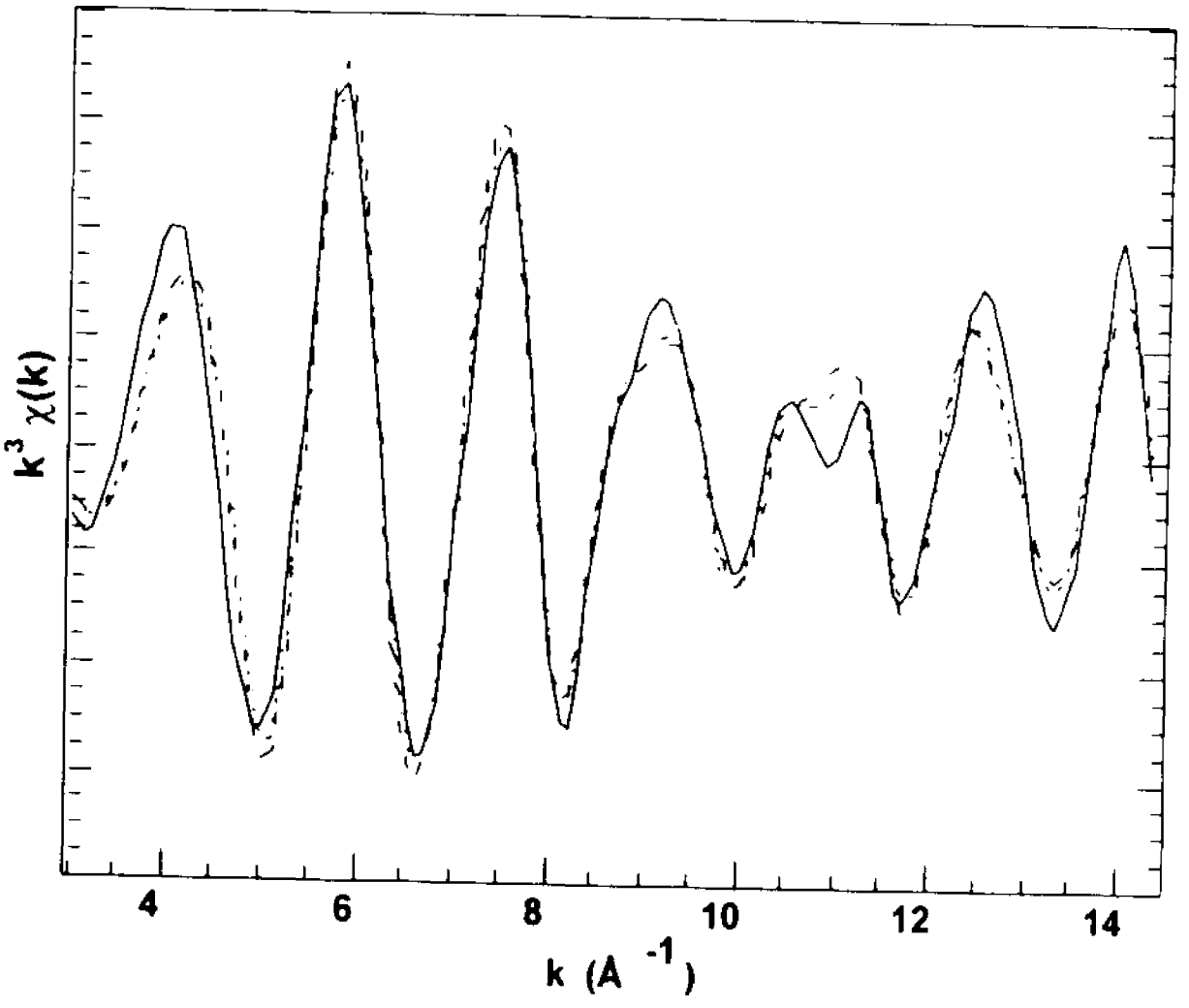

Figure 4.2. Fourier filtered EXAFS of IDS oxidized nitrogenase (shown solid) with the 4 component (short dash) and the 5 component (dashed) fit results

Table 4.1. Results of curve fitting for Fe EXAFS.

	Fe-S ΔE_0 = -3eV			Fe-Fe ΔE_0 = -8eV			Fe-Mo ΔE_0 = -6eV			Fe-Fe ΔE_0 = -10eV		
	N	R, Å	σ^2 x 10^5 Å^2	N	R, Å	σ^2 x 10^5 Å^2	N	R, Å	σ^2 x 10^5 Å^2	N	R, Å	σ^2 x 10^5 Å^2
P^{2+}/M^+												
4-shell	3.6	2.29	555	3.2	2.66	988	0.2	2.72	443	1.3	3.73	369
5-shell	3.6	2.29	501	1.6	2.61	333	0.2	2.72	443	1.3	3.74	395
				1.6	2.74	333						
P^{2+}/M												
4-shell	3.6	2.31	506	3.2	2.65	871	0.2	2.71	290	1.3	3.74	347
5-shell	3.6	2.31	475	1.6	2.59	333	0.2	2.71	290	1.3	3.75	344
				1.6	2.70	333						
P/M												
4-shell	3.6	2.31	599	3.2	2.63	634	0.2	2.71	295	1.3	3.73	361
5-shell	3.6	2.31	582	1.6	2.58	333	0.2	2.71	295	1.3	3.74	392
				1.6	2.67	333						
P/M$^-$												
4-shell	3.6	2.33	578	3.2	2.60	938	0.2	2.66	398	1.3	3.72	245
5-shell	3.6	2.33	655	1.6	2.54	333	0.2	2.66	398	1.3	3.72	243
				1.6	2.66	333						

Christiansen at the University of California, Davis, before further analysis was undertaken within the single scattering formalism. Using symmetrized models for the M-center and P-cluster cores, and analyzing for possible multiple scattering contributions with FEFF5,[23] he detected no significant multiple scattering contributions in the 1-3 Å range for either Fe or Mo. The largest multiple scattering pathway predicted for the < 3 Å range for Fe was a 3.6 Å Fe-S-Fe path that contributed 7% to the large Fe-S interaction at ≈ 2.3 Å. There is a predicted contribution of 25% to the long Fe-Fe interaction at 3.7 Å. There is no significant multiple scattering predicted for the cubane cores of the P-clusters. It should be noted that FEFF5 requires that the analyst input a structural geometry prior to analysis. If, in fact, the nitrogenase metal clusters are *significantly* asymmetric, then the multiple scattering predictions could be in error. However, examination of the crystallographic models and previous EXAFS data tends to support the proposal that the short distance interactions in Av1 are dominated by single scattering.

The average Fe-Fe distance of 2.65 Å is not significantly different from the 2.63 Å value for resting enzyme. However, the large σ^2 value of ~0.09 $Å^2$ for the 2.65 Å Fe-Fe interaction may be significant. In fact, it was the observation of this large value for σ^2 that inspired this analysis. Typical values for thermal motion disorder of short bridged metal-metal distances are on the order of 0.05 Å or less, so a σ^2 of ~0.09 $Å^2$ indicates a measure of 'static' as opposed to 'thermal' disorder. One could argue that the short Fe-Fe distances

nitrogenase simply get more disordered upon oxidation, yielding an average distance of 2.65 Å. An alternative view is that the P-cluster Fe-Fe interactions have all expanded while the cofactor interactions have remained the same upon IDS oxidation, yielding an average of 2.65 Å.

Nitrogenase crystallographic data from the laboratories of both Rees[21] and Bolin[22] indicate that the short Fe-Fe distances in the cofactor are smaller than the short distances in the P-cluster. The EXAFS analysis in the previous chapter determined an average Fe-Fe distance of 2.64 Å for as-isolated Av1. Reanalysis of the same data in this study by fixing N at 3.2 (from inspection of the crystallographic models) and fixing the Fe-Mo interaction at 2.71 Å (see above) resulted in a distance fit of 2.63 Å. The σ^2 values in both cases were slightly higher than expected for a short interaction, but not totally unreasonable. Crystallographically modeled values of this short Fe-Fe distance in Cp1 average 2.71 Å in the P-cluster, with a root mean square deviation of 0.13 Å, and 2.60 Å in the M-center, with a root mean square deviation of 0.13 Å.[22]

A "split shell" EXAFS analysis was effected by defining N = 1.6 for both P-cluster and M-center, and fitting the 2.65 Å Fe-Fe distance with two shells instead of one. The EXAFS resolution criterion $\Delta R \approx \pi/2\Delta k$ over the data range of k = 3-14.5 $Å^{-1}$ does not allow complete resolution of identical backscatterers that have distances that differ by less than 0.14 Å.[24] Nevertheless, it seemed reasonable to attempt a "split shell" EXAFS analysis of Av1 in different

oxidation states, to determine if any consistent changes or trends were indicated. Allowing for two different short Fe-Fe components while constraining as many other parameters as possible resulted in a somewhat improved fit if σ^2 and R were allowed to vary. Short Fe-Fe distances of 2.59 Å and 2.70 Å were determined for IDS oxidized Av1, as shown in Table 4.1.

The previously reported as-isolated and thionine-oxidized Av1 Fe EXAFS were reinterpreted with the new model[1] (Table 4.1). As expected, the thionine-oxidized spectrum, which produced the largest $\sigma_{Fe\text{-}Fe}$ values in the 4-shell fits, gave the largest difference in Fe-Fe distances when fit with the "split-shell" model, with an average M-center short Fe-Fe of 2.61 Å, compared to a P-cluster short Fe-Fe of 2.74 Å. A 2.74 Å Fe-Fe distance has been observed in a synthetic Fe_4S_4 cluster,[25] while the 2.61 Å distance is similar to the 2.64 Å value reported for isolated FeMoco.[3] The as-isolated spectrum also gave a relatively short M center Fe-Fe distance of 2.58 Å, which is approaching the distance seen in Fe-Fe bonding interactions.

The reduced Av1 E_1 EXAFS was extracted from the E0 + E1 mix by subtracting the EXAFS of as-isolated Av1 scaled to 50% amplitude (see above). The subtraction process resulted in an increase of the noise level in the pure E_1 EXAFS which was significant above k = 11. To provide additional constraints for the more complex Fe analysis, the Mo EXAFS data was fit first. The Mo EXAFS was Fourier-filtered to select the region from 1-3 Å and backtransformed. The fits yielded Mo-(O,N), Mo-S, and Mo-Fe distances of

2.13, 2.36, and 2.65 Å respectively (Figure 4.3 and Table 4.2). Of these distances, the most significant result is the apparent 0.06 Å contraction in the Mo-Fe distance. This Mo-Fe distance and the associated σ^2 of 0.004 $Å^2$ were then used as constraints in the analysis of the Fe EXAFS of the E_1 enzyme (P/M).

The Fe EXAFS was Fourier filtered, and the ~1-3.5 Å region was backtransformed and fit with both single Fe-Fe shell and split Fe-Fe shell simulations, as described above for IDS oxidized Av1. The Fe-Mo distance and σ of 2.65 Å and 0.06 Å determined in the Mo analysis were held fixed. The results are summarized in Table 4.1 and Figure 4.4. Using a single short Fe-Fe interaction, Fe-S and Fe-Fe distances of 2.33 Å and 2.60 Å were determined. Allowing for a split Fe-Fe distribution gave subshell average distances of 2.54 and 2.66 Å. A fit of the Fourier filtered 3.2-4.5 Å region showed an Fe-Fe interaction at 3.72 Å, only slightly shorter than the 3.74 Å distance seen in resting Av1.

4.4 Discussion

Figure 4.5 depicts the overall distance trends in the short Fe-Fe and the short Mo-Fe interaction, respectively, for the 4 defined oxidation states examined. Many of the individual changes are small, within the generally accepted EXAFS error of ± 0.02 Å,[26] but a clear trend is still apparent. Examination of Table 4.1 and Figure 4.5 shows that reduction results in a slight contraction of the average metal-metal distances, and a slight expansion in the

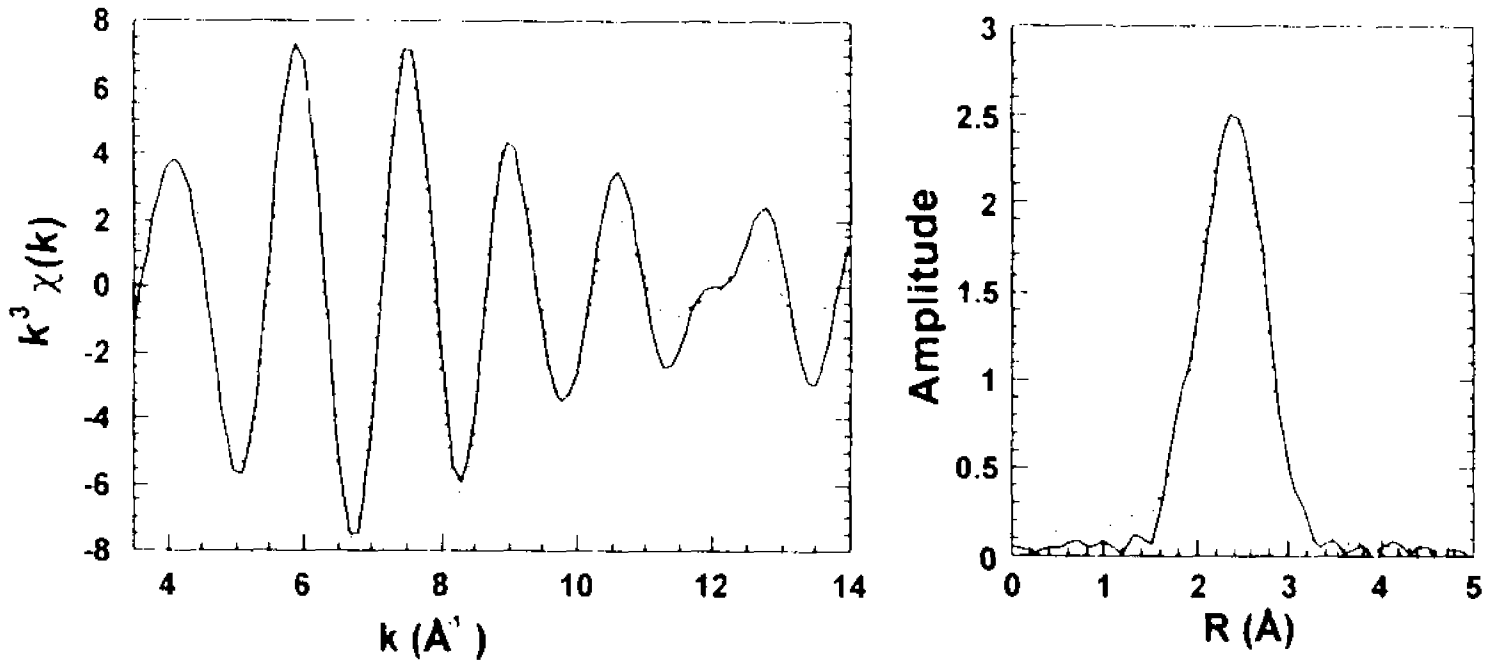

Figure 4.3 Mo Fourier filtered EXAFS (left) data (solid) and fit (dashed). Fourier transform (right) of the Mo data (solid) and fit (dashed).

Table 4.2 Results of curve fitting for Mo EXAFS.

	Mo-O/N ΔE_0 = -3.3 eV			Mo-S ΔE_0 = -14 eV			Mo-Fe ΔE_0 = -10 eV		
	N	**R, Å**	**σ^2 x 10^5 Å^2**	**N**	**R, Å**	**σ^2 x 10^5 Å^2**	**N**	**R, Å**	**σ^2 x 10^5 Å^2**
P^{Z+}/M^{+}	3.0	2.17	317	3.0	2.38	399	3.0	2.72	435
P/M	3.0	2.20	283	3.0	2.36	340	3.0	2.71	310
P/M'	3.0	2.13	263	3.0	2.36	178	3.0	2.65	397

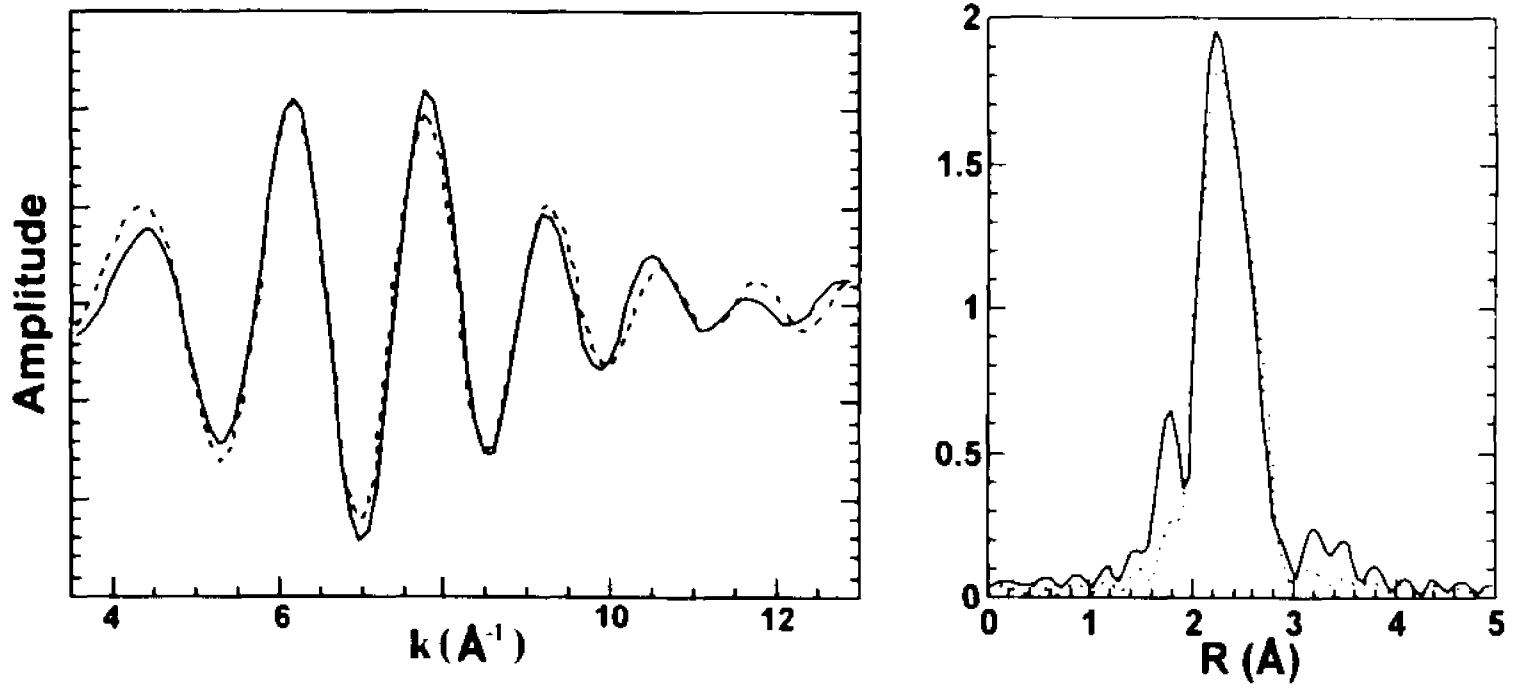

Figure 4.4 Fe Fourier filtered EXAFS (left) data (solid) and fit (dashed). Fourier transform (right) of the Fe data (solid) and fit (dashed).

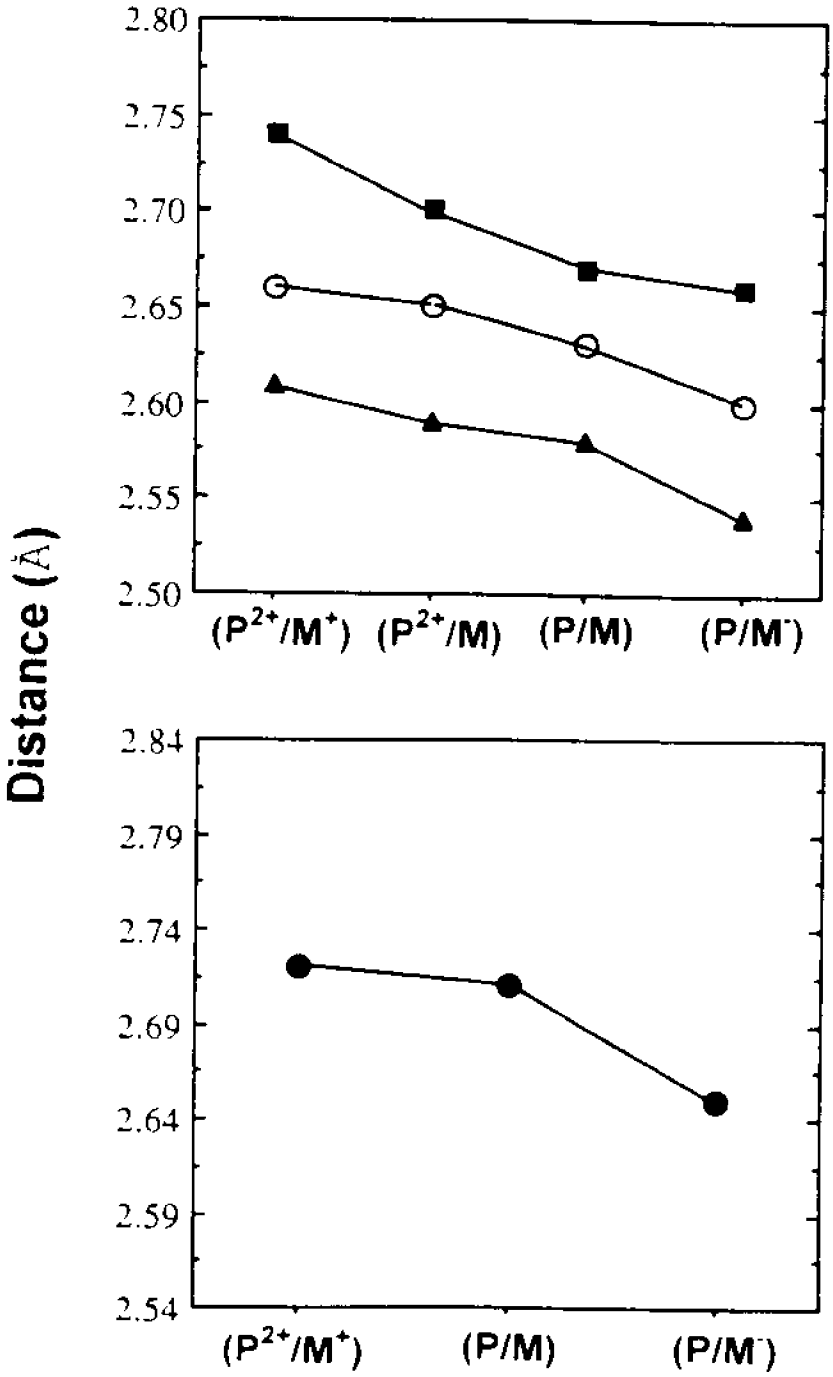

Figure 4.5. Plots showing the trends in metal-metal distances during metal cluster oxidation/reduction. Top: The variation in Fe-Fe distances as the protein goes from fully oxidized (P^{2+}/M^{+}) to reduced (P/M^{-}). The center plot indicates the variation in the 4 component fits while the outer data points indicate the trend demonstrated in the split-shell fits. Bottom: Trend in the Fe-Mo interaction for different redox states of the protein.

average Fe-S distance. This trend follows for both short Fe-Fe interactions in the split-shell model, as well as the single interaction fit with only one shell.

The split-shell analysis may be defended as chemically reasonable in light of the crystallographically modeled Fe-Fe average distances in the P-cluster and M-center cited above.[21,22] EXAFS of extracted cofactor has shown shorter Fe-Fe distances than those observed in intact Av1.[3] Also, the Fe in the M-center is 3-coordinate according to the proposed models, and a tighter structure may exist in the M-center than in the P-cluster due to stronger Fe-Fe interactions. The average "split" of 0.11 Å between the proposed P-cluster and M-center distances in the "split-shell" model actually approaches the predicted resolution of 0.14 Å cited above.[24]

Perhaps the most important result of this analysis is that very little EXAFS resolvable structural change takes place in either the M-center or P-cluster in the oxidation range examined. The E_1 state is catalytically competent to reduce H^+ and the E_1 EXAFS showed small changes from the as-isolated Av1, but no dramatic structural rearrangements were apparent. In every oxidation state examined, the long Fe-Fe interaction at ≈ 3.75 Å was apparent, which also argues against large structural rearrangements.

The binding site of N_2 on, near, or in the cofactor cluster is as yet unknown. It has been proposed that N_2 somehow gets inside the cofactor cluster, perhaps by the cofactor breaking apart to accomodate it.[27] Theoretical studies by Deng and Hoffman suggest that the lowest energy binding site(s) are

on the surface of the cofactor, not inside it.[28] They estimate that the short Fe-Fe would have to expand to ≈ 3.0 Å to accomodate N_2. In this study, no change of that magnitude was observed in the oxidation states examined.

Contraction of metal clusters upon reduction is atypical behavior.[29] In most documented cases, they have been shown to expand as they become more reduced. There are examples of metal cluster distance contractions as electrons are added. Mo clusters have been shown to have 2.6 Å, 2.5 Å, and 2.1 Å Mo-Mo distances in Mo(V)-Mo(V), Mo(IV)-Mo(IV), and Mo(II)-Mo(II) bonds, respectively.[30] However, in both $[Fe_6S_6L_6]^{n-}$ prismanes and $[Fe_4S_4]^{n+}$ clusters, addition of electrons results in longer Fe-Fe distances,[31] as is also the case with the Mo-capped prismanes.[19] So, the observed distance contraction in Av1 is atypical for synthetic Fe-S-containing clusters, but the three coordinate Fe in the M-center is also atypical.

It should be stressed here again that EXAFS only reports average distances. Thus, an asymmetric distortion in the P-cluster, M-center, or both upon change in oxidation state could result in a combination of long and short distances for the same apparent absorber-backscatterer interaction. This undoubtedly occurs to some extent, since the resting state enzyme crystallographic model shows some distance distribution for the short Fe-Fe distance.[21,22] However, very large distortions can result in anomalous EXAFS behavior. Asymmetric distance distributions that tail to long distances can yield EXAFS that overemphasizes the short interactions, to the extent that the

distances found in optimized curve fits are actually less than the true average distance.[32] This could be happening in Av1, in either the M-center or the P-cluster upon oxidation or reduction, but EXAFS is not capable of determining this.

If the split-shell analyses do, in fact, give a reasonably accurate model of the M-center and P-cluster short Fe-Fe interactions, then the especially short Fe-Fe in the M-center warrants some discussion. The reduced M-center value of 2.54 Å is very close to that in clusters where metal-metal bonding is suspected. $Fe_2(CO)_9$ shows an Fe-Fe distance of 2.52 Å, and it has been speculated that it may or may not have an Fe-Fe bond.[33,34] In any event, the short Fe-Fe distance in Av1 may allow for significant electronic interaction between the Fe atoms, resulting in an "activated" cofactor surface, competent to reduce N_2. The distance changes observed for the various redox states may indicate that the cofactor and/or P-cluster undergo some sort of "breathing" or pulsating motion during the substrate reduction cycle.

References

1. Chen, J.; Christiansen, J.; Tittsworth, R.C.; Hales, B.J.; George, S.J.; Coucouvanis, D.; Cramer, S.P. *J. Am. Chem. Soc.* **1993**, *115*, 5509-5515

2. a) Flank, A.M.; Weininger, M.; Mortenson, L.E.; Cramer, S.P. *J. Am. Chem. Soc.* , **1986**, *108*, 1049-1055 b) Chen, J.; Christiansen, J.; Campobasso, N.; Bolin, J.T.; Tittsworth, R.C.; Hales, B.J.; Rehr, J.J.; Cramer, S.P. *Angew. Chem. Int. Ed. Engl.* **1993**, *32*, 1592-1594

3. a) Conradson, S.D.; Burgess, B.K.; Newton, W.E.; Mortenson, L.E.; Hodgson, K.O. *J. Am. Chem. Soc.* , **1987**, *109*, 7507 b) Arber, J.M.; Flood, A.C.; Garner, C.D.; Gormal, C.A.; Hasnain, S.S.; Smith, B.E. *Biochem. J.* **1988**, *252*, 421-425 c) Antonio, M.R.; Teo, B.K.; Orme-

Johnson, W.H.; Nelson, M.J.; Groh, S.E.; Lindahl, P.A.; Kauzlaurich, S.M.; Averill, B.A. *J. Am. Chem. Soc.*, **1986**, *108*, 1049-1055

4. Lowe, D.J.; Thorneley, R.N.F. *Biochem J.* **1984**, *224*, 877-886.

5. Fisher, K.; Lowe, D.J.; Thorneley, R.N.F. *Biochem J.* **1991**, *279*, 81-85

6. Orme Johnson, W.H.; Paul, L.; Meade, J.; Warren, W.; Nelson, M.; Groh, S.; Orme Johnson, N.R.; Munck, E.; Huynh, B.N.; Emptage, M.; Rawlings, J.; Smith, J.; Roberts, J.; Hoffman, B.; Mims, W.B.; In *Current Perspectives in Nitrogen Fixation* ; Gibson, A.H.; Newton, W.E., eds.; Elsevier, North-Holland, New York, **1981**, 79-84

7. Munck, E.; Rhodes, H.; Orme Johnson, W.H.; Davis, L.C.; Brill, W.J.; Shah, V.K. *Biochim. Biophys. Acta* **1975**, *400*, 32-53

8. (a) Hagen, W.R. in *Iron Sulfur Proteins* (Sykes, A.G., Cammarck, R. Eds) pp165-122, *Advances in Inorganic Chemistry*, **1992**, Vol. 38, Academic Press, New York; (b) Surerus, K.K.; Hendrich, M.P.; Christie, P.D.; Rottgardt, D.; Orme-Johnson, W.H.; Munck, E.J. *J. Am. Chem. Soc.* **1992**, *114*, 8579-8590; (c) Plerik, A.J.; Wassink, H.; Haaker, H.; Hagen, W.R. *Eur. J. Biochem.* **1993**, *212*, 51-61

9. Hagen, W. R. In *Advances in Inorganic Chemistry: Iron-Sulfur Proteins*; A. G. Sykes and R. Cammack, Ed.; Academic Pres: 1992; Vol. 38; pp 165-222.

10. Surerus, K. K.; Hendrich, M. P.; Christie, P. D.; Rottgardt, D.; Orme-Johnson, W. H.; Münck, E. *J. Am. Chem. Soc.* **1992**, *114*, 8579-8590.

11. Pierik, A., J.; Wassink, H.; Haaker, H.; Hagen, W. R. *Eur. J. Biochem.* **1993**, *212*, 51-61.

12. Smith, B. E.; Lowe, D. J.; Chen, G.-X.; O'Donnell, M. J.; Hawkes, T. R. *Biochem. J.* **1983**, *209*, 207-213.

13. Tittsworth, R.C.; Hales, B.J. *J. Am. Chem. Soc.* **1993**, *115*, 9763-9767.

14. Cramer, S.P.; Tench, O.; Yocum, M.; George, G.N. *Nucl. Instrum. Methods A266*, **1988**, 586-591

15. Sansone, M.; Via, G.; George, G.N.; Metizner, G.; Hewitt, R., In *X-Ray Absorption Fine Structure*; S.S. Hasnain, Ed.; **1991**, pp 656-658, Ellis Horwood Ltd.: W. Sussex, England

16. Cramer, S.P.; Hodgson, K.O.; Steifel, E.I.; Newton, W.O. *J. Am. Chem. Soc.* **1978**, *100*, 2478-2760

17. McKale, A.G.; Knapp, G.S.; Chan, S-K. *Phys. Rev. B* **1986**, *33*, 841-846

18. Marquardt, D.W. *J. Soc. Ind. Appl. Math.* **1963**, *11*, 443

19. Coucouvanis, D. in *Molybdenum Enzymes, Cofactors and Model Systems*; Steifel, E.I.; Coucouvanis, D.; Newton, W.E. eds.; ACS Symposium Series 535, New York; **1993**, 304-331.

20. Kim, J.C.; Rees, D.C. *Science* **1992**, *257*, 1677.

21. Chan, M.K.; Kim, J.; Rees, D.C. *Science* **1993**, *260*, 792-794.

22. Campobasso, N., *Ph.D. Thesis, Purdue U.*, **1994**.

23. (a) Rehr, J.J.; Mustre de Leon, J.; Zabinsky, S.I.; Albers, R.C. *J. Am. Chem. Soc.* **1991, *113*,** 5135; (b) Mustre de Leon, J.; Rehr, J.J.; Zabinsky, S.I.; Albers, R.C. Phys Rev B, **1991**, *44*, 4146.

24 Lee, P.A.; Citrin, P.H.; Eisenberger, P.; Kincaid, B.M. *Rev. Mod. Phys.* **1981**, *53*, 769-806

25. Laskowski, E.J.; Frankel, R.B.; Gillum, W.O.; Papaefthymiou, J.R.; Ibers, J.A.; Holm, R.H. *J. Am. Chem. Soc.* **1978**, *100*, 5322-5337

26. *X-Ray Absorption: Principles, Applications, Techniques of EXAFS, SEXAFS and XANES*; Prins, R.; Königsberger, D., eds.; Wiley: New York, **1988.**

27. a) Schrauzer, G.N.; Docemeny, P.A.; Palmer, J.G. *Zeitschrift Fur Naturforschung Section B-A Journal of Chemical Sciences*, **1993**, *48*, 1295-1298 b) Schrauzer, G.N. *J. Inorg. Biochem.* **1993**, *51*, 370

28. Deng, H.; Hoffman, R. *Angew. Chem. Int. Ed. Engl.* **1993**, *32*, 1062-1065

29. Lauher, J.W. *J. Am. Chem. Soc.* **1978**, *100*, 5305-5315

30. Cramer, S.P.; Gray, H.B.; Dori, Z.; Bino, A. *J. Am. Chem. Soc.* **1979**, *101*, 2770-2772

31. Stiefel, E. I.; George, G. N. In *Bioinorganic Chemistry*, Bertini, I.; Gray, H. B.; Lippard, S. J.; Valentine, J. S. Eds; University Science, Mill Valley **1994**, 365-453.

32. Eisenberger, P.; Brown, G.S. *Sol. State. Comm*, **1979**, *29*, 481-484.

33. Barnett, B.L.; Krüger, C. *Angew. Chem. Int. Ed. Engl.*, **1971**, *10*, 910-911.

34. Mealli, C.; Prosperio, D.M. *J. Organomet. Chem.* **1990**, *386*, 203-28.

Chapter 5 EPR Studies of the One-Equivalent-Oxidized P-clusters of the Nitrogenase MoFe Protein.

5.1 Introduction

The nitrogenase MoFe protein of *Azotobacter vinelandii* (Av1) contains one Fe_7S_9Mo cofactor cluster, or FeMoco, in each of its two α subunits, and two P-clusters, which are each composed of two Fe_4S_4 cubane clusters coupled by two bridging cysteine thiols and one sulfide. One P-cluster spans each $\alpha\beta$ interface.[1-3] It has been shown that the cofactor clusters are necessary for catalysis, and it is widely accepted that catalysis occurs on or near the cofactor. The role of the P-clusters is not yet known, but it is reasonable to propose that they are somehow involved in the catalytic function of nitrogenase, perhaps as electron acceptors from component 2. In any event, the reduction of dinitrogen is a redox process, and elucidation of the possible stable redox states accessible to the P-clusters may be fundamental to understanding the catalytic mechanism of nitrogenase.

5.2 Background

As-isolated Av1 exhibits an S = 3/2 EPR signal[4] with *g*-factors of 4.3, 3.7, and 2.0, which has been assigned to the FeMo cofactor. This signal is bleached during catalytic turnover, presumably due to reduction of the cofactor.[5] Chemical oxidation also results in loss of the S = 3/2 EPR signal[6], which may be restored by chemical reduction with sodium dithionite (DTN). The P-clusters are diamagnetic in as-isolated Av1, but become paramagnetic

upon oxidation. Magnetic circular dichroism[7,8] (MCD) and Mossbauer spectroscopy[6] of oxidized Av1 have indicated spin states of S = 5/2-7/2 and S = 3/2-9/2, respectively. Integer-spin[9-11] EPR signals have been observed in Av1 that has been oxidized by four or more equivalents with the redox dye thionine. They have been proposed to arise from an S = 3 spin system of 2-equivalent oxidized P-clusters (P^{2+}). Spin quantitation of these signals indicates that there are approximately two spins per Av1 molecule, which is what would be expected if each P-cluster was oxidized by two equivalents, forming an integer spin system on each cluster. Further oxidation with a large molar excess of thionine solution or by stirring over solid thionine results in the appearance of S = 7/2 and S = 1/2 EPR signals that have been assigned to 3-equivalent oxidized P-clusters (P^{3+}).[11,12] Oxidation past this point has been shown to result in irreversible deactivation of Av1, along with the appearance of an S = 5/2 EPR signal at g = 4.3, which is typical of high-spin Fe^{3+}, a possible metal cluster degradation product. All of the oxidations up to and including P^{3+} are reversible, and cause essentially no loss of catalytic activity.

Thionine titrations of Av1 have been shown to follow a well established pattern.[6] The first four oxidizing equivalents have no effect on the S = 3/2 cofactor signal, but the integer spin EPR signals assigned to P^{2+} attain maximal amplitude at 4 equivalents. The cofactor EPR signal is removed by the next two equivalents of oxidant, so it follows that the first four equivalents of oxidant most likely oxidize the P-clusters. It has been proposed that the P-clusters are

oxidized by 2 equivalents each in an n = 2 Nernstian process, and go directly from P^0 to P^{2+}.[9-11] However, an S = 1/2 EPR signal that has been observed in thionine titrations of Av1[13] and $K_3Fe(CN)_6$ oxidized Kp1[14] (the component 1 nitrogenase of *Klebsiella pneumoniae*) indicates that P^+ (singly oxidized P-cluster) may be a stable paramagnetic species, although integrations of these signals show that they arise from a minority species.

Studies of the power saturation behavior of the S = 3/2 cofactor EPR signal of Av1 during stepwise thionine titrations have demonstrated that a dipolar interaction occurs between the P-clusters and M-centers as the titration proceeds through the first four oxidizing equivalents.[15] This interaction results in a measurable change in the power saturation behavior of the S = 3/2 EPR signal and is nonlinear, showing maximum change at the 2-equivalent-oxidized step. This strongly suggests the existence of a paramagnet that is created during the early stages of the thionine titration, and the most likely candidate is the P-cluster, since it is in relatively close proximity to the M-center ($\approx$ 14 Å).[3] The fact that the perturbation to the power saturation behavior of the M-center is maximized at 2 oxidizing equivalents and there are 2 P-clusters per Av1 molecule indicates that the paramagnetic species created may actually be P^+, or 1-equivalent oxidized P-cluster. Further EPR studies and theoretical analysis that confirm and explain the existence of the stable P^+ species are presented here.

5.3 Experimental

Since both nitrogenase component proteins are purified and stored in the presence of the reductant sodium hydrosulfite (sodium dithionite or DTN), it was necessary to remove it prior to conducting oxidative titrations. This was done by gel filtration chromatography, using Sephadex G-25 (Pharmacia) and anaerobic 0.025 TRIS-HCl (pH 7.4) buffer with 0.2 M NaCl. The Av1 was loaded onto pre-equilibrated 13 cm x 1.5 cm columns and eluted with the previously mentioned buffer. Collected fractions were assayed for residual DTN with methyl viologen indicator.

The dithionite-free Av1 was titrated with thionine solution prepared by dissolving saturating amounts of thionine (ICN) in the same buffer. The thionine solutions were filtered with 0.2 μm syringe filters to remove any solid oxidant. Titrations were carried to endpoint, which is indicated by a persistent bluish tint in the protein solution. Assuming the apparent endpoint to be at the 6-equivalent-oxidized step (4 equivalents for the P-clusters, and 2 more to oxidize the FeMo cofactor), appropriate aliquots of oxidant were used to titrate separate Av1 samples in a stepwise fashion, from 0 to 6 equivalents oxidized. Also, incremental titrations were done using small aliquots (< 1 oxidizing equivalent per step) while monitoring the S = 3/2 FeMo cofactor EPR signal, since it has been shown that it retains full amplitude until the 4th oxidizing equivalent and is removed by the 5th and 6th equivalents.[6,15] The S = 3/2 EPR

signal of Av1 served as an "internal standard" which allowed accurate calibration of the oxidative titrations.

All experimental samples were allowed to stand in the glove box for at least 30 min. to assure equilibration and then were loaded anaerobically into quartz EPR tubes and frozen in liquid nitrogen. The final protein concentration varied from 11 to 30 mg/ml Av1. The samples were checked for nitrogenase activity by acetylene reduction assay and were found to show no significant loss of activity.

EPR spectra were recorded on a computer interfaced Bruker ER300D spectrometer operating in perpendicular mode at X-band (9.44 GHz) frequency. The spectrometer was fitted with a rectangular TE_{102} resonant cavity. An Oxford Instruments ESR-900 helium flow cryostat was used to reach low temperatures ($\geq$ 2.8 K) which were monitored with an Oxford Instruments ITC-4 temperature controller connected to an FeAu/chromel thermocouple positioned directly below the sample tube.

The oxidative titrations described above were designed to access oxidation states available to the metal clusters of nitrogenase in the 0 - 6 equivalent oxidized range. At no time was sufficient oxidant added to create the 3-equivalent-oxidized P-cluster species P^{3+}, and the previously mentioned S = 1/2 and S = 7/2 EPR signals assigned to P^{3+} were not observed in these experiments.[11,12]

5.4 Results

Figure 5.1 shows EPR spectra of 2-equivalent-oxidized (A), and as-isolated Av1 (B). Both spectra show the typical S = 3/2 FeMo cofactor signal, but the spectrum of 2-equivalent-oxidized Av1 also shows inflections in the g = 2 and the g = 5 - 8 regions which are not observed in the as-isolated Av1 spectrum. These inflections attain maximum amplitude in the 2-equivalent-oxidized samples of Av1, and are abolished by the 4-equivalent-oxidized step.

Figure 5.2 is an EPR spectrum of the g = 2 region of 2-equivalent-oxidized Av1, showing, inflections at g = 2.06, 1.95, 1.89, and 1.82. The inflections at g = 2.06, 1.95, and 1.82 exhibit similar saturation behavior and amplitude variation, and may be assigned to the same signal, which arises from an S = 1/2 spin state. This signal is reminiscent of the S = 1/2 EPR signals of reduced ferredoxins, which arise from FeS clusters.[16] It also exhibits power saturation behavior that is typical of these species, saturating very easily at low (< 5 K) temperature. As mentioned previously, observation of a similar signal has been reported by other investigators in thionine oxidized Av1[13] and $K_3Fe(CN)_6$ oxidized Kp1.[14] The small inflection at g = 1.89 will be discussed below.

EPR spectra of the g = 5 - 8 region recorded at (A) 15 K and (B) 8 K of 2-equivalent-oxidized Av1 are shown in Figure 5.3. Inflections are apparent at g = 6.67, 7.3, and 5.30 in spectrum A, which are diminished in amplitude in spectrum B. Since spectrum A was recorded at 15 K and B recorded at 8 K, it may be concluded that these inflections arise from an excited state. The

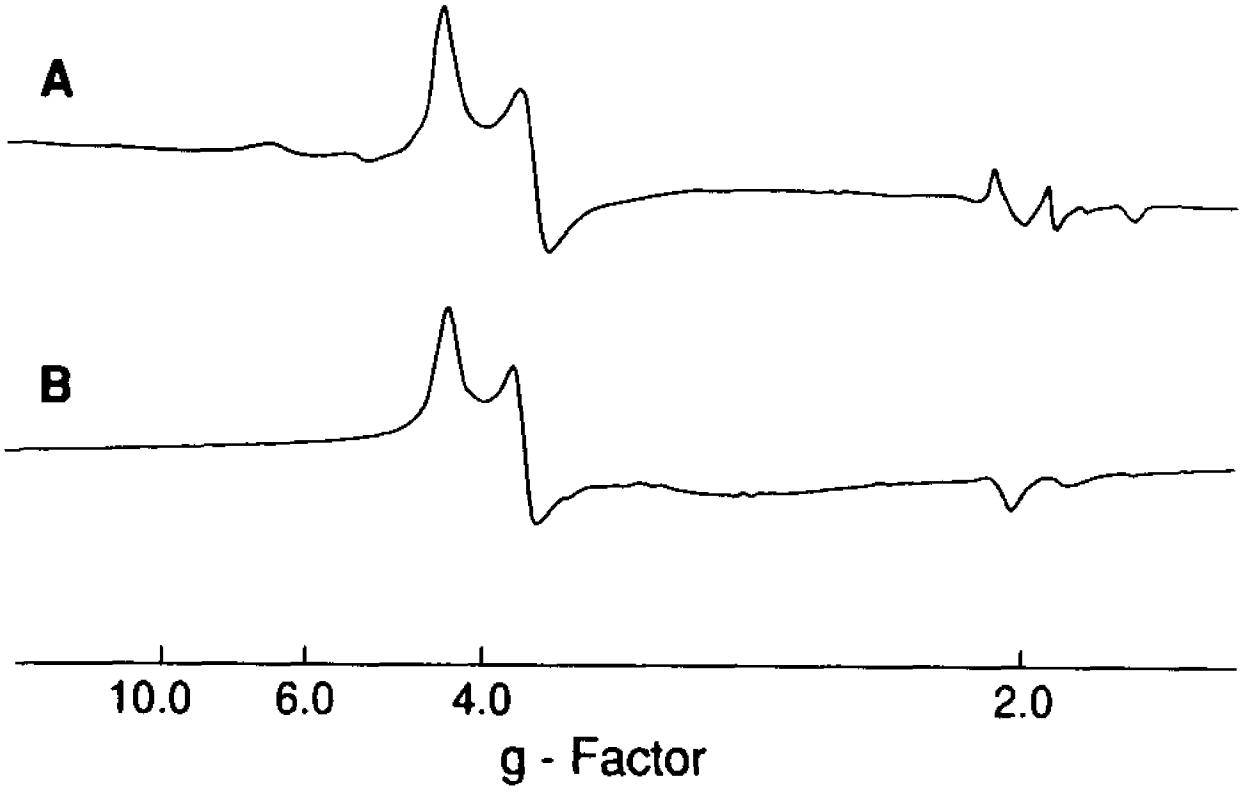

Figure 5.1. EPR spectra of (A) two-equivalent oxidized and (B) as-isolated Av1. Spectra have been normalized for spectrometer gain and protein concentration. EPR spectrometer conditions: microwave frequency, 9.45 GHz, modulation frequency, 100 kHz, modulation amplitude, 1.25 mT; microwave power, 20 mW, temperature, 15 K.

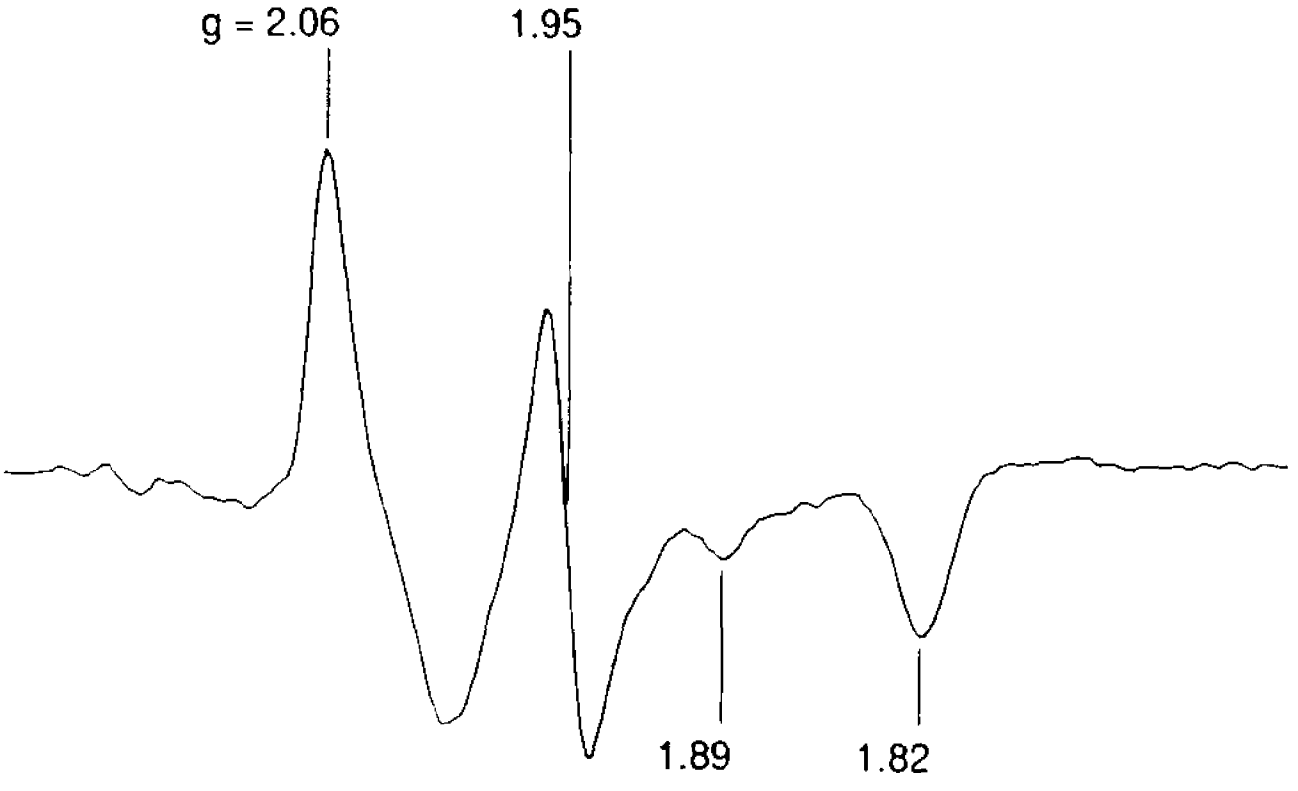

Figure 5.2. EPR spectrum of the $g = 2$ region of two-equivalent oxidized Av1. The signals at $g = 2.06$, 1.95 and 1.82 are assigned to the same $S = 1/2$ spin state. The signal at $g = 2.01$ is the high-field inflection the $S = 3/2$ FeMoco signal of Av1. The origin of the small inflection at $g = 1.89$ is unknown (see text). EPR spectrometer conditions: microwave frequency, 9.45 GHz; modulation frequency, 100 kHz; modulation amplitude, 1.25 mT; microwave power, 20 mW; temperature, 15 K.

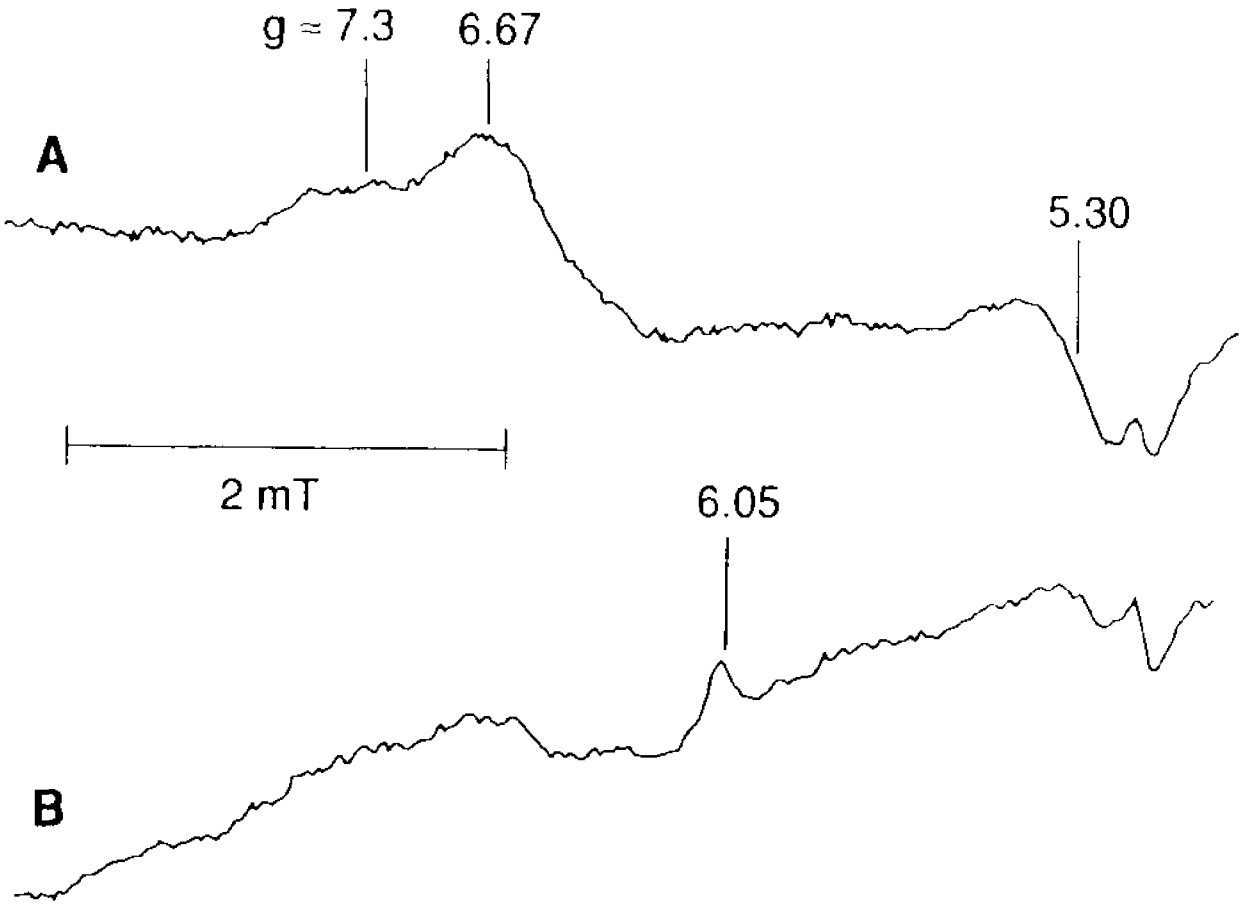

Figure 5.3. EPR spectra of the g = 5-8 region of two-equivalent oxidized Av1 at (A) 15 K and (B) 8 K. The signals at g = 6.67 and 5.30 are assigned to the same S = 5/2 spin system, while the signal at $g \approx 7.3$ may arise from another S = 5/2 spin state. The increased amplitudes of these proposed S = 5/2 signals at 15K indicate that they are excited states. The small inflection at g = 6.05 in (B) is probably the excited state transition ($|\pm 3/2\rangle$) of the S = 3/2 FeMoco spin manifold

absorbance shaped inflection at g = 6.67 and the derivative-shaped inflection at g = 5.30 were assigned to the $|\pm 1/2\rangle$ doublet of an inverted S = 5/2 spin system with $\lambda = |E/D| \approx 0.029$ (where D and E are the axial and rhombic zero field splitting parameters, respectively) using "RHOMBO" (Figure 5.4; also, see Materials and Methods), which was donated to us by Professor W. R. Hagen.[9] A predicted third inflection at g = 1.97 was not observed. This inflection may have been obscured by the g = 2.0 inflection of the S = 3/2 FeMo cofactor signal, or it may be unobservable due to g-strain line broadening.[9] There was no spectral evidence of any transition within the $|\pm 3/2\rangle$ or $|\pm 5/2\rangle$ doublets of the S = 5/2 system with g = 6.67 and g = 5.30. Inflections predicted at g = 5.97, 0.68, and 0.70 for the $|\pm 3/2\rangle$ doublet and g = 0.006, 0.006, and 9.99 for the $|\pm 5/2\rangle$ doublet were not observed at any temperature. The transition probability within these doublets is essentially zero, due to relatively low rhombicity and large g-factor anisotropy.[9]

The inflection at $g \approx 7.3$ may be tentatively assigned to the low field resonance of another S = 5/2 spin system. Unequivocal assignment of a spin state is impossible when only one spectral line is observed. The $g \approx 7.3$ inflection may possibly arise from the $|\pm 1/2\rangle$ doublet of an S = 5/2 spin system. It is an absorbance-shaped inflection, and therefore is most likely the extreme low-field inflection of a spin system with $S \geq 5/2$. If, in fact, the $g \approx 7.3$ signal does arise from the $|\pm 1/2\rangle$ doublet of an inverted S = 5/2 signal, two other inflections, one at g = 4.3, and one at g = 1.89 are predicted. The

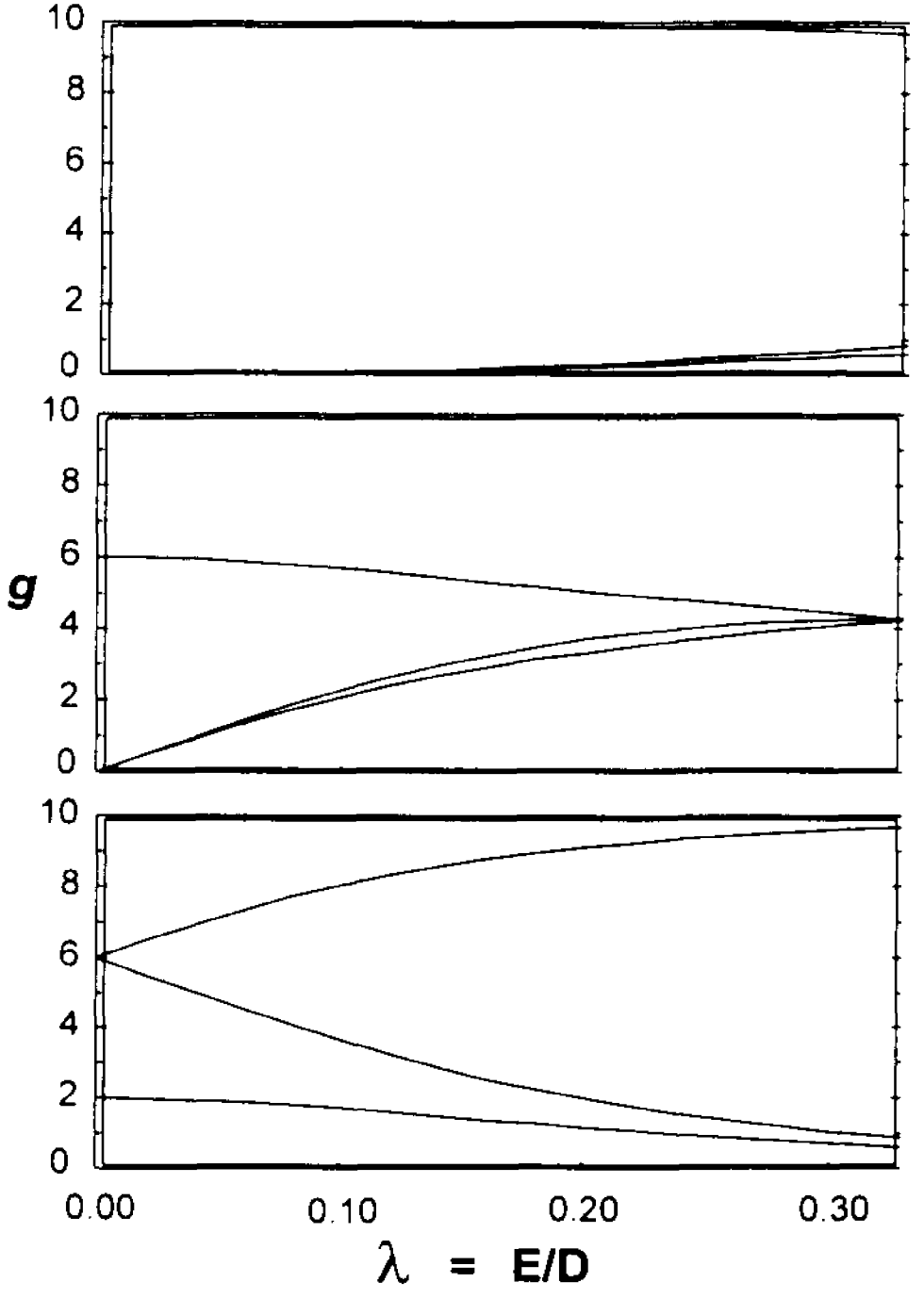

Figure 5.4. "Rhombogram" calculated for an S = 5/2 spin system. Dashed lines indicate predicted *g*-factors for the signals at $g = 6.67$ and $g = 7.3$. The doublets are: (top), $|\pm 5/2\rangle$; (middle), $|\pm 3/2\rangle$; (bottom), $|\pm 1/2\rangle$. The spin system discussed in the text is "inverted", i.e., the $|\pm 1/2\rangle$ doublet is the excited state.

predicted inflection at g = 4.3 was not observed, and could have been obscured by the dominant line of the S = 3/2 FeMoco signal at g = 4.3. A sharp inflection was observed at g = 1.89. It is unlikely that this feature arises from the same spin state as the g = 7.3 inflection, since it is sharper than the inflection at g = 7.3. High field inflections in the EPR spectra of transition metal clusters and complexes often show g-strain broadening, and are rarely sharper than the corresponding low-field inflections.[9] No signals were observed that could be assigned to predicted transitions within the $|\pm 3/2\rangle$ and $|\pm 5/2\rangle$ doublets of the S = 5/2 spin system. Lines predicted at g = 10, 0.023, and 0.024 for the $|\pm 5/2\rangle$ doublet would be unobservable due to low transition probability, and predicted lines at g = 5.9, 1.3, and 1.4 arising from the $|\pm 3/2\rangle$ doublet also have a relatively low transition probability. Assignment of the g = 7.3 inflection to higher spin states, such as S = 7/2 or S = 9/2 is doubtful, because an observable line at g = 7.3 would lead to the prediction of other observable lines arising from other doublets in the spin system, and none were observed at any temperature. Exact assignment of the g = 7.3 signal is impossible considering the limited available data, but it should be stressed that an unequivocal assignment of S is not absolutely required to propose a logical model for P-cluster oxidation.

The S = 5/2 signals arise from excited states, as determined by temperature-dependent depopulation experiments. The signals were integrated by the method of Aasa and Vänngård.[17] Integrated signal areas

were multiplied by the absolute temperature for Curie law correction. Since the signals at g = 6.67 and g = 7.3 overlap, a perpendicular line was constructed from the baseline to the minimum between the peaks to separate the two areas, and then each was integrated. This has the obvious effect of cutting off the low-field wing of the g = 7.3 inflection and the high-field wing of the g = 6.67 inflection, possibly introducing serious inaccuracy in the integrations. Although the absolute integrated areas of the two S = 5/2 signals are probably inaccurate, their relative integrated areas are quite dependable. Temperature-dependent depopulation data was fitted to the Boltzmann distribution expression for the intensity of an EPR signal arising from the $|\ \pm 1/2\ \rangle$ doublet of an inverted S = 5/2 spin system. The expression used was:

$$AT = e^{-6D/kT} / (1 + e^{-2D/kT} + e^{-6D/kT})$$

where A is the signal area, T is the absolute temperature, D is the axial zero-field splitting parameter, and k is the Boltzmann constant. Curve fits of the experimental data in the 0 - 25 K temperature range yielded D = -3.2 ± 0.2 cm^{-1} for the g = 6.67 signal and D = 3.2 ± 0.2 cm^{-1} for the g = 7.3 signal. Line broadening made integration impossible for temperatures above 25 K. The uncertainties expressed are calculated standard deviations for the curve fits.

A weak low-field EPR signal appeared at g = 11.6 as the titration proceeded, and gained maximal amplitude at the 4-equivalent-oxidized step of the titration. This is shown in Figure 5.5. The g = 11.6 signal remained at full amplitude after ≥ 6 electrons were removed by thionine titration, at which point

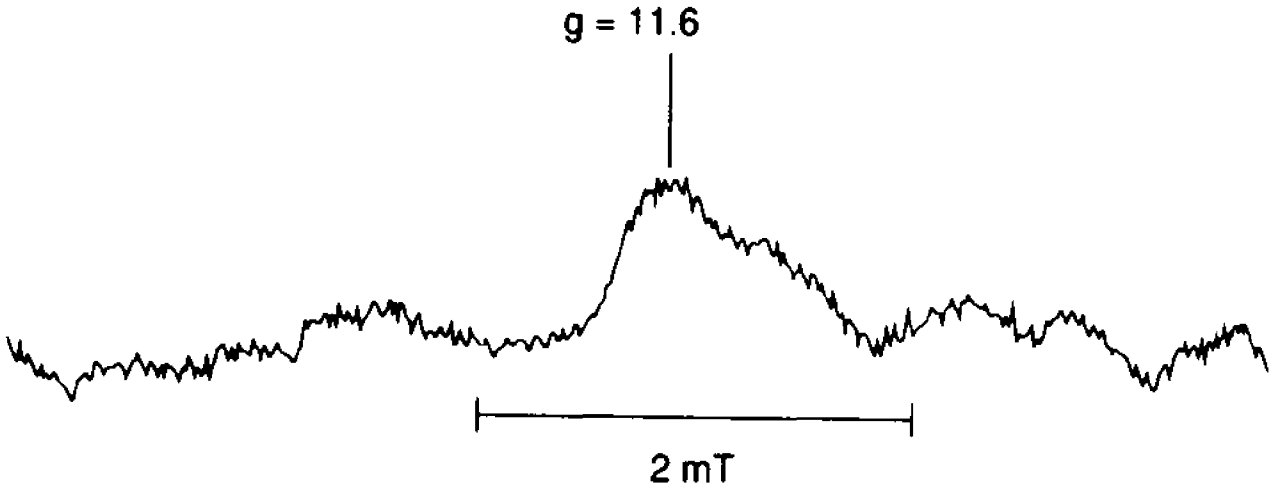

Figure 5.5 EPR spectrum of the g = 11 region of four-equivalent oxidized Av1. The spectrum has been corrected by subtraction of a sloping baseline. EPR spectrometer conditions: frequency, 9.45 GHz; modulation frequency, 100 kHz; modulation amplitude, 1.25 mT; microwave power, 50 mW; temperature, 15 K.

the S = 3/2 cofactor signal is entirely abolished. As mentioned above, an integer-spin (proposed S = 3) signal assigned to P^{2+} with g = 11.9 has been observed in previous parallel-mode EPR studies of oxidized Av1.[9-11] Perpendicular-mode EPR studies of the same species have revealed a signal at g = 11.6 ± 0.4 that is very similar to the one shown in Figure 5.5.[11] The signal arises from an excited state, as verified by temperature studies, in agreement with the reports cited above. Also, oxidative titration with excess indigodisulfonate can induce this signal, while the S = 3/2 FeMoco signal remains unaffected, thus supporting the proposal that it arises from the P^{2+} species.

Population corrected maximum signal areas assigned to the different P-cluster oxidation states expressed as a percentage of the S = 3/2 cofactor signal in the same sample are shown in Table 5.1. D values for population correction were experimentally determined by us (D = -3.2 ± 0.02 cm^{-1} for both S = 5/2 signals), or obtained from the literature[4] (D = 5.1 cm^{-1} for the S = 3/2 FeMoco signal). The relative intensity of of the absorbance shaped integer-spin signal at g = 11.6 was determined by single integration, but could not be compared directly to the the S = 3/2 FeMoco signal, since the g = 11.6 signal arises from an integer spin system observed by perpendicular-mode EPR.

5.5 Discussion

Figure 5.6 shows the relative integrated areas of the EPR signals arising from the the S = 1/2, S = 5/2, and S = 3 P-cluster signals normalized to

Table 5.1 EPR parameters of oxidized metal centers in Av1

Identity	Spin State	g_x	g_y	g_z	D (cm-1)	$\|E/D\|$	Maximum % per M-center
P+	S = 1/2	2.06	1.95	1.82	---	---	8 ± 2[a]
P+	S = 5/2	[b]6.67	5.30	[c](1.97)	- 3.2 ± .2[a]	.029	29 ± 6
P+	S = 5/2	[b]7.3	(4.6)	[d](1.9)	- 3.2 ± .2	.059	34 ± 5
M center	S = 3/2	6.05	[e](< .5)	[e](< .5)	---	---	--
[f]P2+	S = 3	---	---	11.6	---	---	---
[g]P3+	S = 7/2	[b]10.4	5.5	(1.8)	- 3.7	.043	65 ± 10
[g]P3+	S = 1/2	1.97	1.88	1.68	---	---	12.5 ± 1.5

[a]Uncertainties are calculated standard deviations among data sets [b]g-factors listed arise from the $|\pm 1/2\rangle$ doublet [c]g-factors predicted but not observed are in parentheses. [d]See text [e]Out of range of spectrometer [f]Refs 9, 10, 11 [g]Refs 11,12

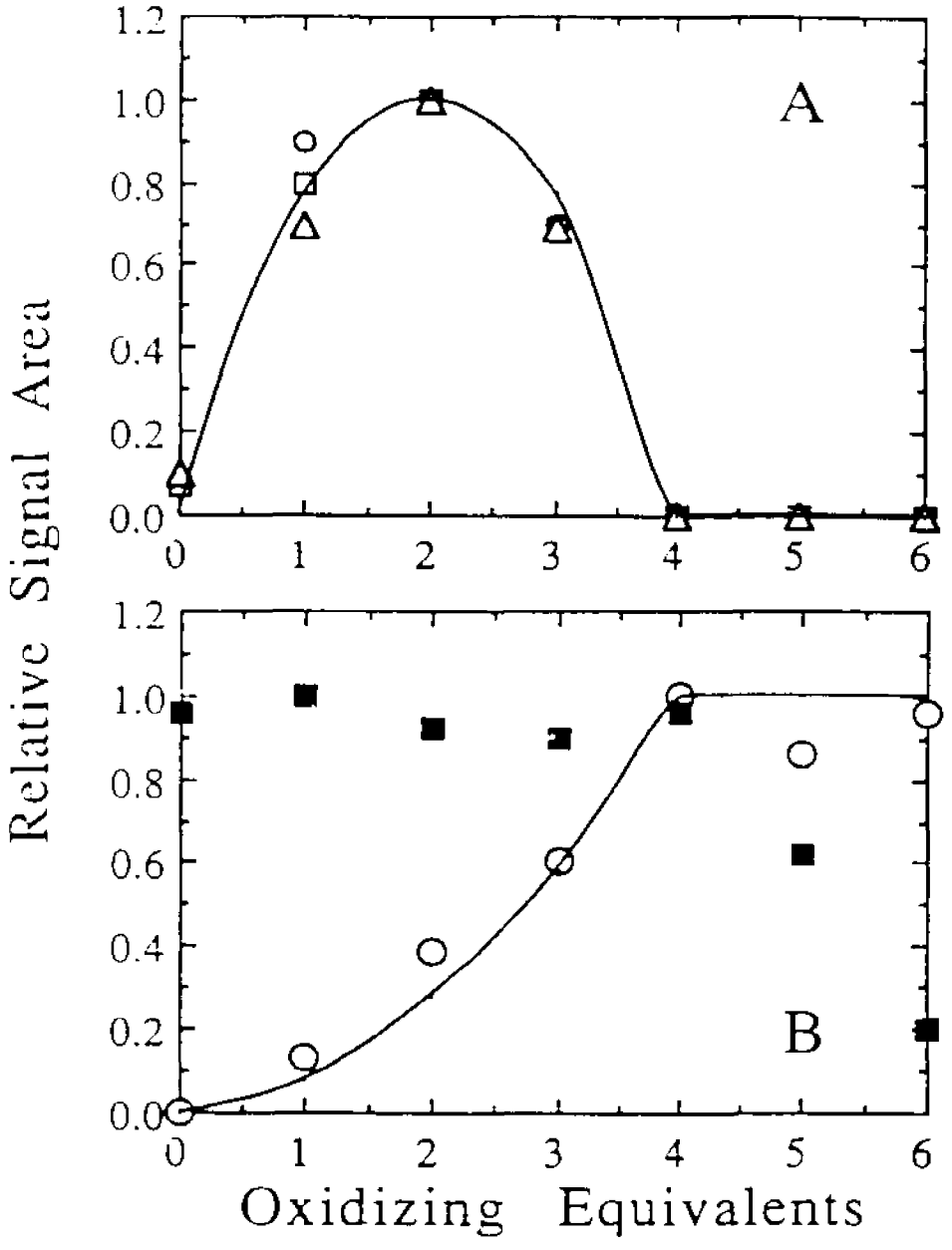

Figure 5.6 Relative EPR spectral areas for (A) half-integer (S = 5/2, 1/2) and (B) integer (S = 3) spin states. In (A), relative spectral areas of the S = 5/2 with g = 7.3 (Δ), S = 5/2 with g = 6.67 (O), and S = 1/2 (□) are plotted as a function of oxidizing equivalents. The relative spectral areas of the S = 3/2 FeMoco signal (■) and the S = 3 signal (O) with g = 11.6 are plotted in (B). Theoretical plots are also shown (——) predicting the relative spectral amplitudes of both the half-integer (S = 5/2, 1/2, arising from P^{+}) and integer (S = 3, arising from P^{2+}) signals

maximal area for each signal, along with the S = 3/2 FeMoco signal, plotted as a function of oxidizing equivalents. The S = 1/2 and both S = 5/2 P^{+} signals attain maximum area at 2 oxidizing equivalents, while the S = 3 P^{2+} signal attains maximum area at 4 oxidizing equivalents. Note that the half-integer P^{+} signals have been completely removed at the point in the oxidation (4 equivalents oxidized) that the P^{2+} integer-spin signals attain maximal amplitude. Also, the S = 3/2 cofactor signal remains essentially constant until after the 4th equivalent of oxidant, in agreement with previously reported Mössbauer results which indicate that the first 4 equivalents of oxidant go to oxidize the P-clusters.[6]

The relative spectral intensities shown in Figure 5.6 suggest a possible model for P-cluster oxidation. It appears that the P-clusters in Av1 oxidize 1 equivalent at a time, and the first oxidizing equivalent gives rise to the S = 5/2 and S = 1/2 species, which may be assigned to P^{+}. The next oxidizing equivalent creates the P^{2+} species, from which we observe the integer-spin EPR signal at g = 11.6. The signals arising from the P^{+} and P^{2+} states maximize at 2 and 4 oxidizing equivalents, respectively, because there are 2 P-clusters per Av1 molecule. This behavior is strikingly similar to earlier results reported from this laboratory which show a non-linear change in the relaxation time of the S = 3/2 cofactor signal as a function of oxidizing equivalents in the 0-4 equivalent range.[15] This change in the relaxation behavior of the S = 3/2

cofactor signal is most likely due to magnetic interaction of the cofactor spin-system with the paramagnetic P-cluster species P^{+}.

A simple theoretical model may be proposed to explain the oxidation behavior of the P-clusters and to simulate the observed spectral data. A similar model was previously proposed to model the change in relaxation behavior of the S = 3/2 FeMoco signal during oxidative titration.[15] The model is constructed with the following constraints: (1) The first 4 electrons removed in the oxidative titration are taken from the P-clusters. (2) There are 4 equivalent sites (2 on each P-cluster) from which 1 electron can be removed during the initial oxidation. (3) In a titration with limiting thionine solution, each site can only be oxdized by 1 equivalent, resulting in P^{+} (1 site oxidized), or P^{2+} (2 sites oxidized), but not P^{3+} (which is unattainable at the thionine concentrations that were used). (4) If 2 sites on the same P-cluster are oxidized, they interact magnetically.[15] (5) The P-cluster oxidation is completely random. Any site is just as likely to be oxidized by 1 equivalent as any other, even if the other site on the same P-cluster has already been oxidized. (6) If one site on a P-cluster is oxidized (P^{+}), it becomes paramagnetic with a half-integer spin. (7) When both sites on the same P-cluster are oxidized (P^{2+}), the sites interact magnetically and give rise to an integer-spin state.[9-11] This model is not able to distinguish between different S = n/2 spin states, but it can predict the occurrence of integer and half-integer spin states as the oxidative titration proceeds.

The intensity variation of the P^+ half-integer and P^{2+} integer spin EPR signals may be modeled using the following equation:

$$(Ox)^4 + 4(Ox)^3(Red) + 6(Ox)^2(Ox)^2 + 4(Ox)(Red)^3 + (Red)^4 = 1$$

where the fraction of sites oxidized is given by Ox = n/4 with $4 \geq n \geq 0$ and n is the number of oxidizing equivalents. It follows that the fraction of sites reduced may be represented by Red = (1 - n/4). Using this equation, the fraction of Av1 proteins in the various oxidation states may be calculated as the titration proceeds. For example, $(Ox)^4$ represents the fraction of Av1 molecules with all 4 available sites oxidized, while the term $6(Ox)^2(Ox)^2$ represents the fraction with 2 sites oxidized and 2 reduced. The binomial coefficients for each term represent the degeneracies of the various possible redox states; i.e., there are 6 ways to oxidize the 4 sites in Av1 by 2 equivalents, which is the state defined by the term $6(Ox)^2(Ox)^2$. The equation was used to calculate the relative populations of half-integer and integer spin species as the oxidative titration proceeded in a step-wise fashion, and the contributions from each term to integer and half-integer spin states were tabulated. The results of the calculation, normalized to maximal amplitude, are shown as the solid lines in Figure 5.6. The theoretical model gives a reasonable fit to the experimental data, and predicts the relative amplitudes of integer and half-integer spin EPR signals quite well.

Unfortunately, the theoretical model is not as accurate in predicting absolute spectral areas. The model predicts that the maximum attainable area

for the half-integer spin species arising from P^+ occurs at 2 oxidizing equivalents, in agreement with experiment, but that the area only attains 44% of the area of the S = 3/2 FeMoco EPR signal. Examination of Table 5.1 reveals that the sum of the areas of the EPR signals of half-integer spin species assigned to P^+ is 71 ± 8%, which is greater than predicted. There are several possible sources of error that may have contributed to this deviation. First, spin quantitation of small amplitude overlapping signals is extremely difficult, and significant error (more than the reported error for the integrations of the S = 5/2 signals, which is the standard deviation of the mean among data sets) may have been introduced in integration of the S = 5/2 EPR signals. Also, as was stated previously, assignment of the g = 7.3 inflection to an S = 5/2 spin system is tentative at best, since only one spectral inflection was observed. The assignment is plausible, for reasons previously stated, but certainly not definitive. Furthermore, integration by the method of Aasa and Vänngård requires knowledge of all of the g-factors of an EPR spectrum.[17] If, in fact, the assignment is incorrect and the g = 7.3 signal arises from some spin state other than S = 5/2, then it follows that the g-factor assignment is incorrect, the determination of D is incorrect, the population correction is in error, and thus the integrated area is incorrect. The assignment of the g = 6.67 and g = 5.30 signals to an S = 5/2 spin system is much more reliable since 2 predicted g-factors were observed. Finally, the model assumes random statistics, meaning that the probability of the $P \rightarrow P^+$ oxidation is the same as the $P^+ \rightarrow P^{2+}$

oxidation. This may not be the case, although the fit of the experimental data to the theoretical model indicates that the two probabilities are similar. If, for example, they were very different and P^+ was strongly favored, then all of the P^+ would be created before any of the P^{2+}. This was not the case, as is readily apparent upon examination of Figure 5.6. It appears that the most significant source(s) of error are the assignment of the g = 7.3 signal and the integration of the g = 6.67 and g = 7.3 signals.

The EPR data indicates that P^+ gives rise to at least two, and possibly three, different spin states. Mixed spin states in transition metal clusters are not unprecedented. In fact, the nitrogenase component 2 protein, which contains an Fe_4S_4 cluster, exhibits mixed-spin EPR spectra with an S = 3/2 and S = 1/2 signal which are apparently at equilibrium.[18-20] In the case of Av2, the mixed spin state may be due to conformational differences in the cluster and/or the polypeptide ligands binding the cluster, since the equilibrium between the two spin states can be shifted by changing the solvent.[18-20] If we view P^+ in this manner, then the paramagnetism of the 1-equivalent oxidized cluster could be delocalized upon the entire double-cubane cluster, and conformational differences stabilize the various possible spin states. The second oxidation step would then create P^{2+}, which would exhibit the integer spin EPR signal at g = 11.6. Alternatively, if we think of the P-cluster as a double-cubane structure, consisting of two Fe_4S_4 oxidation sites, then the P^+ species would be formed by oxidation of one or the other cubane. Oxidation of the second cubane in the P-

cluster would give rise to a second paramagnetic species which would couple with the first to form the integer-spin species, giving rise to the P^{2+} signal at g = 11.6. In this case, formation of P^{2+} occurs by two separate oxidations of P-cluster halves, which may explain why the oxidations $P \rightarrow P^{+}$ and $P \rightarrow P^{2+}$ appear to be equally probable.

In conclusion, it has been demonstrated that the P-clusters of Av1 may be oxidized 1 equivalent at a time to form the species P^{+}, which gives rise to S = 1/2 and proposed S = 5/2 spin states that are observable by EPR spectroscopy. The second oxidizing step forms P^{2+}, an integer-spin (proposed S = 3) species observable in parallel[9-11] and perpendicular mode[11] EPR. A theoretical model which assumes equal probability for both oxidation steps gives a reasonable fit to the experimental data, supporting the assertion that the P^{2+} species is ultimately formed by two single equivalent oxidations of the P-clusters, one equivalent at a time. It remains to be shown if any of the P^{ox} states are relevant to the physiological function of Av1.

References

1. Kim, J.; Rees, D. C. *Science* **1992**, *257*, 1677-1682.
2. Chan, M. K.; Kim, J.; Rees, D. C. *Science* **1993**, *260*, 792-794.
3. Kim, J.; Rees, D. C. *Nature* **1992**, *360*, 553-560.
4. Münck, E.; Rhodes, H.; Orme-Johnson, W. H.; Davis, L. C.; Brill, W. J.;Shah,V. K. *Biochim. Biophys. Acta.* **1975**, *400*, 32-53.
5. Mortenson, L. E., Zumft, W. G., Palmer, G., *Biochim. Biophys. Acta*, **1973**, *292*, 422-435.

6. Zimmermann, R.; Münck, E.; Brill, W. J.; Shah, V. K.; Henzl, M. T.; Rawlings, J.; Orme-Johnson, W. H. *Biochim. Biophys. Acta.* **1978**, *536*, 185-207.

7. Johnson, M. K.; Thomson, A. J.; Robinson, A. E.; Smith, B. E. *Biochim. Biophys. Acta.* **1981**, *671*, 61-70.

8. Morningstar, J. E.; Johnson, M. K.; Case, E. E.; Hales, B. J. *Biochemistry* **1987**, *26*, 1795-1800.

9. Hagen, W. R. In *Advances in Inorganic Chemistry: Iron-Sulfur Proteins*; A. G. Sykes and R. Cammack, Ed.; Academic Pres: 1992; Vol. 38; pp 165-222.

10. Surerus, K. K.; Hendrich, M. P.; Christie, P. D.; Rottgardt, D.; Orme-Johnson, W. H.; Münck, E. *J. Am. Chem. Soc.* **1992**, *114*, 8579-8590.

11. Pierik, A., J.; Wassink, H.; Haaker, H.; Hagen, W. R. *Eur. J. Biochem.* **1993**, *212*, 51-61.

12. Hagen, W. R.; Wassink, H.; Eady, R. R.; Smith, B. E.; Haaker, H. *Eur. J. Biochem.* **1987**, *169*, 457-465.

13. Orme-Johnson, W. H.; Paul, L.; Meade, J.; Warren, W.; Nelson, M.; Groh, S.; Orme-Johnson, N. R.; Münck, E.; Huynh, B. N.; Emptage, M.; Rawlings, J.; Smith, J.; Roberts, J.; Hoffmann, B.; Mims, W. B. In *Current Perspectives in Nitrogen Fixation*; A. H. Gibson and W. E. Newton, Ed.; Elsevier, North-Holland, New York: 1981; pp 79-84.

14. Smith, B. E.; Lowe, D. J.; Chen, G.-X.; O'Donnell, M. J.; Hawkes, T. R. *Biochem. J.* **1983**, *209*, 207-213.

15. Oliver, M. E.; Hales, B. J. *J. Am. Chem. Soc.* **1992**, *114*, 10618-10623.

16. Sweeney, W. V.; Rabinowitz, J. C. In *Annual Review of Biochemistry*; E. Snell E., P. D. Boyer, A. Meister and C. Richardson, Ed.; Annual Reviews, Inc.: Palo Alto, CA, 1980; Vol. 49; pp 139-161.

17. Aasa, R.; Vänngård, T. *J. Magn. Reson.* **1975**, *19*, 308-315.

18. Lindahl, P. A.; Day, E. P.; Kent, T. A.; Orme-Johnson, W. H.; Münck, E. *J. Biol. Chem.* **1985**, *260*, 11160-11173.

19. Hagen, W. R.; Eady, R. R.; Dunham, W. R.; Haaker, H. *FEBS Lett.* **1985**, *189*, 250-254.

20. Watt, G. D.; McDonald, J. W. *Biochemistry* **1985**, *24*, 7226-7231.

Chapter 6 Oxidative Titration of the Enzymatically Reduced VFe Protein of *Azotobacter vinelandii*

6.1 Introduction

Azotobacter vinelandii expresses an alternative form of nitrogenase with V replacing Mo as the M-center heteroatom in the component 1 protein (Av1').[1-3] The vanadium system expresses a distinct component 2 protein (Av2') which appears to be very similar in structure to Av2. Although crystallographic data is not available for Av1', amino acid sequence homology,[4] metal analysis,[3] EXAFS spectroscopy,[5-8] and Mössbauer spectroscopy[9,10] indicate striking similarities to Av1. EXAFS and Mössbauer studies of Av1' have yielded spectra that are very similar to those observed in studies of Av1, strengthening the proposal that Av1 and Av1' have virtually identical metal cluster composition.

In Chapter 5, an oxidation study of the MoFe nitrogenase of Azotobacter vinelandii was presented and a simple probability model was proposed to model P-cluster behavior during oxidative titrations, as monitored by EPR spectroscopy. It was demonstrated that the P-clusters in Av1 could be oxidized by one equivalent to form the paramagnetic species P^+, with spin states of S = 5/2 and S = 1/2. EPR signals arising from these paramagnetic species attain maximal area at the 2-equivalent oxidized step of the titration, and disappear by the 4-equivalent oxidized step. During the initial steps of the titration a low field signal at g = 11.6 grows in, attaining maximum amplitude at 4-oxidizing equivalents. This signal was previously assigned to an integer spin system (S

= 3) in P^{2+}, the two equivalent oxidized P-cluster[11-13]. The variation of the relative EPR signal areas of the S = n/2 (P^{+}) and S = 3 (P^{2+}) species gives a reasonable fit to the proposed random probability model for P-cluster oxidation. The reduction of dinitrogen to ammonia is a redox process, so an understanding of the possible redox states available to the nitrogenase metal clusters may be fundamental to elucidating the mechanism of nitrogenase catalysis.

To better understand the analogous oxidation states of the metal clusters in V-nitrogenase, an EPR spectroscopic study of the oxidative titration of V-containing Av1' was conducted. In the as-isolated state, the vanadium cofactor (M-center) of Av1' is similar to the M-center of Av1 in that it is a paramagnetic, EPR-active species with $S = 3/2$.[3,14] Unlike the spectrum of Av1, the EPR spectrum of as-isolated Av1' contains an additional axial $S = 1/2$ signal which has not been unequivocally assigned. As-isolated Av1' also displays $S = 5/2$ EPR signals very similar to those associated with the 1-equivalent oxidized P-cluster (P^{+}) in Av1[15]. These P^{+} signals can be removed by enzymatic reduction of Av1' without change to the $S = 3/2$ vanadium cofactor signal, thus demonstrating that the P-clusters may be reduced enzymatically by Av2'. Oxidative titrations of enzymatically reduced Av1' reveal the concurrent oxidation of both clusters in this protein compared to the consecutive oxidation observed with Av1.

A novel form of Av1', called $Av1'_A$, has recently been isolated and characterized in this laboratory.[16] $Av1'_A$ appears to be an $\alpha\beta_2$ trimer containing only one M-center, one complete P-cluster and an additional Fe_4S_4 cluster. In its as-isolated state, $Av1'_A$ exhibits an EPR spectrum very similar to the tetrameric form of Av1' mentioned above (now called $Av1'_B$), and is similarly enzymatically reducible, resulting in EPR-silent P-clusters. However, the oxidation behavior of enzymatically reduced $Av1'_A$, as observed by EPR spectroscopy, is strikingly different from that of $Av1'_B$. We believe that we observe a redox gating of electron flow in $Av1'_A$ where a redox-induced conformational change in $Av1'_A$ produces an intramolecular electron transfer from reduced P-clusters to oxidized M-centers, an event that may be fundamental to the catalytic role of nitrogenase.

6.2 Experimental

Vanadium-containing nitrogenase was purified from the LS-15 mutant strain of *Azotobacter vinelandii* using a variation of previously published methods[17] modified[16] to separate forms $Av1'_A$ and $Av1'_B$. The specific activity of purified VFe protein (Av1'), as determined by acetylene reduction assay, ranged from 200-260 nmol C_2H_2 reduced $min.^{-1}$ mg^{-1} protein. All purification steps were conducted under anaerobic conditions in the presence of 2 mM sodium dithionite. Protein concentration was determined by the Biuret method. Purified protein was frozen and stored in liquid nitrogen.

The metal clusters of Av1' were reduced enzymatically to their "native" forms prior to performing oxidative titrations. This reduction was effected by incubating Av1' with Av2' in the presence of Mg-ATP and sodium dithionite. The reduction reaction mixtures consisted of Av1' and Av2' in a 20:1 molar ratio, Mg-ATP in 20-fold molar excess to Av1', and a 50-fold molar excess of sodium dithionite in 0.025 M Tris-HCl pH 7.4 with 0.1M NaCl. The enzymatic reduction was conducted at ambient temperature in a Vacuum Atmospheres glove box under an Ar atmosphere with $[O_2] < 2$ ppm. The enzymatic reaction was allowed to go to completion (20 min) after which the excess sodium dithionite and Mg-ADP were removed by gel filtration with Sephadex G-25, using the same buffer (without sodium dithionite) as the eluent. The eluted protein fractions were monitored for residual sodium dithionite with methyl viologen indicator. Final concentration of Av1' ranged from 13-25 mg/ml.

Oxidative titrations were performed using solutions of thionine (Eastman) or indigosulfonate (ICN), which were prepared in anaerobic 0.025 M Tris-HCl pH 7.4 with 0.1 M NaCl, and filtered with 0.2-μm syringe filters to remove any undissolved oxidant. Using the procedure established for oxidative titration of the MoFe protein,[15,18,19] reduced Av1' was divided into equal aliquots which were titrated to endpoint, as indicated by persistent color of the oxidant. After establishing the volume of oxidant necessary to reach the endpoint, separate aliquots of protein were titrated incrementally with smaller volumes of oxidant calculated to assure that there would be at least 6 equal steps before reaching

the apparent endpoint. Titrations were carried past the observed endpoint, to assure maximum oxidation of the metal centers. Titrated samples were allowed to equilibrate for at least 30 min. before loading into quartz EPR tubes and freezing in liquid nitrogen. For reference, aliquots of untitrated reduced protein were similarly allowed to stand in the glove box for the duration of the titration procedure, loaded into EPR tubes and frozen simultaneously with the titrated samples.

EPR spectra were recorded on a computer-interfaced Bruker 300D spectrometer with ESP 200 data collection software. The instrument was fitted with a TE_{102} perpendicular-mode cavity resonating at X-band frequencies. An Oxford Instruments ESR-900 helium flow cryostat was used to generate low temperatures. Temperature was monitored and controlled with an Oxford Instruments ITC-4 temperature controller connected to an FeAu/chromel thermocouple positioned directly below the sample tube.

Values for *D* (the axial zero field splitting parameter) were determined by curve fitting Boltzmann distribution expressions for the relative populations of the doublets in question to Curie law corrected spectral areas recorded in temperature-dependent depopulation experiments. The expressions used were: $AT = e^{-6D/kT}/(1 + e^{-2D/kT} + e^{-6D/kT})$ and $AT = e^{-3.5D/kT}/(1 + e^{-3.5D/kT} + e^{-7D/kT})$ for the $|\pm 1/2\rangle$ doublet of the inverted $S = 5/2$ system and the $|\pm 3/2\rangle$ doublet of the rhombic $S = 5/2$ spin system, respectively, where *A* is the integrated signal area, T is the absolute temperature and *k* is the Boltzmann

constant. EPR spectral assignments were done using "RHOMBO", which was supplied to us by Professor W. R. Hagen.[21]

6.3. Results

Prior to performing a controlled oxidative titration of a multi-cluster protein, it is imperative that all of the clusters be fully reduced. However, recent Mössbauer studies of as-isolated Av1' have indicated the presence of oxidized P-clusters.[9] This situation can be contrasted to that of the MoFe protein (Av1) under the same conditions where both cluster types exist only in their reduced native (P and M) forms.[10] Mössbauer spectroscopy has also demonstrated that full reduction of the Av1' clusters to their P and M states occurs following the limited enzymatic reduction (described above) without any of the M-centers existing in the "super-reduced" M^- state.[9]

The presence of oxidized P-clusters in as-isolated Av1' can also be detected in the EPR spectrum of this protein. Previous oxidative titrations of Av1 strongly suggest that singly oxidized P-clusters (P^+) give rise to $S = 1/2$ and $S = 5/2$ EPR signals that reach maximal amplitude at 2 oxidizing equivalents per protein.[15] Figure 6.1 compares the EPR spectra in the $g = 3$-12 region of as-isolated $Av1'_B$, enzymatically reduced $Av1'_B$, and 2-equivalent thionine oxidized Av1. The difference spectrum (Fig. 6.1C) of as-isolated (Fig. 6.1A) minus enzymatically reduced $Av1'_B$ (Fig. 6.1B) reveals a broad inflection at $g = 4.3$ and inflections at $g = 6.67$ and 5.2. We have observed these inflections in numerous difference spectra and do not feel that they are

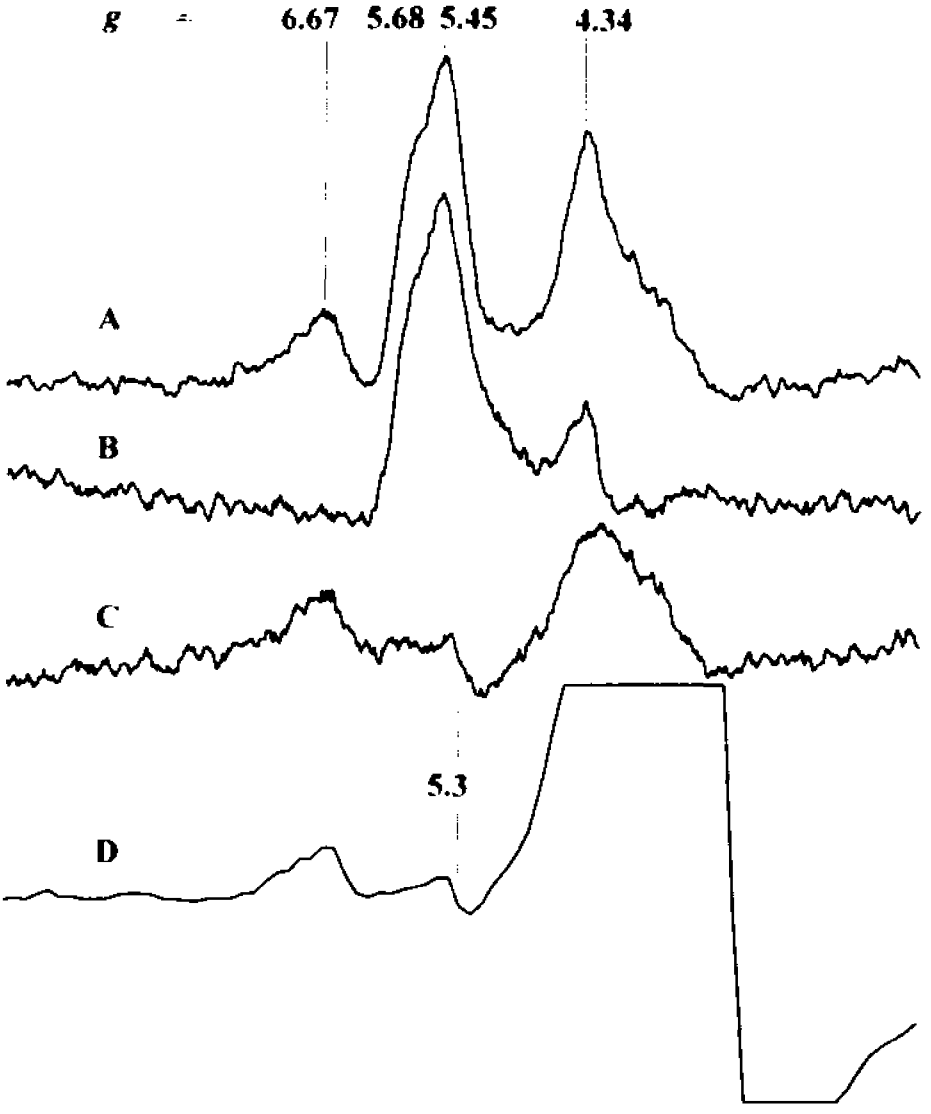

Figure 6.1 EPR spectra of the g = 3 -12 region of (A), as-isolated Av1'$_B$; (B), enzymatically reduced Av1'$_B$; (C), a difference spectrum (C = A - B); and (D), 2-equivalent oxidized Av1. The large off-scale features in (D) are the S = 3/2 FeMo cofactor signals at g = 4.3 and g = 3.7. The spectra are normalized for protein concentration and instrument gain. EPR spectrometer conditions: microwave frequency, 9.45 GHz; modulation frequency, 100 kHz; modulation amplitude, 1.0 mT; microwave power, 20 mW; temperature, 12 K (A, B, and C), 16 K (D).

subtraction artifacts. The spin state of the broad absorbance-shaped inflection centered at g = 4.3 is unknown, but this signal presumably arises from an oxidized cluster of $Av1'_B$ (see Discussion). A similar signal is not observed during the oxidation of Av1; however, its presence may be masked by the intense g = 4.34 inflection of the paramagnetic M-center (FeMoco). The remaining inflections at g = 6.67 and 5.2 are associated with an excited state, as determined by temperature studies. These signals may be tentatively assigned to the excited $|\pm 1/2\rangle$ doublet of an inverted S = 5/2 spin system with D = -1.6 cm ± .22 cm^{-1} and rhombicity E/D = 0.029. Partially oxidized Av1 protein ($P \rightarrow P^+$, Fig. 6.1D) shows analogous signals at g = 6.67 and g = 5.30 similarly assigned to the $|\pm 1/2\rangle$ doublet of an S = 5/2 spin system with D = -3.2 ± .20 cm^{-1} and E/D = 0.029.[15] The slightly broader g = 6.67 signal in $Av1'_B$ compared to that in Av1 may indicate a greater heterogeneity in the environment of the P-clusters in the former protein.

The spectrum of as-isolated $Av1'_B$ (Fig. 6.1A) also shows the S = 3/2 signal of the M-centers (FeVco) which arises from the ground and excited doublets of an inverted (D = -0.74 cm^{-1}) spin system with g-factors of 5.68 and 5.45 (E/D = 0.29). Previously observed g-factors were 5.80 and 5.40.[12] We observe these g-factors to change to 5.71 and 5.42 (E/D = 0.28) upon enzymatic reduction (Fig. 6.2). It is possible that this change arises from a change in paramagnetic interaction between the oxidized P-clusters and the vanadium cofactor in as-isolated $Av1'_B$, where enzymatic reduction of the

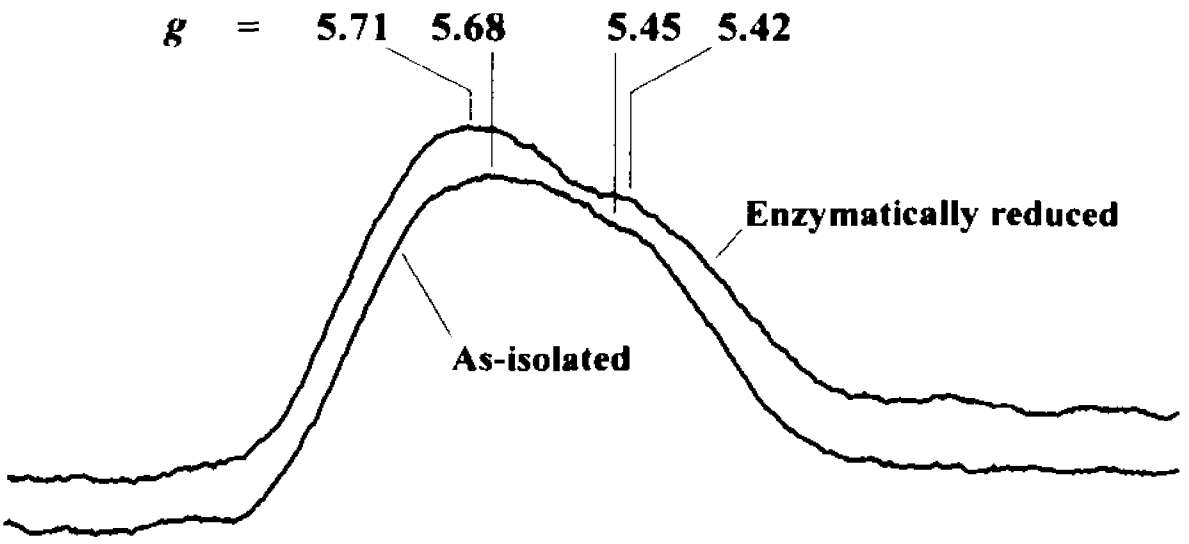

Figure 6.2 Low-temperature EPR spectra of the cofactor in as-isolated and enzymatically reduced $Av1'_B$. As-isolated $Av1'_B$ exhibits g -factors of 5.68 and 5.45. Enzymatic reduction results in a change in rhombicity with an observed shift to g = 5.71 and g = 5.42. The spectra are normalized for protein concentration and instrument gain. EPR spectrometer conditions: microwave frequency, 9.45 GHz; modulation frequency, 100 kHz; modulation amplitude, .6 mT; microwave power, 20 mW; temperature, 3.2 K.

P-clusters to their native diamagnetic state would remove this interaction. However, previous studies of Av1 have shown that oxidation of the P-clusters to the P^+ state does not change the rhombicity of the cofactor (FeMoco), but does produce changes in its spin relaxation behavior.[18] Furthermore, paramagnetic interactions usually result in line broadening, which is opposite to what is observed with $Av1'_B$. While it is questionable that spectral broadening occurred, it is clear that the rhombicity (*E/D*) of the cofactor signal in $Av1'_B$ decreases as the P-clusters become oxidized. This change in rhombicity implies a structural change about the cofactor upon oxidation of the P-clusters.

Oxidative titrations of enzymatically reduced $Av1_B$ were performed and monitored by EPR spectroscopy. Changes in the EPR spectrum (recorded at 12 K) of the g = 5-8 region during a thionine titration are shown in Figures 6.3 and 6.4. In this region of the spectrum, enzymatically reduced $Av1'_B$ (Fig. 6.3A) exhibits EPR signals associated with the vanadium cofactor (g = 5.71 and g = 5.42) along with a small, sharp inflection at g = 4.34. A 1.5 equivalent/protein oxidation (Fig. 6.3B) restores both the g = 6.67 and the broad g = 4.3 EPR signals previously observed in as-isolated $Av1'_B$ (Fig. 6.1A), while slightly diminishing the vanadium cofactor signal. Superimposed on the broad g = 4.3 signal is a sharp inflection at g = 4.34 which increases in intensity upon further oxidation (Fig. 6.3C and 6.3D). Oxidation by 3 equivalents (Fig. 6.3C) results in a further attenuation of the Av1' cofactor signal by approximately 50% yet enhances the g = 6.67 and g = 4.3 signals to their maximal amplitude. Finally,

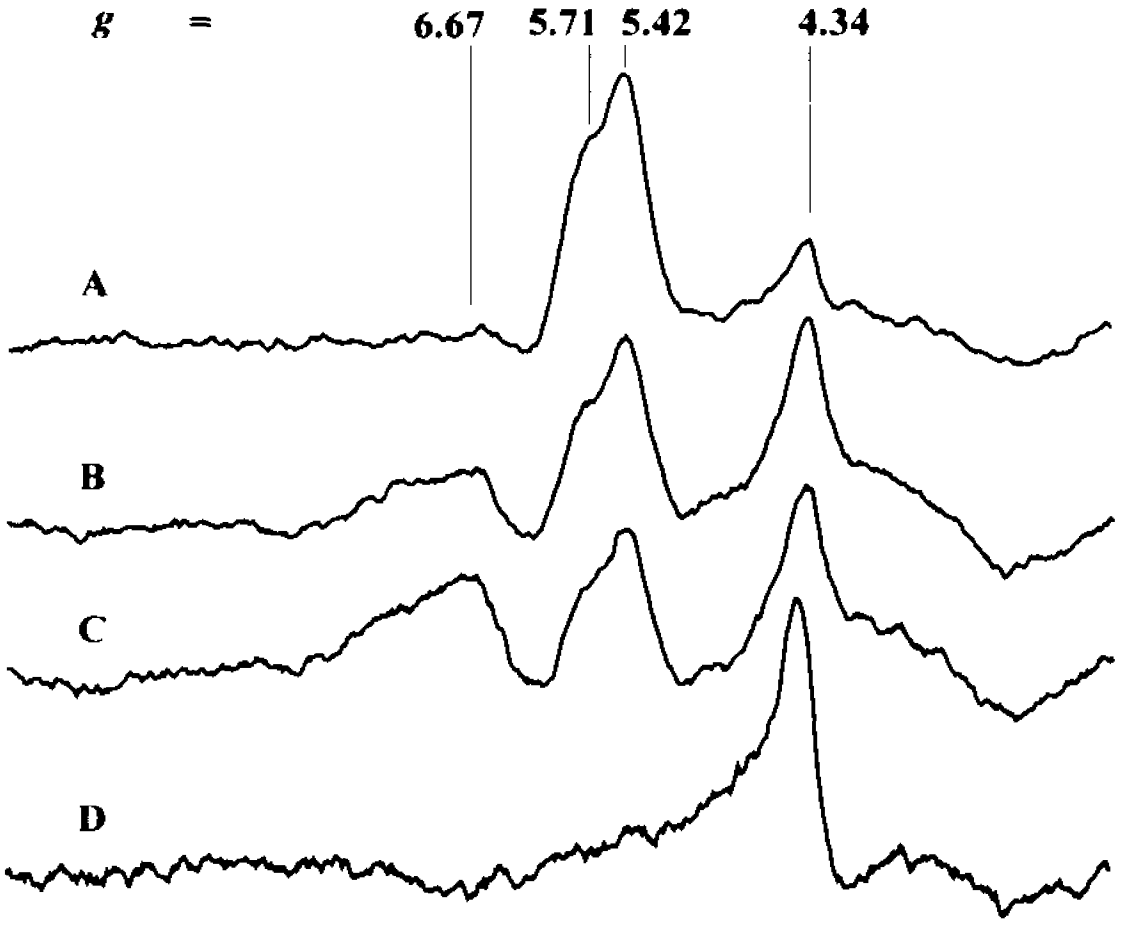

Figure 6.3. EPR spectra of thionine-titrated enzymatically reduced Av1'$_B$. (A), Enzymatically reduced Av1'$_B$; (B) reduced Av1'$_B$ titrated with 1.5 equivalents of thionine, in which the inflections at g = 6.67 and g = 4.3 have reappeared; (C), 3-equivalent oxidized Av1'$_B$ and (D), 6-equivalent oxidized Av1'$_B$. EPR spectrometer conditions: microwave frequency, 9.45 GHz; modulation frequency, 100 kHz; modulation amplitude, 1.0 mT; microwave power, 20 mW; temperature, 12 K.

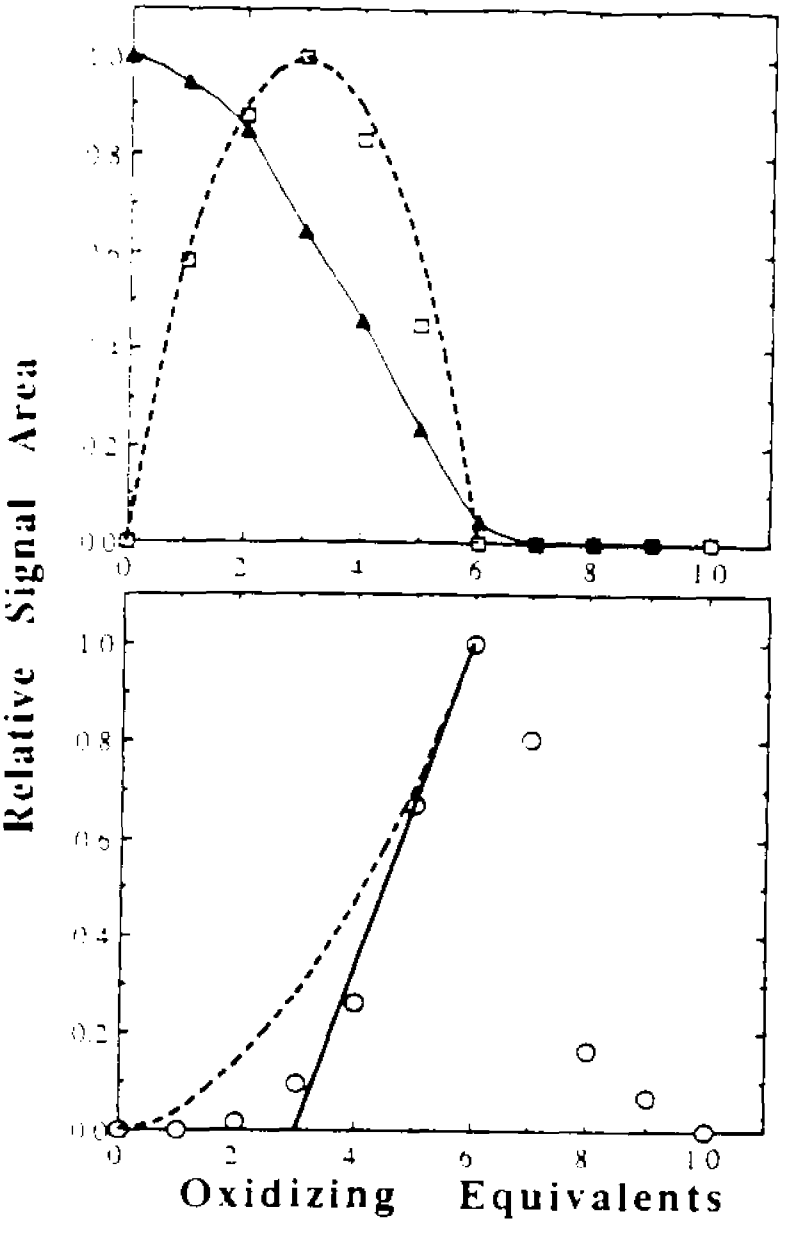

Figure 6.4 Top Relative EPR spectral areas of the S = 5/2 (P^*) signal at g = 6.67 and the S = 3/2 VFe cofactor signal as a function of oxidizing equivalents Experimental data (□) for the g = 6.67 (P^*) signal and a theoretical line (----) calculated with the random probability P-cluster oxidation model (see text) are shown Also, the area of the S = 3/2 cofactor signal (▲) is plotted along with a line (—) interpolated through the data points Bottom Experimental data (O) for the relative signal area of the S = 3 (P^{2*}) signal with g = 11.5 plotted along with the theoretical models. The random oxidation model is represented by (----) and the consecutive model by (—)

except for the sharp line at g = 4.34, all of the spectral signals of $Av1'_B$ decrease in amplitude upon further oxidation (Figs. 6.3D and 6.4).

The as-isolated VFe protein also exhibits an axial S = 1/2 EPR signal with inflections at g = 2.04 and g = 1.93 (Fig. 6.5A).[1,2] The origin of this signal is currently unknown but it is presumed to be associated with either the P-clusters or M-centers. During enzymatic reduction this signal was occasionally, but not always, removed. In the cases where it was not removed by enzymatic reduction (Fig. 6.5B), it disappeared upon introduction of the first aliquot (< 1 equivalent) of oxidant (Fig. 6.5C). On the other hand, in those cases where this signal was removed by enzymatic reduction (Fig. 6.5D), it reappeared upon introduction of the first aliquot of titrant (Fig. 6.5E), and was subsequently abolished by the addition of the second aliquot (similar to Fig. 6.5C), suggesting that it may represent a minor component of the protein.

Oxidation of Av1 has been shown to induce a 2-equivalent-oxidized P-cluster species (P^{2+}) which gives rise to an integer-spin EPR signal.[11-13] This signal has been assigned to an excited state doublet of an S = 3 or 4 spin system and, typical of integer-spin EPR signals, exhibits absorptions in both parallel and perpendicular mode EPR with g-factors of 11.9 and 11.6, respectively. A similar EPR signal, at g = 11.5 in perpendicular-mode (Fig. 6.6) and g = 12.8 in parallel mode (not shown), is generated during thionine oxidation of $Av1'_B$. This signal attains maximal amplitude at the 6-equivalent-oxidized step in the titration and may be assigned to the 2-equivalent-oxidized

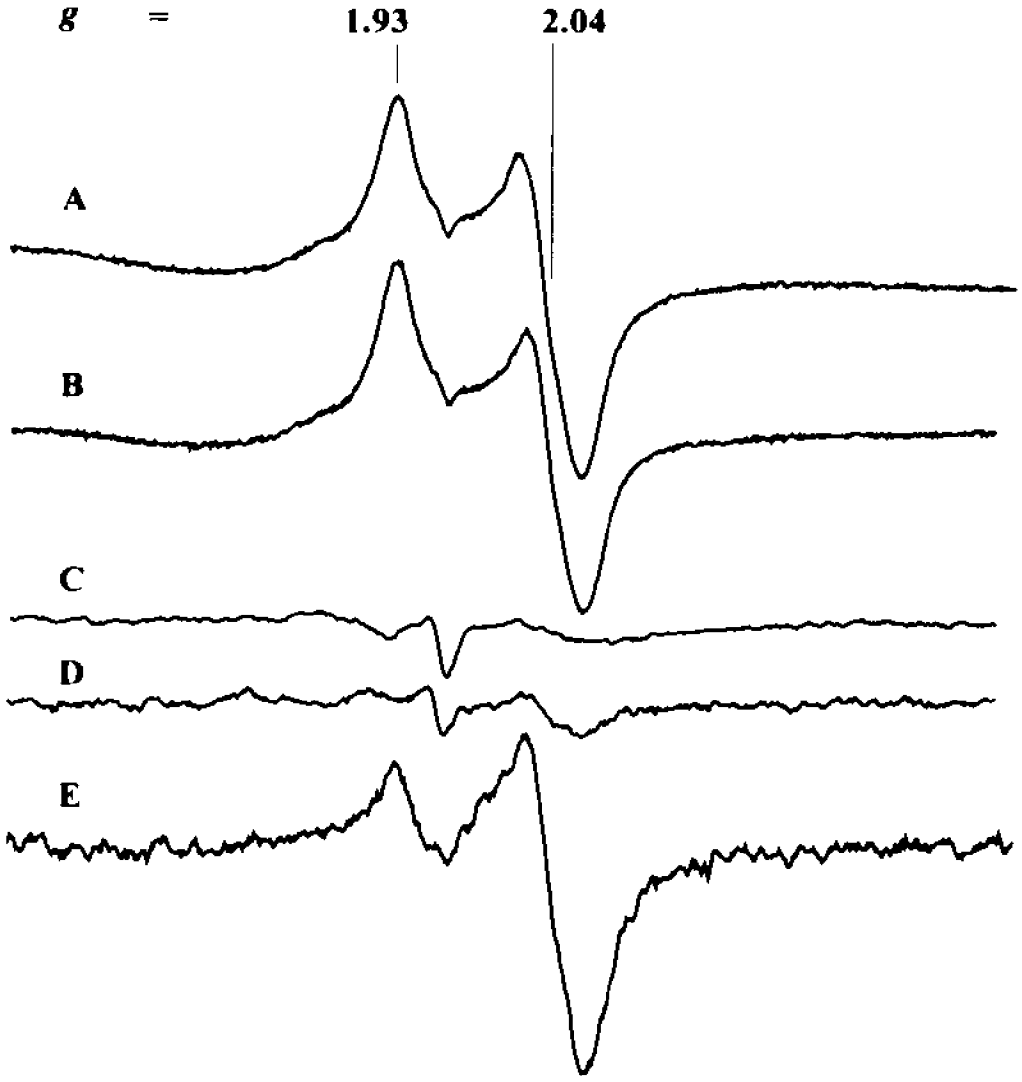

Figure 6.5. EPR spectra of the g = 2 region of $Av1'_B$. (A), As- isolated $Av1'_B$ showing the axial S = 1/2 signal with g = 1.93 and g = 2.04; (B), enzymatically reduced $Av1'_B$ in which the S = 1/2 signal was not removed; (C), thionine oxidized $Av1'_B$ (< 1 equivalent), in which the S = 1/2 signal has disappeared; (D), enzymatically reduced $Av1'_B$ in which the S = 1/2 signal is not present; (E), thionine titrated $Av1'_B$ in which the S = 1/2 signal was restored by the first aliquot (< 1 equivalent) of titrant. This last signal was removed by addition of the next aliquot of titrant. EPR spectrometer conditions: microwave frequency, 9.45 GHz; modulation frequency, 100 kHz; modulation amplitude, 1.0 mT; microwave power, 20 mW; temperature, 12 K.

P-cluster (P^{2+}). Temperature studies indicate that it arises from a ground-state transition of a probable $S = 3$ spin system, in contrast to the integer spin signal observed in Av1 mentioned above, which arises from an excited-state doublet.

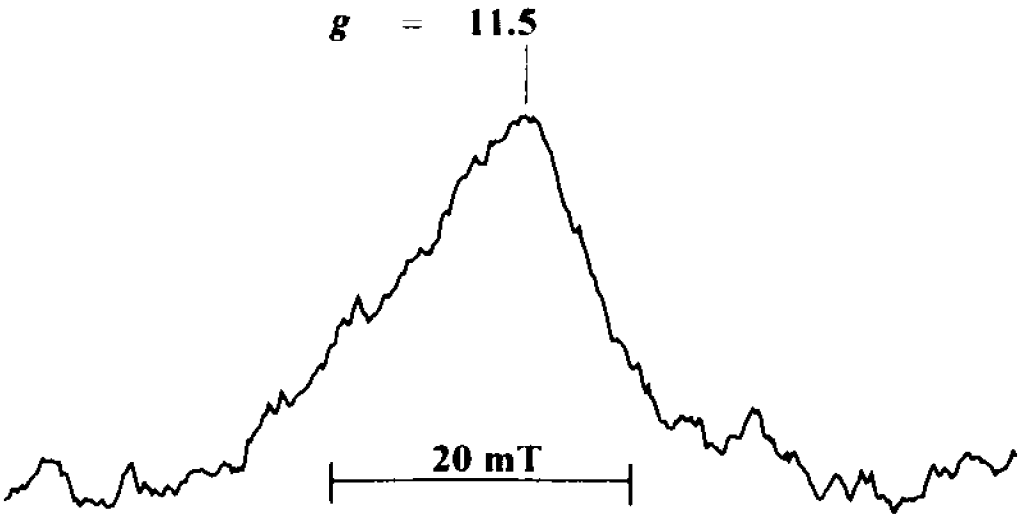

Figure 6.6. Perpendicular-mode EPR spectrum of 6-equivalent oxidized $Av1'_B$, showing a signal at $g = 11.5$ which arises from the integer-spin state ($S = 3$) of P^{2+}. EPR spectrometer conditions: microwave frequency, 9.45 GHz; modulation frequency, 100 kHz; modulation amplitude, 1.0 mT; microwave power, 20 mW; temperature, 3.2 K.

A second form of Av1' called $Av1'_A$, has recently been isolated and characterized.[16] It has been determined to have an $\alpha\beta_2$ conformation, as opposed to the $\alpha_2\beta_2$ structure of $Av1'_B$. This form contains only one cofactor and one P-cluster in the $\alpha\beta$ half of the protein with an additional Fe_4S_4 cluster in the second β subunit. In spite of its smaller subunit structure, $Av1'_A$ is still enzymatically active, exhibiting approximately 75% of the specific activity of

form $Av1'_B$ in acetylene reduction assays. However, oxidative titrations of $Av1'_A$ yield very different spectral data from those described above for $Av1'_B$.

The 12 K EPR spectrum (g = 4-12 region) of as-isolated $Av1'_A$ (Fig. 6.7A) is indistinguishable from that of $Av1'_B$ (Fig. 6.1A), showing an inflection at g = 6.67 (the P^+ state of the P-clusters), two signals with g = 5.68 and 5.45 (the M state of the VFe cofactor) and a broad inflection at g = 4.3 with a sharper superimposed signal at g = 4.34. Enzymatic reduction of this species (Fig. 6.7B) is also similar to that of $Av1'_B$, resulting in the attenuation of both the g = 6.67 and the broad g = 4.3 signals. The only new feature in the spectrum of enzymatically reduced $Av1'_A$ is a minor sharp first-derivative-shaped signal at g = 4.31 (Fig. 6.7B). However, the initial thionine oxidation of $Av1'_A$ results in the oxidation of *only* the cofactor ($M \rightarrow M^+$) without any detectable oxidation of the P-clusters to P^+. This is exactly opposite of what occurs during the oxidation of Av1, where the P-clusters oxidize prior to the cofactor.[15,18,19] Also, during the initial oxidation of $Av1'_A$, the new inflection at g = 4.31 (Fig. 6.7B) increases in amplitude, reaching a maximum at approximately 1 oxidizing equivalent (Fig. 6.7C and Fig. 6.8) at which point the signal of the cofactor has disappeared. Addition of the next equivalent of oxidant produces a unique series of spectral changes, i.e., the g = 4.31 signal disappears while the signals of P^+ (g = 6.67), the reduced cofactor M (g = 5.68, 4.45), and the broad absorbance (g = 4.3) all suddenly appear (Fig. 6.8). This sudden change suggests that the cofactor, oxidized during the initial titration, is re-reduced with a concurrent oxidation of

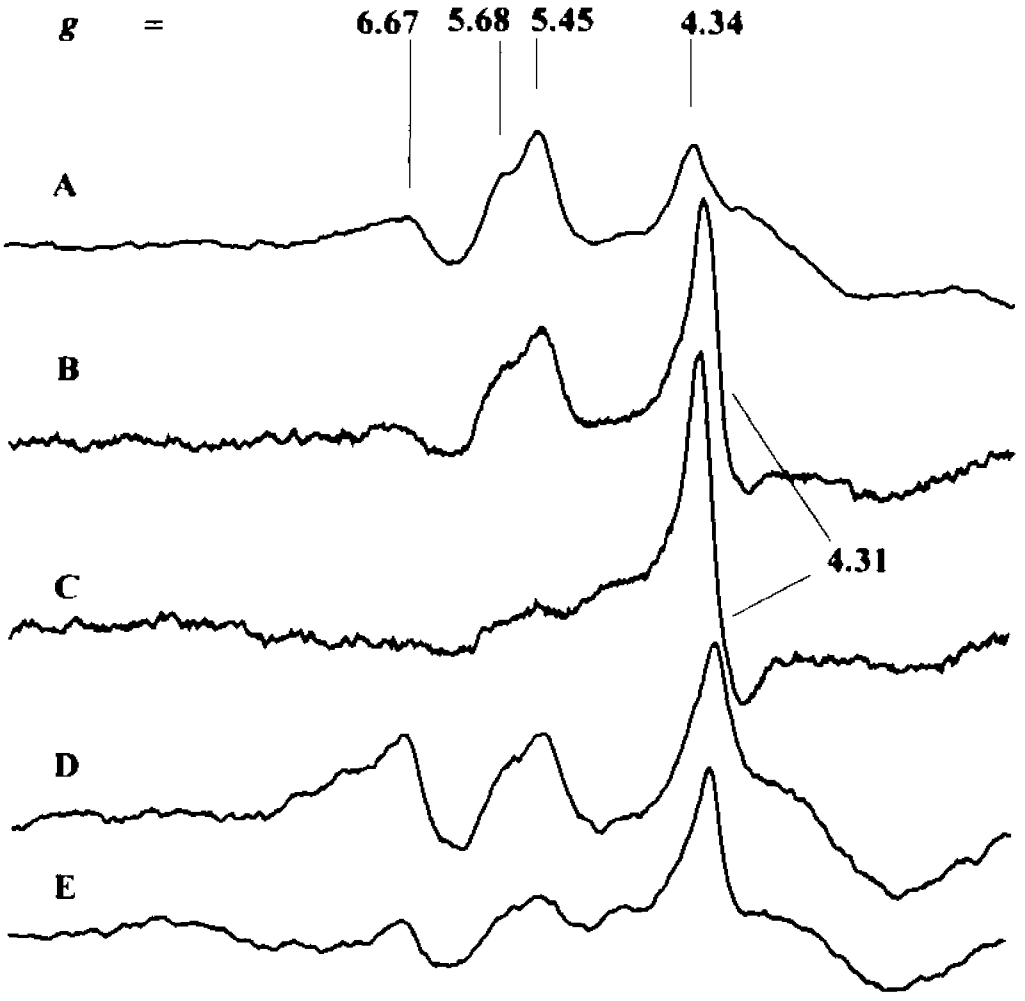

Figure 6.7. EPR spectra of Av1'$_A$. (A), As-isolated Av1'$_A$ showing the S = 3/2 cofactor signal, the S = 5/2 (P^+) signal at g = 6.67, and the broad inflection at g = 4; (B), enzymatically reduced Av1'$_A$ showing a sharp inflection at g = 4.31 and loss of both the P^+ signal at g = 6.67 and the broad inflection at g = 4; (C), 1-equivalent oxidized Av1'$_A$, showing the g = 5.31 signal at maximal amplitude while the S = 3/2 cofactor signal has been abolished; (D), 1.2-equivalent oxidized Av1'$_A$, showing the S = 5/2 (P^+) and S = 3/2 cofactor signal which have returned to full amplitude; (E), 2.5-equivalent-oxidized Av1'$_A$ in which the P^+ and cofactor signal have diminished. EPR spectrometer conditions: microwave frequency, 9.45 GHz; modulation frequency, 100 kHz; modulation amplitude, 1.0 mT; microwave power, 20 mW; temperature, 12 K.

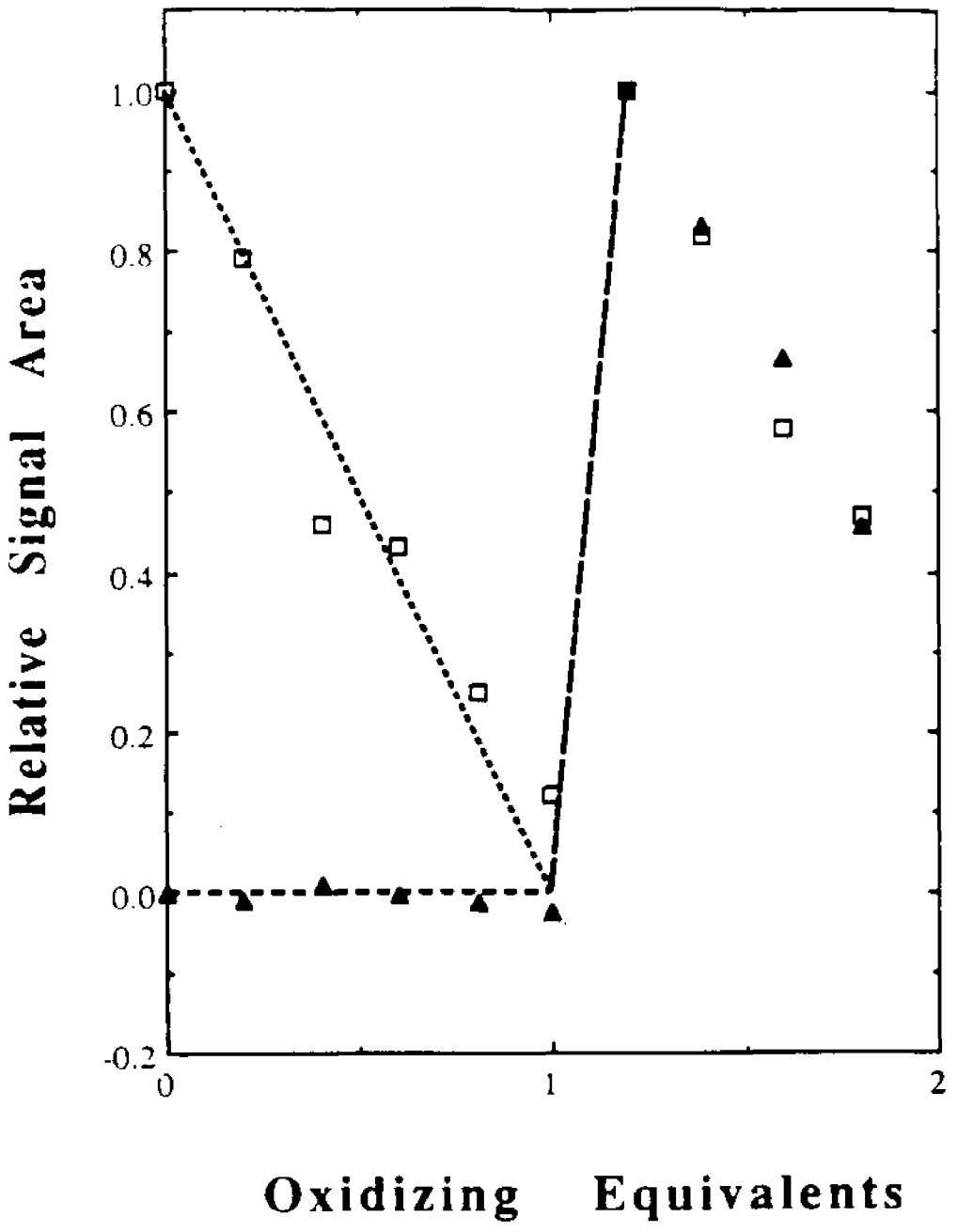

Figure 6.8 Relative EPR signal areas of the S = 5/2 (P^*) (▲) and the S = 3/2 cofactor signals (□) in $Av1'_A$ plotted as a function of oxidizing equivalents. The dashed and dotted lines represent predicted oxidation behavior for the P-cluster and cofactor, respectively, for the coupled ($P \rightarrow P^*$) and ($M^* \rightarrow M$) redox-gated electron flow between these clusters (see text).

the P-cluster ($P \rightarrow P^{+}$ is coupled to $M^{+} \rightarrow M$). All of these new spectral changes gain maximal amplitude by the addition of the next (< 0.3 equivalent) equivalent of oxidant (Fig. 6.7D). After this point in the titration, the oxidative behavior of $Av1'_A$ mimics that of $Av1'_B$, with a simultaneous decrease of both the cofactor ($M \rightarrow M^{+}$) and P^{+} EPR signals ($P^{+} \rightarrow P^{2+}$) as well as a loss of the broad inflection at g = 4.3 (Fig. 6.7E and Fig. 6.8). During this final oxidation, a different first-derivative shaped inflection at g = 4.3 appears (Fig. 6.7E). This signal exhibits the same temperature dependence ($|D|$ = 2.47 ± .22 cm^{-1}) as the g = 4.3 signal observed in the later stages of the oxidative titration of enzymatically reduced $Av1'_B$ (Fig. 6.3C) but differs from the signal (Fig. 6.7C) at g = 4.31 observed in the early stages of the oxidation of $Av1'_A$ ($|D|$ = 3.24 ± .22 cm^{-1}).

The EPR spectrum of the P^{2+} state in $Av1'_A$ was investigated at 3.2 K (Fig. 6.9). At this temperature, the spectrum of the 1-equivalent oxidized species (Fig. 6.9A) exhibits the same derivative-shaped inflection at g = 4.31 and attenuated vanadium cofactor signal observed at 12 K (Fig. 6.7). Following a 1.2-equivalent-oxidation of $Av1'_A$ (Fig. 6.9B), the EPR spectrum of the reduced cofactor reappears along with a broad inflection at g = 4.3 (as observed at 12 K) along with the first indication of a broad inflection at g = 11.3 identical to the integer-spin species previously assigned to P^{2+} (Fig. 6.6). This signal gains maximum amplitude with approximately 3 equivalents (Fig. 6.9C) while the amplitude of the S = 3/2 cofactor signal has diminished and the

inflection at g = 4.3 has increased. Finally, it should be noted that the g = 6.67 signal assigned to P^+ (Fig. 6.7D) is not visible in these low-temperature spectra (Fig. 6.9) since it arises from an excited-state doublet.

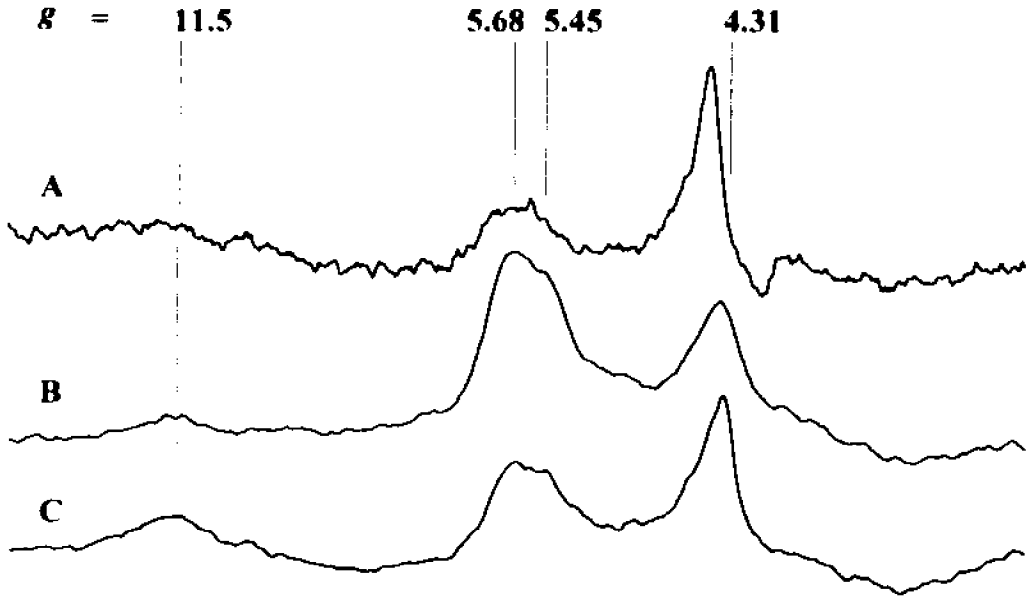

Figure 6.9 EPR spectra of thionine-oxidized Av1'$_A$. (A), 1-equivalent-oxidized Av1'$_A$ showing the attenuated S = 3/2 cofactor signal and an inflection at g = 4.31; (B), 1.2-equivalent-oxidized Av1'$_A$ showing the restored cofactor signal and the disappearance of the inflection at g = 4.31; (C), 2.5-equivalent oxidized Av1'$_A$ showing the proposed S = 3 (P^{2+}) signal and the diminished cofactor signal, along with a first-derivative shaped inflection at g = 4.34.

6.4 Discussion

Av1' in its as-isolated state (in the presence of 2 mM dithionite) contains oxidized P-clusters, as evidenced by the S = 5/2 EPR signal at g = 6.67 (Fig. 6.1A) which is very similar to the one previously assigned to P^+ in 2-equivalent oxidized Av1.[15] Also, Mössbauer studies[9] clearly demonstrate that as-isolated Av1' contains a mixture of oxidized and reduced P-clusters and M-centers. Attempts at chemical reduction of the P-clusters using 10 mM dithionite and the redox mediators methyl viologen and benzyl viologen have been unsuccessful. However, full reduction of the clusters in Av1' to their "native" forms can be effected through enzymatic reduction with a small mount of Av2' and excess MgATP in the presence of dithionite. The reduction is verifiable by both EPR (Fig 6.2B) and Mössbauer spectroscopy.[9] These results are significant for two reasons. First, they suggest that the clusters of Av1' have redox midpoint potentials lower than the clusters in Av1 (since all the clusters in the latter protein are fully reduced in the presence of 2 mM dithionite and methyl viologen). Second, and perhaps more importantly, these results demonstrate that *enzymatic reduction* is able to reduce oxidized P-clusters. Although the enzymatic role of P-clusters is unknown, it has been proposed that they serve to mediate electron transfer from component 2 to the M-centers (as opposed to component 2 reducing the M-centers directly). The EPR data presented here along with the previously cited Mössbauer studies clearly demonstrate that

oxidized P-clusters can be reduced by component 2, thus strengthening this proposal.

Previous oxidative titrations of Av1 showed that the native-state (P^0) P-clusters could be oxidized by one equivalent, generating P^+.[15,18] Further oxidation converted the P-clusters into the 2-equivalent oxidized state ($P^+ \rightarrow P^{2+}$) with an apparent mid-point potential approximately identical to that of the first oxidation step. The EPR spectrum of P^+ in Av1 revealed both S = 5/2 and S = 1/2 spin states. The presence of nearly identical S = 5/2 inflections in the spectra of partially oxidized Av1' (Figs. 6.1C and Fig. 6.3B) clearly establishes the existence of similar P^+ states in this protein. The S = 1/2 EPR signal assigned to the P^+ state in Av1 is not observed in as-isolated or thionine oxidized Av1'.[21,22] Apparently, the S = 5/2 signals represent the presence of the P^+ state in both proteins, while the S = 1/2 signal appears to be a minor component (~10%) unique to the MoFe-protein. If the S = 1/2 and 5/2 spin states assigned to P^+ in Av1 represent the one-equivalent oxidation of separate Fe_4S_4 units at opposite halves of the P-cluster pair and the mid-point potentials ($P \rightarrow P^+$) for the two units are similar, then the units are randomly oxidized and both P^+ spin states will be observed during the oxidative titration of the protein, as is the case for Av1.[15,18] If the midpoint potentials of the two units are significantly different, then the oxidation of one will be preferred over the other. So, if this model holds, the oxidation profile of Av1' should be different from that of Av1. Av1 has been shown to approximate the random oxidation model,

yielding statistical amounts of P^+ and P^{2+} as an oxidative titration proceeds.[15] If, in fact, the P^+ state that gives rise to the g = 6.67 EPR signal in Av1' is electrochemically favored, then no P^{2+} should be generated until after all of the P^+ has been produced, and should lag the production of P^{2+} in Av1. The theoretically predicted formations of P^{2+} for both of these situations are shown in Fig. 6.4B where it can be seen that there is a lag in the formation of P^{2+}, thus strengthening the hypothesis that the S = 1/2 and 5/2 spin states of Av1 P^+ represent separate oxidations of the two Fe_4S_4 units of the P-cluster.

The broad absorption-shaped signal (Figs. 6.1, 6.3 and 6.7) centered at g = 4.3 is very likely associated with P^+ since it is only observed when the g = 6.67 S = 5/2 signal is also present in either $Av1'_A$ or $Av1'_B$. In the oxidative titrations of $Av1'_A$ and $Av1'_B$, the g = 4.3 signal mimics the amplitude variation of the S = 5/2 P^+ signal. Also, in the initial oxidation of $Av1'_A$, during which only the M-centers are oxidized ($M \rightarrow M^+$) while the P-clusters remain reduced, the g = 4.3 signal is not generated (Fig. 6.7). When the P-cluster signal at g = 6.67 is restored, so is the signal at g = 4.3. Other than the fact that this broad g = 4.3 signal obviously arises from a state with S > 1/2, the observation of only one inflection makes the identification of the spin state of this signal ambiguous.

During the oxidation of Av1', a sharp inflection appears at g = 4.34 (Figs. 6.3D and 6.7E) which increases in intensity as more oxidant is added. This inflection is still present following the oxidation of both metal clusters in Av1' ($M \rightarrow M^+$ and $P \rightarrow P^{2+}$). Addition of oxidant beyond this 6-equivalent point results

in a decrease in the intensity of the P^{2+} signal with a further increase in the amplitude of the sharp g = 4.34 inflection. At this point in the titration it was also noted that Av1' was starting to become irreversibly inactivated. Signals in the region of g = 4.34 often reflect the presence of adventitously bound high-spin iron. Therefore, these results suggest that the g = 4.34 signal may arise from the oxidative destruction of one or both of the metal clusters in Av1'. By comparison, Av1 has been oxidized to the P^{3+} (S = 7/2) state (a state not observed by us in Av1') without detectable inactivation.[13]

The oxidative titration of $Av1'_B$ (Figs. 6.3 and 6.4) illustrates the concurrent oxidation of both the P-clusters and M-centers. This situation differs from the analogous oxidation of Av1 using thionine, which shows a 2-equivalent oxidation of the P-clusters to the P^{2+} state preceding the oxidation of the M-centers.[15,18,19] and suggests similar redox mid-point potentials for both metal clusters in the $Av1'_B$ protein. At present it is unknown whether either the similar redox potentials of the clusters in $Av1'_B$ or the fact that both of these potentials are more negative than those of the corresponding clusters in Av1 has any correlation with the apparent lower substrate-reduction efficiency of the vanadium form of the enzyme.[1,3]

The 2-equivalent oxidation of the P-clusters ($P \rightarrow P^{2+}$) in various MoFe proteins has been shown to yield an integer spin state.[11-13] Except for the protein isolated from *Xanthobacter autotrophicus* (Xa1)[12], where P^{2+} exhibits a ground-state EPR signal with g = 15.6, all previously observed P^{2+} EPR signals

have occurred in the g = 12 region and are associated with excited states. The P^{2+} state in both $Av1'_A$ and $Av1'_B$ similarly (Figs. 6.5 and 6.9) exhibits an EPR signal in the g = 12 region associated with an integer spin state, as verified by parallel mode EPR spectroscopy.(kindly performed for us by Dr. Michael Finnegan in Professor Michael Johnson's lab at the University of Georgia). However, unlike the analogous signal in the MoFe proteins, temperature studies indicate that the signal in the Vfe protein arises from a ground state. The ground state of a non-inverted integer-spin system is a singlet, where no EPR transitions are possible, so the observed signal at g = 11.5 most likely represents the transition $\Delta m_S = 2S$ of an integer spin system with negative zero-field splitting ($D < 0$) and the restriction $g \leq 4S$. Using these restrictions with g = 12.8 determined by parallel mode EPR, this inflection can be assigned to an S = 3 state.

The behavior of $Av1'_A$ during an oxidative titration (Fig. 6.7) is highly unusual. To explain this behavior, a model will be proposed which presumes the existence of two different redox forms of this protein, called $Av1'_{A1}$ and $Av1'_{A2}$. Form $Av1'_{A1}$ is generated during the initial enzymatic reduction of the protein. In this protein, the M-centers have a redox mid-point potential more negative than that of the P-clusters and, therefore, oxidize first upon addition of thionine. Following oxidation of the M-centers, $Av1'_{A1}$ converts to form $Av1'_{A2}$ upon addition of more oxidant to the medium. To trigger this conversion, $Av1'_{A1}$ must possess a redox receptor that responds to the environmental potential.

The only known redox active sites in component 1 are the M-centers, the P-clusters and the Fe_4S_4 cluster in $Av1'_A$. Since the M-centers have already been oxidized, it is doubtful that they will respond to further oxidation. The same is true for the Fe_4S_4 cluster which is also oxidized (and EPR silent) at this point in the oxidation. Also, it is difficult to rationalize the Fe_4S_4 acting as the redox receptor since it is probably over 67 Å from both the cofactor and P-cluster. Therefore, the most likely candidate for the redox receptor is the reduced P-cluster. In other words, it must be the establishment of the equilibrium $P \rightarrow P^+ + e^-$ in $Av1'_{A1}$ that triggers its conversion into $Av1'_{A2}$. Form $Av1'_{A2}$ has a redox profile like that of $Av1'_B$ discussed above, where the mid-point potential of the M-center is slightly more positive than that of the P-clusters. Because of this, the initial oxidation of the P-clusters induces the conversion of $Av1'_{A1}$ to $Av1'_{A2}$, inverting the relative redox potentials of the two metal clusters and promoting a redistribution of the electrons in the protein, and electrons flow from the P-clusters to reduce the previously oxidized M-centers.

Why is this phenomenon only observed in $Av1'_A$ and not in $Av1'_B$? The major structural difference between $Av1'_A$ and $Av1'_B$ is the absence of an α subunit in $Av1'_A$. The absence of this subunit appears to render $Av1'_A$ susceptible to a P-cluster oxidation-induced change from $Av1'_{A1}$ to $Av1'_{A2}$ which gates the oxidation changes [$P \rightarrow P^+$ and $M^+ \rightarrow M$]. A similar coupling of the oxidation of the P-clusters with a concurrent reduction of the M-center may also take place in $Av1'_B$ or the MoFe protein but may occur at a different redox level.

outside the range of these titrations. Obviously, this coupling would be mechanistically important because it would force the cofactor into a more reduced state, possibly necessary for N_2 reduction. Even though redox gating is not observed during the oxidative titration of $Av1'_B$, the observed change in rhombicity (Fig. 6.2) of the $S = 3/2$ cofactor signal upon P-cluster oxidation does suggest a coupling between P-cluster oxidation and structure about the cofactor. Similar couplings have already been proposed to occur during catalysis.[23]

How does the oxidation of the P-cluster induce a redox and rhombicity change detected at the cofactor? The structure of component 1 may suggest a possible mechanism for the coupling of redox and conformational changes. An aspect of the P-cluster structure not typically observed in Fe-S clusters is the bridging of the cluster between different subunits. An analogous situation exists in the component 2 protein where a single Fe_4S_4 cluster is bridged between identical subunits.[24] In component 2, MgATP binding, which has been proposed to occur about 20 Å from the Fe_4S_4 cluster, induces a dramatic lowering of the mid-point potential of the cluster and changes the rhombicity of the EPR spectrum of the reduced cluster.[25] Small angle x-ray scattering studies have shown that MgATP binding induces a conformational change in the protein.[26] Also, MgATP binding to component 2 greatly enhances the chelation of the [4Fe-4S] cluster by bathophenanthrolinedisulfonate.[27] In other words, MgATP binding to component 2 induces both a conformational change

in the protein as well as a change in redox mid-point and spectral rhombicity of the cluster, i.e., conformational and redox changes are coupled in component 2. Therefore, it would not be unexpected that a similar situation exists in component 1 where a redox change in the P-cluster induces a conformational shift from $Av1'_{A1}$ to $Av1'_{A2}$. In summary, it may be found that the bridging of a metal cluster between different subunits of a protein is an effective way of coupling a redox change in the cluster with a conformational change in the protein.

References

1. Hales, B. J., Case, E. E., Morningstar, J. E., Dzeda, M. F., Mauterer, L. A. *Biochemistry* **1986**, *25*, 7251-7255.

2. Hales, B. J., Langosch, D. J., Case, E. E. *J. Biol. Chem.* **1986,** *261*, 15301-15306.

3. Eady, R. R., Robson, R. L., Richarson, T. H., Miller, R. W., & Hawkins, M. *Biochem. J.* **1987**, *244*, .

4. Bishop, P. E., Joerger, R. D., Loveless, T. M., Pau, R. N., Michenall, L. A., Simon, B. H. *J. Bacteriol.* **1990** *172*, 3400-3408.

5. Arber, J. M., Dobson, B. R., Eady, R. R., Hasnain, S. S., Garner, C. D., Matsushita, T., Nomuras, M., & Smith, B. E. *Biochem. J.* **1989**, *258*, 733-737.

6. Arber, J. M., Dobson, B. R., Eady, R. R., Stevens, P., Hasnain, S. S., Garner, C. D., & Smith, B. E. *Nature* **1987**, *325*, 372-374.

7. George, G. N.; Coyle, C. L.; Hales, B. J.; Cramer, S. P. *J. Am. Chem. Soc.* **1988**, 110, 4057-4059.

8. Chen, J.; Christiansen, J.; Tittsworth, R.C.; Hales, B.J.; George, S.J.; Coucouvanis D.; Cramer, S.P. *J. Am. Chem. Soc.* **1993**, *115*, 5509-5515.

9. Ravi, N., Moore, V., Lloyd, S., Hales, B. J., & Huynh, B. H. *J. Biol. Chem.* **1994,** *269*, 20920-20924.

10. Münck, E., Rhodes, H., Orme-Johnson, W. H., Davis, L. C., Brill, W. J., Shah, V. K. *Biochim. Biophys. Acta.* **1975,** *400*, 32-53.

11. Hagen, W. R. In *Advances in Inorganic Chemistry: Iron-Sulfur Proteins*; A. G. Sykes and R. Cammack, Ed.; Academic Pres: 1992; Vol. 38; pp 165-222.

12. Surerus, K. K.; Hendrich, M. P.; Christie, P. D.; Rottgardt, D.; Orme-Johnson, W. H.; Münck, E. *J. Am. Chem. Soc.* **1992**, *114*, 8579-8590.

13. Pierik, A., J.; Wassink, H.; Haaker, H.; Hagen, W. R. *Eur. J. Biochem.* **1993**, *212*, 51-61.

14. Morningstar, J. E., Johnson, M. K., Case, E. E., & Hales, B. J. *Biochemistry* **1987,** *26*, 1795-1800.

15. Tittsworth, R.C.; Hales, B.J. *J. Am. Chem. Soc.* **1993**, *115*, 9763-9767

16. Blanchard and Hales, *submitted for publication.*

17. Burgess, B. K.; Jacobs, D. B.; Stiefel, E. I. *Biochim. Biophys. Acta.* **1980**, *614*, 196-209.

18. Oliver, M. E., Hales, B. J. *J. Am. Chem. Soc.* **1992,** *114*, 10618-10623.

19. Zimmermann, R., Münck, E., Brill, W. J., Shah, V. K., Henzl, M. T., Rawlings, J., & Orme-Johnson, W. H. *Biochim. Biophys. Acta.* **1978**, *536*, 185-207.

20. Hales, B. J., True, A. E., & Hoffman, B. M. *J. Am. Chem. Soc.* **1989** *111*, 8519-8520

21. Orme-Johnson, W. H., Paul, L., Meade, J., Warren, W., Nelson, M., Groh, S., Orme-Johnson, N. R., Münck, E., Huynh, B. N., Emptage, M., Rawlings, J., Smith, J., Roberts, J., Hoffmann, B., & Mims, W. B. (1981) in *Current Perspectives in Nitrogen Fixation* (A. H. Gibson & W. E. Newton, Eds.) pp. 79-84, Elsevier, North-Holland, New York.

22. Smith, B. E., Lowe, D. J., Chen, G.-X., O'Donnell, M. J., & Hawkes, T. R. *Biochem. J.* **1983,** *209*, 207-213.

23. Chan, M. K., Kim, J., Rees, D. C. *Science* **1993,** *260*, 792-794.

24. Georgiadis, M. M., Komiya, H., Chakrabarti, P., Woo, D., Kornuc, J. J., & Rees, D. C. *Science* **1992,** *257*, 1653-1659.

25. Zumft, W. G., Palmer, G., & Mortenson, L. E. *Biochim. Biophys. Acta.* **1973,** *292*, 413-421.

26. Hodgson, K. O., Chen, L., Gavini, N., Tsuruta, H., Eliezer, D., Burgess, B. K., & Doniach, S. *J. Biol. Chem.* **1994**, *269*, 3290-3294.

27. Ljones, T., & Burris, R. H. *American Chemical Society* **1978,** *17*, 1866-1867.

Chapter 7 Conclusions

7.1 EXAFS Spectroscopy

The Fe K-edge EXAFS studies of Av1 and Av1' reported in Chapter 3 resulted in the assignment of a number of absorber-backscatterer interacations, which corroborate and extend previous EXAFS studies. This is the first Fe EXAFS reported on the intact nitrogenase component 1. Assuming a symmetrical M-center structure, plausible distance assignments were made in the cofactor model. Furthermore, a long 4.3 Å Fe-S interaction which had been previously unreported was modeled in the EXAFS analysis of Av1 and Av1'. The fact that this interaction was observable and reproducible argues strongly for significant symmetry in the cofactor cluster, since a very wide distance distribution at this great a distance would probably result in this interaction being unobservable. Perhaps this Fe-Fe interaction at 4.3 Å and a very long Mo-Fe interaction at 5.09 Å observed by us in Mo EXAFS (Chapter 4) may serve as useful constraints as the crystallographic models are refined.

EXAFS analysis can only determine an average distance value and cannot distinguish between P-cluster and M-center Fe-X interactions. Obviously, the P-cluster Fe_4S_4 cubanes contribute greatly to the short distance EXAFS Fe-Fe and Fe-S interactions, and we observed a distribution of P-cluster and M-center interactions. Still, the distributions were not so broad that we could not fit and interpret the EXAFS reasonably, and assign an M-center model with little reference to the crystallographic data.

Thione oxidation of Av1 and Av1' had very small but reproducible effects on the EXAFS of both proteins. The short Fe-Fe interaction at 2.7 Å expanded slightly upon oxidation, and the short Fe-S interaction at 2.3 Å contracted slightly. Some change occurs upon oxidation, although it appears to be very small (see below).

Importantly, the Fe-EXAFS of Av1 and Av1' are strikingly similar. Fe-EXAFS of the intact nitrogenase component 1 probes all of the Fe in both types of clusters. Av1 and Av1' have nearly identical EXAFS radial distance distributions. Even with the caveat that we are only observing average distances, it would seem highly unlikely that Av1' has a very different metal-cluster structure than Av1. Previously cited amino-acid analysis, metal analysis, and Mössbauer spectroscopy also support the proposal that Av1 and Av1' have very similar metal cluster structure. Since no one has been able to grow crystals of Av1', the Fe-EXAFS data reported here, previously cited EXAFS results, and the above mentioned corroborative data make the best argument available for metal cluster homology between Av1 and Av1'.

The EXAFS micro-analysis of Av1 in various oxidation states presented in Chapter 3 is somewhat speculative, since the distance differences between the proposed P-cluster and M-center Fe-Fe interaction that were modeled are slightly less than the generally accepted resolution limit for identical or similar atomic number backscatterers. Also, the changes observed for any particular absorber-backscatterer distance are very close to the accepted EXAFS

distance resolution of 0.02 Å. Nevertheless, there were distinct observable trends in the data.

First of all, the "split shell" model for the short Fe-Fe is chemically reasonable, since the M-center is proposed to contain mostly three coordinate Fe by the crystallographic model (except for the possibility of hydride coordination which cannot be ruled out conclusively), and probably has a tighter structure and shorter Fe-Fe distances for this interaction than the cubane P-cluster. Furthermore, both crystallographers cited model this distance as shorter in the M-center than in the P-cluster. Also, the original fits attempted on IDS oxidized Av1 using "true" coordination numbers gotten by inspection of the crystal models yielded a very large root mean square deviation for the short Fe-Fe interaction at 2.65 Å. Armed with these observations, it seemed logical to attempt a "split shell" model on Av1 in various oxidation states.

Consistent trends in the short metal-metal interactions emerged as a function of oxidation state. The short metal-metal interactions were observed to contract as Av1 became more reduced. The short Fe-S interaction at 2.65 Å was observed to expand slightly. The proposed M-center short Fe-Fe distance approaches that of Fe-Fe bonding interactions in the reduced (P/M') Av1. This state is proposed to be competent to bind H^+, so we may be observing M-center dimensions in a catalytically "activated" cofactor. Perhaps the most important result of the experiment is that very large changes were not observed over the oxidation range examined.

Now that strutural refinement of the nitrogenase protein and its metal clusters are proceeding rapidly and we have a more informed view of the clusters and their polypeptide environments, EXAFS and XANES can make the greatest contribution to nitrogenase research by exploring the mechanistic realm. We have taken some halting steps in this direction, but now it is imperative that we try to move toward studies of nitrogenase catalyzing the reduction of dinitrogen to ammonia. Unfortunately, spectroscopy and enzymology do not always have the smoothest of interfaces, and nitrogenase presents its own special problems, the most serious being the requirement for significant amounts of the component 2 protein in any reaction mixture that will reduce nitrogen. Also, concentration, salt, and viscosity effects may cause problems.

One suggested experiment is Mo EXAFS and XANES of high flux enzymatic turnover mixes. These could be done with H^+, C_2H_2, and N_2 as substrates, with no interference from component 2 Fe. Also, detectable concentrations of Av1 could be attained. Of course, no one knows what will happen to Av1 when the sample is frozen, even by rapid freeze techniques. Will the frozen states resemble the catalytic states at all or will the protein relax from the purported "higher" E_n states required to reduce N_2 during the freezing process? At any rate, Mo XANES and EXAFS could possibly yield some useful information about oxidation state, coordination, and distance changes in catalytically active samples..

Mo and Fe L-edge studies are also a possibility. Coupled with rapid freeze techniques, it may be possible to observe oxidation state changes, if they occur, in deep turnover samples. The component 2 Fe would give appreciable interference in the Fe L-edge studies, but it may be possible to subtract it. L-edges are very sensitive to redox changes, so perhaps some evidence of the higher E_n states may be observable. The L-edge experiments would be difficult, both from a sample prep and x-ray detection perspective, but most of the easy x-ray experiments have been done.

7.2 EPR Spectroscopy

Oxidative titration of Av1 resulted in the observation and assignment of EPR signals proposed to arise from P^+, or the 1-equivalent oxidized P-cluster. Previous to this work and the power saturation study by Dr. Melinda Oliver cited in Chapter 5, understanding of the possible stable P-cluster oxidation states was less clear. It had been proposed that the P-clusters oxidize in an n = 2 process, going from $P \rightarrow P^{2+}$. We have shown that a stable P^+ redox state exists, which gives rise to the previously cited S = 1/2 EPR signal and the proposed S = 5/2 signals that we observed. Also, a simple probability model was proposed for P-cluster oxidation from $P \rightarrow P^+ \rightarrow P^{2+}$ that fit the experimental data reasonably. Elucidation of the possible redox states available to the P-clusters is important, since they may be directly involved in the catalytic process. The physiological relevance of the observed P-cluster oxidation states has yet to be demonstrated, but this writer has observed inflections

matching those of the S = 1/2 P^+ EPR signal in CO inhibited enzymatic turnover samples.

The oxidative titrations performed on the vanadium nitrogenase, Av1', have yielded the most interesting and exciting observations of all, at least from a P-cluster perspective. Both forms of Av1', $Av1'_A$ and $Av1'_B$, show spectral evidence of oxidized P-clusters in the as-isolated protein that we have been unable to reduce chemically. We can, however, reduce these clusters enzymatically with the component 2 protein. In and of itself, this is an important result. It shows that the P-clusters get electrons somehow from component 2. It does not show which way the electrons go first, or what route they take to reduce the P-clusters. Spectral evidence exists for M-center reduction, but no one has reported a direct EPR observation of the enzymatic reduction of the P-clusters. This result hints strongly at P-cluster involvement in the catalytic process of nitrogenase.

The oxidative titration behavior of enzymatically reduced $Av1'_B$ is similar but not identical to that of Av1. The P^+ and the P^{2+} state can be induced by chemical oxidation, but they follow a consecutive rather than a random probabilistic oxidation profile. Also, unlike Av1, the M-centers oxidize concurrently with the P-clusters, indicating similar oxidation potentials. This may be related to the lower catalytic efficiency of Av1' as compared to Av1, if an electron transfer takes place between the P-cluster and the M-center during catalysis.

$Av1'_A$ exhibits striking and exciting oxidation behavior. Like $Av1'_B$, it is enzymatically reducible. However, the oxidative titration behavior of $Av1'_A$ is much different than that of $Av1'_B$. Instead of "titrating in" the P^+ EPR signal, as in $Av1'_B$ and Av1, we "titrate out" the M-center signal in the initial stages of the titration. Upon the addition of the next aliquot of titrant after the M-center signal has been abolished, the M-center signal and the P^+ signal amazingly reappear. We believe that we are observing a redox-gated electron transfer from the P-cluster to the M-center. The P-cluster "dumps" its electrons to the oxidized M-center. This sort of interaction has been widely speculated, but no strong spectral evidence has been reported for it.

EPR is a sensitive technique, and it could potentially be of great importance in further mechanistic studies of nitrogenase. Again, attempts should be made to at least approach the conditions where nitrogenase is actually reducing nitrogen. The reduced component 2 proteins are paramagnetic, and may cause significant problems in spectral interpretation. Also, there must be an adequate supply of reducing equivalents, ATP, and substrate available in the sample under consideration. None of these concerns are trivial, and constitute real difficulties in experimental design.

Further study of $Av1'_A$ undergoing enzymatic turnover with various substrates and inhibitors may prove informative. $Av1'_A$ is an active, although apparently somewhat amputated, nitrogenase variant in which we have made some interesting observations. If the intramolecular redox environment of $Av1'_A$

enables us to observe the proposed redox gated electron flow between P and M^+ in oxidative titrations, it may yield interesting results in enzymologic studies.

Vita

Roland Carroll Tittsworth was born in Baltimore City, Maryland and attended Howard County, Maryland public schools. He received his Bachelor of Arts in Biochemistry/Molecular Biology from the University of Maryland, Baltimore County. He currently resides in Baton Rouge, Louisiana.

DOCTORAL EXAMINATION AND DISSERTATION REPORT

Candidate: Roland Carroll Tittsworth

Major Field: Chemistry

Title of Dissertation: X-Ray Absorption and Electron Paramagnetic Resonance Studies of Azotobacter vinelandii Nitrogenase

Approved:

Major Professor and Chairman

Dean of the Graduate School

EXAMINING COMMITTEE:

Date of Examination:

June 15, 1995